AGARD-R-732

AGARD REPORT No.732

Short-Crack Growth Behaviour in an Aluminum Alloy — an AGARD Cooperative Test Programme

NORTH ATLANTIC TREATY ORGANIZATION

ADVISORY GROUP FOR AEROSPACE RESEARCH AND DEVELOPMENT

(ORGANISATION DU TRAITE DE L'ATLANTIQUE NORD)

AGARD Report No.732

SHORT-CRACK GROWTH BEHAVIOUR IN AN ALUMINUM ALLOY – AN AGARD COOPERATIVE TEST PROGRAMME

by

J.C.Newman, Jr
Materials Division
NASA Langley Research Center
Hampton, Va, USA

and

P.R.Edwards
Materials and Structures Department
Royal Aerospace Establishment
Farnborough, Hants
England

This Programme was sponsored by the Structures and Materials Panel of AGARD.

THE MISSION OF AGARD

According to its Charter, the mission of AGARD is to bring together the leading personalities of the NATO nations in the fields of science and technology relating to aerospace for the following purposes:

- Recommending effective ways for the member nations to use their research and development capabilities for the common benefit of the NATO community;
- Providing scientific and technical advice and assistance to the Military Committee in the field of aerospace research and development (with particular regard to its military application);
- Continuously stimulating advances in the aerospace sciences relevant to strengthening the common defence posture;
- Improving the co-operation among member nations in aerospace research and development;
- Exchange of scientific and technical information;
- Providing assistance to member nations for the purpose of increasing their scientific and technical potential;
- Rendering scientific and technical assistance, as requested to other NATO bodies and to member nations in connection with research and development problems in the aerospace field.

The highest authority within AGARD is the National Delegates Board consisting of officially appointed senior representatives from each member nation. The mission of AGARD is carried out through the Panels which are composed of experts appointed by the National Delegates, the Consultant and Exchange Programme and the Aerospace Applications Studies Programme. The results of AGARD work are reported to the member nations and the NATO Authorities through the AGARD series of publications of which this is one.

Participation in AGARD activities is by invitation only and is normally limited to citizens of the NATO nations.

Published December 1988

ISBN 92-835-0493-3

Printed by Specialised Printing Services Limited
40 Chigwell Lane, Loughton, Essex IG10 3TZ

PREFACE

In 1982 the Structures and Materials Panel organized a Specialists' Meeting on the "Behaviour of Short Cracks in Aircraft Structures". The Meeting revealed the complexity of the short-crack growth behaviour and that a short-crack effect does exist, at least under certain test conditions. It also indicated that differences in test technique existed that made it very difficult to compare the data obtained by individual researchers and to assess the significance of the short-crack effect.

In 1984 the Panel organized a Cooperative Test Programme with as objectives: the development of a standard test method for the measurement of short-crack growth, the establishment of relevant short-crack growth data, to improve existing analytical crack growth models and to define the significance of the short-crack effects.

The programme was devised in two parts; a "core" and a "supplemental" portion. The "core" programme objectives included the establishment of a common test procedure, the gathering of test data on the same airframe alloy — AA 2024-T3, data analysis and the development of improved models of short-crack behaviour. The "supplemental" programme focuses on the short-crack phenomenon in other allovs.

This report describes the results obtained under the "core" programme. A computerised data base has been established, together with associated software for using the data base, thus allowing engineers and scientists in the NATO nations to make the maximum use of the results. The results of the "supplemental" programme will be made available as a separate AGARD report in the near future.

The cooperative programme was guided by a Panel sub-committee with the valuable assistance of two coordinators. Over the years the following Panel Members participated in the sub-committee.

P.Bascary (FR)
H.J.G.Carvalhinhos (PO)
K.I.Collier (UK)
A.Deruyttere (BE)
M.Doruk (TU)
J.L.Engerand (FR)
J.M.Fehrenbach (FR)
G.Z.Harris (UK)
L.A.Harris (US)
W.G.Heath (UK)
R.Labourdette (FR)
H.P. van Leeuwen (NL)
R.D.J.Maxwell (UK)
C.W.Skingle (UK)
A.Salvetti (IT)
R.Schmidt (US)
W.Wallace (CA)

The cooperative tests were performed by thirteen laboratories in nine nations represented by:

A.Ankara, METU, (TU)
A.F.Blom, FAA, (SW)
M.H.Carvalho, LNETI, (PO)
G.Cavallini, Univ. of Pisa, (IT)
J.Cieslowski, Johns Hopkins Univ., (US)
R.Cook, RAE, (UK)
P.R.Edwards, RAE, (UK)
J.Foth, IABG, (GE)
M. de Freitas, CEMUL (PO)
R.Galatolo, Univ. of Pisa, (IT)
P.Heuler, IABG, (GE)
C.Kaynak, METU, (TU)
J.J.Lee, Johns Hopkins Univ., (US)
A.Liberge, CEAT, (FR)
D.S.Lock, RAE, (UK)
C.Mazur, AFWAL, (US)
J.C.Newman, NASA, (US)
H.Nowack, DFVLR, (GE)
E.P.Phillips, NASA, (US)
J.Rudd, AFWAL, (US)
W.N.Sharpe, Johns Hopkins Univ., (US)
M.H.Swain, NASA, (US)
R.Wanhill, NLR, (NL)

The coordinators of the programme were:

for Europe — P.R.Edwards
for North America — J.C.Newman

Many thanks are extended to all who participated in the programme, especially to the two coordinators for their considerable efforts in bringing to a successful completion this very valuable piece of research.

H.Zocher
Chairman, Sub-Committee on
Research for Short-Crack Effects

STRUCTURES AND MATERIALS PANEL

Chairman: Prof. Dr-Ing. Hans Förstching
Direktor der DVFLR Institut für
Aeroelastik
Bunsenstrasse 10
D-3400 Göttingen
Germany

Deputy Chairman: Mr Samuel L.Venneri
Director, Materials & Structures Division
(Code RM)
Office of Aeronautics & Space
Technology
NASA Headquarters
Washington DC 20546 — USA

SUB-COMMITTEE ON RESEARCH FOR SHORT CRACK EFFECTS

Chairman: Dipl Ing. Horst Zocher
IABG mbH, Abt TF
Einsteinstrasse, 20
D-8012 Ottobrunn
West Germany

SMP MEMBERS

H.J.G.Carvalhinhos — PO
A.Deruyttere — BE
M.Doruk — TU
R.Labourdette — FR
H.P. van Leeuwen — NL
A.Salvetti — IT

TECHNICAL COORDINATORS

P.R.Edwards — UK (Europe)
J.C.Newman US — (North America)

PANEL EXECUTIVE

Mr Murray C.McConnell — UK

AGARD-OTAN
7, rue Ancelle
92200 Neuilly sur Seine
France

Tel: (1) 4738 5790 & 5792
Telex: 610176F

From USA and CANADA
AGARD-NATO
Attn: SMP Executive
APO New York 09777

ABSTRACT

An AGARD test programme on the growth of "short" fatigue cracks was conducted to define the significance of the short-crack effect, to compare test results from various laboratories and to evaluate an ex sting analytical model to predict the growth of such cracks. The first phase of this programme, the Core Programme, was aimed at test procedure and specimen standardisation and calibration of the various laboratories. A detailed working document has been prepared and is included in this report. It describes the testing fundamentals and procedures and includes the analysis procedures used for handling the test data.

The results from the test programme showed good agreement among the participants on short-crack growth rates, on fatigue life to various crack sizes and breakthrough (surface- or corner-crack became a through crack), and on crack shapes. A crack-growth model, incorporating crack-closure effects was used to analyse the growth of short cracks from small (inclusion) defects in the material along the notch surface. The closure model indicated that the "short-crack" effect was greatest in those tests involving significant compressive loads, such as constant-amplitude loading at stress ratios of -1 and -2, and the Gaussian spectrum loading.

* * *

Un programme d'essais AGARD sur le développement des "petites" fissures a été réalisé afin de déterminer l'importance de ce phénomène, de permettre une comparaison entre les résultats obtenus par les différents laboratoires d'essais et d'évaluer un modèle analytique pour la prévision du développement de telles fissures.

La première phase de ce programme, le programme CORE, a porté sur procédure d'essai à adopter, la standardisation des échantillons et l'étallonage des appareils de mesure dans le différents laboratoires. Un document de travail détaillé a été préparé et il est joint à ce rapport. Il fournit la description des principes d'essai et des procédures adoptées ainsi que les procédures d'analyse mises en oeuvre pour le traitement des données d'essai.

Les résultats obtenus par les différents participants concordent dans une large mesure en ce qui concerne la vitesse de propagation des petites fissures, l'endurance en fatigue de fissures de différentes longeurs, les fissures traversantes (évolution des fissures superficielles et fissures d'angle en fissures traversantes) ainsi que la forme des fissures. Un modèle du développement des fissures, qui tient compte des effets de la fermeture des fissures, a été utilisé pour analyser le développement des petites fissures à partir de petite défaute (inclusions) le long de la surface de l'entaille. Les résultats obtenus du modèle de fermeture indiquent que le phénomène des petites fissures a été le plus marqué lors des essais faisant appel à des charges compressives importantes, telles que les charges à amplitude constante, appliquées avec des rapports de contrainte de -1 et de -2, et les spectres de chargement Gaussiens.

CONTENTS

SHORT-CRACK GROWTH BEHAVIOUR IN AN ALUMINUM ALLOY -AN AGARD COOPERATIVE TEST PROGRAMME-

by

J. C. Newman, Jr.
Materials Division
NASA Langley Research Center
Hampton, Virginia
USA

and

P. R. Edwards
Materials and Structures Department
Royal Aerospace Establishment
Farnborough, Hants
ENGLAND

SUMMARY

An AGARD Cooperative Test Programme on the growth of "short" fatigue cracks was conducted to define the significance of the short-crack effect, to compare test results from various laboratories, and to evaluate an existing analytical model to predict the growth of such cracks. The initiation and growth of short fatigue cracks (5 μm to 2 mm) from the surface of a semi-circular notch in 2024-T3 aluminum alloy sheet material were monitored under various load histories. The cracks initiated from inclusion particle clusters or voids on the notch surface and generally grew as surface cracks. Tests were conducted under several constant-amplitude (stress ratios of -2, -1, 0, and 0.5) and spectrum (FALSTAFF and GAUSSIAN) loading conditions at three stress levels each. Growth of the short cracks was recorded using a plastic-replica technique. Over two hundred and fifty edge-notched specimens were fatigue tested and nearly 950 cracks were monitored by twelve participants from nine countries. Long crack-growth rate data for cracks greater than 2 mm in length were obtained over a wide range in rates (10^{-8} to 10^{-1} mm/cycle) for all constant-amplitude loading conditions. Long crack-growth rate data for the FALSTAFF and GAUSSIAN load sequences were also obtained on the same material.

The results from the cooperative test programme showed good agreement among the participants on short-crack growth rates, on fatigue life to various crack sizes and breakthrough (surface- or corner-crack became a through crack), and on crack shapes. The short cracks exhibited the "short-crack" effect in that they grew faster than long cracks at the same stress-intensity factor range and stress ratio. The short cracks also grew at stress-intensity factor ranges much lower than the thresholds obtained from long-crack tests under constant-amplitude loading. Short-crack growth rates also showed a stress-level effect at the same stress-intensity factor range and stress ratio. The short-crack and stress-level effects were more pronounced as the stress ratio became more negative. This applied for both constant-amplitude and spectrum loading. High stress levels generally produced multi-cracks along the bore of the notch whereas low stress levels produced only a few. The data showed a large amount of "scatter" due to such factors as crack-grain boundary interaction and multi-crack interaction. A crack non-interaction criterion was used to eliminate data where cracks were judged to be interacting and greatly reduced "scatter" in the stress-intensity factor against growth rate data.

A crack-growth model, incorporating crack-closure effects, was used to analyze the growth of short cracks from small (inclusion) defects in the material along the notch surface. This defect size was consistent with experimental observations of initiation sites at inclusion-particle clusters. Reasonable agreement was found between measured and predicted short-crack growth rates, fatigue life to breakthrough, and crack shapes for most loading conditions. However, for R = -2 loading, the model predicted slower growth rates and longer fatigue lives to breakthrough than test results. In contrast, in the high R-ratio (R = 0.5) loading, the model predicted slightly faster rates and shorter fatigue lives to breakthrough than the tests. These particular conditions involved local notch-root yielding either under tension or compression. These discrepancies may be due to the fact that in the model plane-strain conditions were assumed for short-crack growth behaviour, whereas the actual behaviour may have been closer to plane stress. The closure model did indicate, however, that the "short-crack" effect was greatest in those tests involving significant compressive loads, such as constant-amplitude loading at stress ratios of -1 and -2, and the GAUSSIAN spectrum loading. Similar behaviour was observed in the tests.

1. INTRODUCTION

With the increasing acceptance of linear-elastic fracture mechanics methods for damage-tolerance analyses, there has also been a trend towards use of the same methodology for fatigue durability analyses. To obtain acceptably long lives without a significant weight penalty, the analyses must assume a very small initial crack. Numerous investigators [1-18] have observed that the growth characteristics of short fatigue cracks in plates and at notches differ from those of long cracks in the same material. These studies have concentrated on the growth of short cracks ranging in length from 10 μm to 1 mm. On the basis of linear-elastic fracture mechanics (LEFM), the short cracks grew much faster than would be predicted from long crack data. This behaviour is illustrated in Figure 1, where the crack-growth rate is plotted against the linear-elastic stress-intensity factor range, ΔK. The solid (sigmoidal) curve shows typical results for a given material and environment under constant-amplitude loading. The solid curve is usually obtained from tests with long cracks. At low growth rates, the threshold stress-intensity factor range, ΔK_{th}, is usually obtained from load-reduction (K-decreasing) tests. Some typical experimental results for short cracks in plates and at notches are shown by the dashed curves. These results show that

short cracks grow faster than long cracks at the same ΔK level and that they also grow at ΔK levels below threshold.

A Specialists' Meeting in 1982 organized by the AGARD Structures and Materials Panel (SMP) on "The Behaviour of Short Cracks in Aircraft Structures" [15] revealed the complexity of short-crack growth behaviour. Many varied views were expressed on the data obtained from experimental and analytical investigations, but there was no consensus of opinion. Some tests appeared to confirm the existence of the short-crack effect, whereas other experimenters did not confirm these findings. During the round table discussion [15], however, it emerged that tests which did not confirm the existence of the short-crack effect had not included compressive loading cycles. The applicability of LEFM concepts to short-crack growth behaviour was also questioned. Some of the "classical" short-crack experiments [1-3] were conducted at high stress levels which would invalidate LEFM procedures. Nonlinear or elastic-plastic fracture mechanics concepts were also used to explain the observed short-crack effects. The metallurgical similitude [16] also breaks down for short cracks (which means that the growth rate is no longer an average taken over many grains). Thus, the local growth behaviour is controlled by metallurgical features [6,12]. If the material is anisotropic (differences in modulus and yield stress in different crystallographic directions), the local grain orientation will determine the rate of growth. Crack front irregularities and small particles or inclusions affect the local stresses and, therefore, the crack growth response. In the case of long cracks (which have long fronts), all of these metallurgical effects are averaged over many grains. LEFM and nonlinear fracture mechanics concepts are only beginning to explore the influence of metallurgical features on stress-intensity factors, strain-energy densities, J-integrals and other crack-driving parameters. Reference 19 gives a review of two books [17,18], published in late 1986, on the behaviour of short cracks in metallic materials.

As the crack size approaches zero, a crack size must be reached below which the assumptions of the ΔK concept are violated. But for many engineering applications, a ΔK-based analysis that extends into the regime of questionable validity may still be very useful. Certainly from a structural designer's viewpoint, a single analysis methodology that is applicable to all crack sizes is very desirable. Therefore, the application of ΔK analyses to short-crack problems should be thoroughly explored.

The outcome of the AGARD SMP meeting [15] was to encourage further activity on the growth behaviour of short cracks. As a result, an AGARD Cooperative Test Programme was initiated in 1984 to investigate the short-crack growth behaviour under various loading conditions for a common airframe aluminum alloy and to improve methodologies to predict the growth of short cracks. The results from the Cooperative Test Programme are reported herein. This report contains the description, test results, data analysis, crack-growth model analysis, and conclusions of the collaborative fatigue test programme.

A Computerised Data Base which constitutes an operational manual for the data-base computer program was also developed. Data on crack location and size as a function of cycles, generated in the Cooperative Test Programme, are stored on the data base. The computer program and data base together constitutes a means by which engineers and scientists can make maximum use of the data generated in the AGARD Collaborative Programme.

2. COOPERATIVE PROGRAMME OVERVIEW

The objectives of the AGARD Cooperative Test Programme on the Behaviour of Short Cracks were to: (1) define the "short-crack" specimen, core-programme material, and loading conditions, (2) develop standard test methods to measure growth of short cracks, (3) calibrate test techniques used by the participating laboratories, (4) establish relevant short-crack data under specified test conditions, (5) define the regime where long-crack data is applicable to short cracks, (6) improve existing analytical crack-growth models, and (7) define the significance of the short-crack effect.

The "short-crack" specimen used in the cooperative test programme was selected to produce naturally-occurring cracks at material defects and to propagate cracks through a stress field similar to that encountered in aircraft structures. Single-edge-notch tensile specimens made of 2024-T3 aluminum alloy sheet material, as shown in Figure 2, were used. A wide range in loading conditions were applied in the test programme. Tests were conducted under several constant-amplitude and spectrum (FALSTAFF [20,21] and GAUSSIAN [22]) loading conditions at three stress levels each. The core-programme material--2024-T3 aluminum alloy sheet--was supplied by the National Aeronautics and Space Adminstration - Langley Research Center. The United States Air Force Wright Aeronautical Laboratory machined 700 core-programme specimens. Nearly 550 specimens were distributed to fifteen laboratories. Twelve laboratories conducted tests in the Cooperative Test Programme.

Several methods of measuring the growth of "short" cracks (lengths from about 10 μm) were considered. These methods were the electrical-potential method [23], ultrasonic surface wave [24], marker bands [25], and plastic replicas [26]. For the aluminum alloy, the plastic-replica method was found to be accurate for use down to the short-crack lengths required in the programme. This method is very simple to apply, but the method is very labor intensive. Growth of short cracks was recorded by all participants using the plastic-replica method. Over two hundred and fifty edge-notched specimens were fatigue tested and nearly 950 cracks were monitored by twelve participants from nine countries. About sixty specimens were also tested in a preliminary fatigue test programme to establish the test conditions for the Cooperative Test Programme.

The participating laboratories are listed in Table 1. This table shows the country, laboratory, and participants. The code used to present results from each laboratory are as indicated. The test conditions used in the core programme are shown in Table 2. Three types of loading were considered: constant-amplitude loading, the standard maneuver load sequence FALSTAFF, and the standard random load sequence GAUSSIAN. For constant-amplitude loading, four stress ratios (-2, -1, 0 and 0.5) were applied. For each type of loading, three stress levels were selected. The lowest stress level was selected to be near the fatigue limit. The estimated fatigue life for these conditions, supplied to the participants, are as shown. Three specimens were supplied for each condition. The participant test matrix for short-crack

growth is shown in Table 3. The basic "core" programme was constant-amplitude loading with R = -1 and 0, and the FALSTAFF load sequence. The participants were either assigned or they chose other conditions. Each laboratory was required to align their test machines and gripping fixtures to produce a nearly uniform tensile stress field on an un-notched sheet specimen with strain gauges. Those laboratories conducting spectrum load tests were independently checked by a programme coordinator to verify the accuracy of their spectrum loading.

Long crack-growth rate data for cracks greater than 2 mm in length were also obtained over a wide range in rates for all constant-amplitude loading conditions, for the FALSTAFF load sequence, and for the GAUSSIAN load sequence. These results were used to define the regime where long-crack data are applicable to short cracks for the core-programme material.

A semi-empirical crack-growth model, incorporating crack-closure effects [27,28], was used to correlate the long crack-growth rate data over a wide range in rates for various constant-amplitude loading conditions. Using the long-crack data (neglecting the long-crack thresholds), the model was then used to predict crack growth and closure behaviour of short cracks emanating from semi-circular edge notches, to predict fatigue life from an initial defect, and to predict crack shapes. Comparisons were made between experimental and predicted crack-growth rates for short cracks, fatigue life and crack shapes under the constant-amplitude and spectrum loading conditions used in the core programme.

As part of the AGARD Cooperative Test Programme, an experimental study was also conducted to measure the crack-closure behaviour of short cracks using a laser-interferometric displacement technique (see reference 29).

The experimental data from the core programme and the predictions from the analytical crack-closure model were used to assess the significance of the short-crack effect for the 2024-T3 aluminum alloy sheet material.

3. COOPERATIVE TEST PROGRAMME

The cooperative test programme consisted of testing single-edge-notch and center-crack tension specimens made of 2024-T3 aluminum alloy sheet material under constant- and variable-amplitude loading. Tests were conducted at room temperature and under laboratory air conditions. This section describes the short-crack specimen, material, loading conditions, test procedures, and data analysis procedures used to obtain short-crack growth rate data. The procedures used to obtain long-crack growth rate data from center-crack tension specimens are also presented.

3.1 Short-Crack Specimen

The short-crack specimen was selected to produce naturally-occurring cracks at material defects and to propagate cracks through a stress field similar to that encountered in aircraft structures. A single-edge-notch tensile (SENT) specimen, as shown in Figure 2, was used. The notch was semi-circular with a radius of 3.18 mm. The stress-concentration factor was 3.17, based on gross-section stress [30]. Figure 3 shows the normal stress distribution near the notch root for the SENT specimen (solid curve). For comparison, the normal stress distribution for a circular hole in an infinite plate is shown as the dashed curve. The normal stress distribution for the SENT specimen is similar to that for an open hole in an infinite plate, but the stresses are slightly higher because of the finite width. Therefore, the SENT specimen simulates a hole in an aircraft structure, but the side notch allows the notch root to be observed with a microscope and allows plastic replicas to be taken with ease during testing.

The specimen blanks for the SENT specimens were cut from 24 aluminum alloy sheets (610 by 1830 by 2.3 mm). The layout diagram is shown in Figure 4. The long dimension of the specimen was parallel to the rolling direction of the sheet. Each specimen blank was labelled with a specimen number. The blanks were milled to final overall dimensions (50 mm wide by 305 mm long by supplied thickness). Some blanks (60) were reserved for alignment and long-crack specimens. These blanks did not contain a notch. In the remaining blanks, a semi-circular notch was milled with final cuts of 0.25, 0.1 and 0.05 mm using a newly sharpened tool to achieve a final radius of 3.18 mm. This milling sequence was designed to minimize residual stresses at the notch root.

Specimens were tested in either wedge grips, hydraulic grips, or flat plate friction grips. The grip lines are shown in Figure 2. If the grips were not capable of gripping to a depth of 77.5 mm, then the specimen was shortened but the edge of the gripping area remained the same (150 mm between grip lines). In some laboratories, bolt holes were also used in the gripping area to apply pressure in gripping the specimen. The specimens were not gripped directly. Either aluminum or plastic spacers were used between the specimen and the grip jaws. These spacers were used so that the specimen would not crack in the gripping area.

3.2 Material

The core-programme material was 2024-T3 aluminum alloy sheet (2.3 mm thick). This material was taken from a special stock of aluminum-alloy sheets retained at NASA Langley Research Center for fatigue testing. The fatigue and fatigue-crack-growth properties of this material are discussed in references 31 and 32. Tables 4 and 5 give the nominal chemical composition and average tensile properties, respectively. Tensile properties were obtained by using standard American Society for Testing and Materials (ASTM) tensile specimens.

Typical microstructure perpendicular to the rolling direction and parallel to the nominal crack-growth plane is shown in Figure 5. Typical grain dimensions in the crack-growth directions, 2a and c, were 25 μm and 55 μm, respectively. The dimension in the rolling direction was typically 95 μm. Clusters of inclusion particles (black) are evident in Figure 5. Annex A gives a more complete description of a microstructural examination of the core-programme material.

Chemical polishing of the SENT specimens was necessary to smooth machining marks on the notch surface and to debur the edges of the notch. This also provided further assurance that there were no significant residual stresses present at the notch root. The core-programme specimens were chemically polished in a solution of 80 percent phosphoric acid, 5 percent nitric acid, 5 percent acetic acid, and 10 percent water, by volume, heated to 105 degrees Centigrade for five minutes. A layer of material approximately 0.02 mm in thickness was removed by the five-minute polishing process. Some specimens that were chemically polished for one- or three-minutes were also tested for comparison (see Annex B on Preliminary Fatigue Tests on Short-Crack Specimens). Figure 6 shows typical notch surface finishes after one and five minutes of polishing. The five-minute polishing procedure removed more material from the surfaces than the one-minute polishing process. The edges of the five-minute polished specimens were deburred and mildly rounded during the polishing process, thus preventing premature initiation of cracks at the edge of the notch. In some cases, prior to testing, the notch surface was lightly etched to reveal the microstructure.

3.3 Loading

A wide range of loading conditions was applied in the cooperative test programme. Fatigue tests were conducted under several constant-amplitude loading conditions and under two spectrum load sequences. The two standard load spectra were: FALSTAFF [20,21] and a Gaussian spectrum [22]. In all tests, the cyclic frequencies ranged from 5 to 20 Hz.

Each laboratory was required to align their test machines and gripping fixtures to produce a nearly uniform tensile stress field on an un-notched sheet specimen with strain gauges. Three blank specimens (identical to the short-crack specimen without a notch) were supplied to each laboratory for alignment verification. The alignment procedures are presented in Annex C. Those laboratories conducting spectrum load tests were independently checked by a programme coordinator (P. R. Edwards, Royal Aerospace Establishment) to verify the accuracy of their spectrum loading. The results of the on-line spectrum loading accuracy verification are discussed in Annex D.

Anti-buckling guides lined with teflon sheets, shown schematically in Figure 7, were used on all tests where compressive loads were applied. They were loosely bolted together on both sides of the specimen. Guide plates were not used when the minimum applied load was zero or positive. If a test was interrupted, the steady-state minimum load was maintained at a level not lower than the required minimum load in the test. The following sections briefly describe the various load histories.

3.3.1 Constant-amplitude loading

Four stress ratios, $R = -2$, -1, 0 and 0.5, were used in the programme. The large negative stress ratios were selected because, as previously mentioned, the short-crack effect is more pronounced under compressive loading conditions. In contrast, the short-crack effect is less evident at high stress ratios. At each R-ratio, three stress levels were selected, see Table 2. The lowest stress level for each R-ratio was selected to be slightly higher than the fatigue limit. Annex B shows the results of preliminary fatigue tests and analyses conducted to determine the particular stress levels used in the test programme. Table 3 gives a summary of the stress ratios used by the participating laboratories.

Table 6 shows the calculated local notch-root elastic stresses normalized by yield stress at maximum and minimum applied stress for the core-programme conditions. The medium and high $R = -2$ loading conditions yield the notch root under compression. All conditions at $R = -1$ loading were elastic. Consequently, this condition was used to determine initial crack sizes and an effective threshold for crack growth to be used in life predictions (see Annex B). The highest loading at $R = 0$ and all loading at $R = 0.5$ cause the notch root to yield under tension. Both FALSTAFF and GAUSSIAN loading cause the notch root to yield under tension. The GAUSSIAN loading also causes compressive yielding at the notch root.

3.3.2 Standard maneuver load sequence FALSTAFF

Most of the participants carried out fatigue tests under FALSTAFF (Fighter Aircraft Loading STAndard For Fatigue) loading at three different stress levels, see Table 3. These stress levels were selected from preliminary fatigue tests and analyses conducted on SENT specimens. These results are also discussed in Annex B.

FALSTAFF [20,21] is based on a large number of actual flight load-time histories pertaining to five different fighter aircraft types operated by three different air forces. The load sequence represents the load-time history in the lower wing skin near the wing root of a fighter aircraft. The essential properties are summarized as follows. FALSTAFF represents a load sequence, defined by successive peaks and troughs, covering a "block" of 200 flights. The block size conforms to average European annual fighter utilization. Flights in FALSTAFF belong to three different groups of mission types: flights with repetitive patterns of severe maneuvering (air-to-ground missions), flights with severe maneuvering (air combat) and flights with only light to moderate maneuvering (navigation mission). FALSTAFF contains taxi-load cycles and the majority of these are associated with a crossing of the zero-stress level. The complete FALSTAFF sequence consists of 35966 numbers, ranging in magnitude from 1 to 32. The "FALSTAFF load levels" ranging from 1 to 32 are arbitrary units. The "zero"-stress level corresponds to FALSTAFF level 7.5269. The smallest load variation ("omission level") considered is two FALSTAFF levels or about 8 percent of the highest stress contained in FALSTAFF. The highest stress ("truncation level") considered is the one exceeded once in one-hundred flights. References 20 and 21 give a complete FALSTAFF sequence in tabular form and give a FORTRAN listing of the program to generate the sequence.

Figures 8(a) and 8(b) show the cumulative distributions of the FALSTAFF sequence (peaks and troughs) and some typical flights, respectively. The severity of the spectrum is usually identified by referencing the stress that a test specimen experiences at the highest stress level in the sequence (S_{max}). In this report, the same convention is used.

3.3.3 Standard random load sequence GAUSSIAN

Four laboratories carried out fatigue tests using a Gaussian type random load sequence [22] at three different stress levels. This sequence is used for general application in fatigue testing. Again, the particular stress levels used in the cooperative programme (Table 2) were selected from the results of preliminary fatigue tests and analyses conducted on the SENT specimens (see Annex B).

The Gaussian load sequence was originally defined in three forms, each one having a different irregularity factor (ratio of number of zero crossings to number of peaks). The version specific for the cooperative test programme is that with the narrowest bandwidth. The narrow bandwidth sequence has an irregularity factor (I) of 0.99. Herein, this particular sequence is referred to as GAUSSIAN.

The characteristic properties of the GAUSSIAN random load sequence are as follows. The sequence has a frequency distribution of level crossings equal to that of a stationary Gaussian process. Sequence length is defined by about 10^6 mean level crossings (N_0) with positive slope. The number of peaks N_1 (equal to the number of troughs) are dependent upon the irregularity factor $I = N_0/N_1 = 0.99$. The total range of possible peaks and troughs is divided into 32 intervals. For $I = 0.99$, the spectrum shows very little variation in the mean value (nearly zero) and the spectrum is very close to an $R = -1$ variable-amplitude loading.

Figures 9(a) and 9(b) show the GAUSSIAN load sequence (cumulative distribution of peaks and troughs) and a portion of the sequence, respectively. The severity of the spectrum is identified by referencing the stress that a test specimen experiences at the highest stress level in the sequence (S_{max}).

3.4 Short-Crack Test Conditions and Procedures

The test conditions for the core programme are shown in Table 2. Each participant was to test a "common core programme" (constant-amplitude loading at $R = -1$ and $R = 0$; and the FALSTAFF sequence). One additional test condition (either the constant-amplitude test with $R = 0.5$ or $R = -2$; or the GAUSSIAN sequence) was to be selected by the participant. Table 3 gives a summary of the test conditions submitted by the various participants.

All test conditions were to be carried out with the three stress levels specified. The total number of notched specimens sent to each participant was 36. Three specimens were provided for each test condition (load type and stress level). For each test condition, there were two objectives: (1) obtain surface-crack-length-against-cycles data, and (2) obtain surface-crack-depth information. To achieve these objectives, the particular test for each condition was as follows.

For each test condition, one specimen was to be tested to obtain surface-crack-length-against-cycles data (using the plastic-replica method) until one continuous crack was all the way across the notch root. The specimen was then pulled to failure. Another specimen was to be tested under the same condition but only until the total surface-crack length along the bore of the notch was between particular values specified for each participant (see Table 7). The specimen was then statically pulled to failure. An enlarged photograph of the fracture surface showing the surface crack (or cracks) was made so that the surface-crack shape could be measured.

For each test condition, a spare specimen was provided in case a specimen was inadvertently broken. This specimen could be used to obtain more information on crack growth or on crack shape.

3.4.1 Short-crack measurement method

Several methods of measuring the growth of "short" cracks from lengths of 10 μm to 2 mm were considered. These methods were electrical potential [23], ultrasonic surface waves [24], marker bands [25], and plastic replicas [26].

The electrical-potential method is widely used in monitoring the growth of "long" cracks (for example, see reference 33). This method was successfully used to monitor the growth of short cracks in steels and superalloys [23] but the sensitivity of this method for aluminum alloys had not been established. Several factors must be considered for accurate and reproducible electrical potential monitoring of short cracks. First, a calibration between measured voltage and crack size must be established. Also, the electrical probe must be accurately located with respect to the crack location. The cooperative programme objective of monitoring the growth of naturally-initiated cracks and the possibility of multi-crack initiation sites would make the application of this method very difficult.

The ultrasonic surface wave method [24] was shown to be effective in detecting a surface crack (or multi-surface cracks) at the root of a notch in an aluminum alloy material. This method is capable of detecting surface cracks down to about 300 μm. However, reference 24 also demonstrated that the plastic-replica method could detect a surface crack or multi-surface cracks, as small as about 10 μm.

The marker-band method, using either a high R-ratio or a small spike overload marker, could not be used to detect small surface cracks [25]. Reference 25 also showed that the plastic-replica method could be used to monitor the growth of "short" cracks.

Because the replica method was found to be accurate down to the short crack lengths required in the programme, this method was selected as the primary method. Each participant was free to select any other method to monitor short cracks provided that they calibrate their method against the replica method. All participants, however, chose the replica method. This method is very simple to apply, but the method is very labor intensive. Many replicas have to be taken to determine crack length against cycles. The suggested plastic-replica procedures are presented in Annex E.

Figure 10 shows the area over which cracks were to be monitored. The crack length (L_1) was measured along the bore of the notch. The value of L_1 and its location were recorded on a "Data Chart" as a function of cycles. The Data Chart, shown in Figure 11, includes the specimen number, loading type, peak stress, and a grid upon which the information obtained from a replica was recorded. Each record of crack length, location, and cycles was taken at a specified cyclic interval. Replicas were taken at a cyclic interval chosen so that at least 25 to 30 replicas were taken during one test. A test was terminated when a crack had grown across the total specimen thickness, B. The estimated number of cycles to breakthrough (L_1 = B) for the various load histories are shown in Table 2. The cyclic intervals were determined from these estimates. These estimates were obtained from preliminary fatigue tests and analyses (Annex B). Replicas were taken while the specimen was under tensile load. (The loading procedures for taking replicas under constant-amplitude, FALSTAFF, and GAUSSIAN loading are presented in the next section.) When a test was terminated, the specimen was statically pulled to failure. Some test specimens, however, were statically pulled to failure early in life to determine the shape of the cracks (see Section 3.4.3). Figure 12 shows an example of a data chart for a specimen with a single crack.

At the lowest stress levels selected in Table 2, a single crack was expected to initiate naturally and dominate for most of the fatigue life. However, at the higher stress levels several cracks might develop along the bore of the notch, as shown in Figure 13. If several cracks developed in the test, the participant monitored the five largest cracks and recorded these on the Data Chart as L_i (i = 1 to 5). An example of recording multi-crack data is shown in Figure 14. Starting with the lowest number of cycles (early in life) where crack(s) could be measured, the crack(s) were numbered and their lengths recorded in millimeters (± 0.001 mm) on the Data Chart. At the next "cyclic interval," crack lengths were recorded and any new crack(s) were included, such as crack number 3. If two cracks joined together, such as crack numbers 2 and 4 between 40,000 and 45,000 cycles, the lowest number was used as the crack identification number. The total length was recorded as L_2 and it was indicated that L_4 was now measured as part of L_2. Likewise, when cracks 1 and 2 joined together, their total length was recorded as L_1 and it was indicated that L_2 was now measured as part of L_1 (and L_4 was also measured as part of L_1). These data charts provided approximate locations for determining crack initiation sites, for calculating stress-intensity factors, and for applying the crack non-interaction criteria (see Section 4.2).

In addition to the Data Charts, the participants provided a table and plot of stress-intensity factor range against crack-growth rate, a photograph of the fracture surface showing the surface crack(s) and the full thickness of the specimen, and a photograph of a replica taken near the end of each test showing the full thickness. The methods of calculating stress-intensity factors and crack-growth rates are presented in Section 3.5

3.4.2 Constant-amplitude, FALSTAFF, and GAUSSIAN loading

Replicas were taken while the specimen was under tensile load so that any cracks that were present would be open and allow the replica material to infiltrate the cracks. The loading procedures are as follows.

Constant-amplitude loading.- The test was stopped at mean (or minimum) load. The applied load was then manually increased to 80 percent of the maximum test load. This load was held while a replica was taken along the bore of the notch. After the replica was removed from the notch, the load was reduced to mean load and the test was restarted.

FALSTAFF and GAUSSIAN loading.- To take replicas under the spectrum-load conditions, the test machine was programmed (or manually set) to stop and hold at a specified peak level after the desired number of cycles had been completed. The replica was taken along the bore of the notch (see procedures in Annex E). The specified peak levels were: FALSTAFF--Level number 22 and GAUSSIAN--Class number 7, level 26. After the replica was removed from the notch, the test machine was restarted and continued from the specified peak level.

3.4.3 Crack shape

The replica method provides information only on surface- or corner-crack lengths (L) along the notch root. The surface- and corner-crack depths have to be determined by either an experimental or analytical calibration. For each test condition, one specimen was to be tested until the total crack length along the bore of the notch was between particular values specified for each participant. The participant test matrix on crack shape is shown in Table 7. Three crack-size types were selected. One series of tests were to be terminated when the crack length (L) was less than 0.5 mm. The second series of tests were to be terminated when the crack length (L) was between 0.5 and 1 mm. And the third crack-size type was between 1 and 2 mm. Initially, the crack-size types were divided equally among the fifteen laboratories. However, only twelve laboratories submitted results on the cooperative test program. Unfortunately, several laboratories selected for the mid-range did not participate in the test programme. Therefore, results from reference 25, using the same core-programme material and specimen configuration, were used to supplement test results in this range.

The analytical model used in references 25 and 28 was also used to calibrate the relationship between surface-crack length and crack depth.

3.5 Short-Crack Data Analysis Procedures

In the following, approximate stress-intensity factor equations for a surface crack or a corner crack emanating from a semi-circular edge notch are presented. These equations are used later to compare crack-growth rates measured for short cracks with those measured for long cracks as a function of the stress-intensity factor range. The method of calculating the crack-growth rates for short cracks is also presented.

3.5.1 Calculation of stress-intensity factors

The calculation of stress-intensity factors assumes that either a semi-elliptical surface crack is located at the center of the edge notch, as shown in Figure 15(a), or a quarter-elliptical corner crack is located at an edge, as shown in Figure 15(b). (Note definition of a and t in Figure 15.) For a surface crack located at other locations along the bore of the notch, the calculation is adequate if the crack is small compared to thickness. However, if several cracks are close to one another then the calculation is in error. No provisions have been made to account for multi-crack interaction in the calculation of the stress-intensity factors (see Section 4.2 on Short-Crack Growth Rate Data and Non-Interaction Criteria).

To calculate the stress-intensity factor at the point where the crack intersects the notch surface ($\phi = \pi/2$), the crack length (a) and the crack depth (c) must be known. For a surface crack, "2a" (or L) is the projection of the crack on a horizontal plane, as shown in Figure 16. This figure is a montage of photographs of a replica showing a crack and the initiation site. For a corner crack, "a" is equal to L. The crack depth (c) was calculated from the following equation

$$c/a = 0.9 - 0.25(a/t)^2 = 0.9 - 0.25(L/B)^2 \qquad (1)$$

for either a surface crack or corner crack. Equation (1) is in good agreement with experimental measurements and analytical calculations made on surface cracks growing from an edge notch in reference 25. Comparisons are also made later between the crack shapes predicted from Equation (1) and those obtained from the results of the cooperative test programme.

The stress-intensity factor range equation for a surface crack located at the center of the edge notch, Figure 15(a), subjected to remote uniform stress [25], is

$$\Delta K = \Delta S \sqrt{\pi a/Q}\, F_{sn} \qquad (2a)$$

for $0.2 \leq a/c \leq 2$ and $a/t < 1$. Equations for Q, the shape factor, and F_{sn}, the boundary-correction factor, are given in Annex F.

For a corner crack, the stress-intensity factor is

$$\Delta K = \Delta S \sqrt{\pi a/Q}\, F_{cn} \qquad (2b)$$

for $0.2 \leq a/c \leq 2$ and $a/t < 1$, where

$$F_{cn} = F_{sn}(1.13 - 0.09a/c) \text{ for } a/c \leq 1$$

$$F_{cn} = F_{sn}(1 + 0.04c/a) \quad \text{for } a/c > 1$$

The stress range (ΔS) is full range ($S_{max} - S_{min}$) for constant-amplitude and spectrum loading. For example, $\Delta S = 2S_{max}$ for R = -1 loading. For spectrum loading, the highest peak stress is S_{max} and the lowest trough is S_{min}.

3.5.2 Calculation of crack-growth rates

The calculation of crack-growth rate for constant-amplitude and spectrum loading is a simple point-to-point calculation as

$$\frac{da}{dN} = \frac{\Delta a}{\Delta N} = \frac{a_{i+1} - a_i}{N_{i+1} - N_i} \qquad (3)$$

where a_i is the crack length at N_i cycles. The cyclic interval, $N_{i+1} - N_i$, is the interval between replicas. The cyclic interval was chosen so that at least 25 to 30 replicas were taken during a test.

The corresponding stress-intersity factor range (ΔK) is calculated at an average crack length, a, (see Fig. 15) as

$$a = (a_i + a_{i+1})/2 \qquad (4)$$

using Equations 1 and 2.

3.6 Long Crack-Growth Rate Tests

Fatigue crack growth rate tests were conducted on long cracks (lengths greater than 2 mm) at the four constant-amplitude stress ratios [34], under the FALSTAFF load sequence [34], and under the GAUSSIAN load sequence (Annex H). The objective was to generate near-threshold fatigue crack growth rate data for the

core-programme material (2024-T3 aluminum alloy) using a load-shedding procedure. This load-shedding procedure is consistent with the guidelines of the ASTM Standard Test for Measurement of Fatigue Crack Growth Rates (E647-87). Tests were conducted on 50 mm- and 76 mm-wide center-crack tension specimens made of the 2.3 mm-thick aluminum alloy. These data were used to define the regime where long-crack data are applicable to short cracks. The results from this study are presented and discussed in Annex G and H.

4. SHORT-CRACK EXPERIMENTAL DATA

In the following, the experimental data generated in the Cooperative Test Programme on the single-edge-notch-tension specimen is presented. Data generated under various loading conditions on crack-initiation sites, short-crack growth rates, and fatigue lives to various crack sizes from the twelve participants are compared. An analysis of variation among participating laboratories on growth-rate measurements is also presented.

4.1 Initiation Sites for Short Cracks

The method used to quantify the comparison of data on initiation sites is shown in Figure 17. This figure shows a cross section of the notch root. The crack-initiation site location, denoted as t_f, is measured from the centerline of the specimen thickness. One-half sheet thickness is denoted as t. When $t_f = 0$, the crack initiated at the specimen centerline but when $t_f = t$, the crack initiated at the edge of the notch and the specimen surfaces.

The information on initiation sites was obtained from the Short-Crack Data Charts made from plastic replicas taken early in life. Each specimen produced anywhere from one to many crack-initiation sites along the notch root. The program requirements specified that the five largest cracks should be monitored from initiation to breakthrough (L = B). Several participants monitored as many cracks as possible. It was noted that high stress levels tended to produce more multi-cracking than the low stress levels. The low stress levels in the test programme were selected to be slightly higher than the fatigue limit.

First, the initiation-site information from all participants was analyzed together. The distribution of initiation sites along the bore of the notch for nearly 950 cracks (about 250 specimens) is plotted in Figure 18. The "number of cracks" that initiate in ten separate regions along the notch-root surface are plotted against t_f/t. The ten regions are each defined as ten-percent of the specimen thickness. Crack initiation, in general, occurred at inclusion-particle clusters or voids at or near the notch-root surface (see Section 6.2). More than 70 percent of the cracks initiated at t_f/t values less than 0.5 (middle half of specimen thickness). Only about 8 percent of the cracks initiated as corner cracks at the edge of the notch and specimen surfaces. Examination of the microstructure across the specimen thickness showed that the grain structure was uniform whereas the occurrence of inclusion particles was less probable toward the specimen surfaces.

The results shown in Figure 18 were typical for most participants. Test results from the participant who produced the most corner cracks (20 percent) are shown in Figure 19. The results from this participant showed only about 55 percent of the initiation sites fell within the middle half of the specimen thickness. Figure 20 shows the results from the participant who produced the most initiation sites (84 percent) within the middle half of the specimen thickness.

4.2 Short-Crack Growth Rate Data and Non-Interaction Criteria

All of the crack-growth rate data generated by the twelve participants under the six different loading conditions were analyzed using the procedures described in Section 3.5. The crack-growth rate data are presented herein as a function of the stress-intensity factor range (ΔK). For each loading condition, the short-crack growth rate data are compared with long-crack data generated under the same loading conditions on the same material.

As previously mentioned, in most of the tests many cracks initiated along the notch root of each specimen and it was appreciated that as the cracks approached each other they could mutually affect the crack-growth rate of the other. It was noted particularly that in many cases cracks slowed down and stopped propagating because they were affected by the presence of larger cracks in the vicinity. Accordingly, a simple system for rejecting crack-growth rate data, where such interaction could occur, was devised (J. Foth, Industrieanlagen Betriebsgesellschaft, West Germany) and is described in Figure 21. Three cases were considered when data are rejected:

a) Where cracks are in line with each other (such as Cracks 1 and 2) and when the distance ($d_{1,2}$) between the adjacent crack tips is less than the length of the largest crack (L_1), then subsequent data from both cracks are rejected. Here it is expected that as the crack tips approach each other the rate of growth of each would be accelerated.

b) Where cracks intersect the same line parallel to the axis of the specimen (such as Cracks 1 and 3) and when the distance between the two cracks ($h_{1,3}$) is less than the length of the largest (L_1), then subsequent data from Crack 3 is rejected. Here the larger crack (L_1) would be expected to relieve stresses in the region of the shorter crack (L_3) and, consequently, the rate of growth of Crack 3 would slow down.

c) After two cracks have joined (such as Cracks 1 and 2), crack-growth rate data are rejected from both cracks until the combined crack length (L) is twice the length of the combined cracks immediately after joining ($L_1 + L_2$), as illustrated in Figure 21(b). This is to allow for the development of a full crack front for the combined crack.

These three conditions are referred to as the "non-interaction" criteria.

The differences between analyzing all of the data and only data that satisfy the "non-interaction" criteria are illustrated in Figures 22 and 23, respectively. Figure 22 shows all of the crack-growth rate data generated from tests carried out by all participants using the standard load sequence FALSTAFF for all three stress levels. As can be seen, there was a considerable amount of scatter for a given stress-intensity factor range. Figure 23, on the other hand, shows all of the FALSTAFF crack-growth rate data that satisfy the "non-interaction" criteria. The scatter in the data was greatly reduced for the larger values of stress-intensity factor range (or larger crack sizes). For clarity, it was decided that all of the data presented in this report would satisfy the non-interaction analysis.

Figures 23 to 28 show all the data obtained by various participants in the short-crack programme using the non-interaction analysis. No attempt has been made in these diagrams to differentiate between participants or stress levels. This is done in detail in the subsequent section. On each of the figures, long-crack data obtained under the same loading action and on the same material (Annex G and H) are shown for comparison. A straight line giving the best least squares fit to the short-crack data is also shown. This line is used later in the discussion of variations in data between different laboratories.

Figures 29 to 46 show in detail the crack-growth rate data obtained by the various participants under each loading action, respectively. Each figure refers to one stress level and one particular loading action (constant-amplitude or spectrum loading). The individual participants are identified by letters, and the key to each is given in Table 1. Again, the long-crack data (solid curve) are also shown for comparison. For all stress levels and loading actions, the results from the various participants agreed well. The scatter in the data may be caused by interactions between the crack and grain boundary that are not accounted for in the analysis. For almost all of the loading actions, crack-growth rates for short cracks were found to be significantly higher than those for long cracks at the same stress-intensity factor range.

The short-crack growth rates obtained under FALSTAFF loading (Figs. 29-31) were found to be nearly an order-of-magnitude faster than those for long cracks. The crack-growth rate data for long cracks under the GAUSSIAN loading (Figs. 32-34) did not cover the same stress-intensity factor range as the short cracks but an extrapolation of the long-crack data would be expected to show significant differences in rates for the same ΔK.

Under constant-amplitude loading, the higher crack-growth rates for short cracks were most significant for tests conducted at negative stress ratios (R = -2 and -1; Figs. 35-40). The short-crack results at R = 0 test condition (Figs. 41-43) showed about the same rates as long cracks for the same ΔK for ΔK-ranges above the long-crack threshold (ΔK_{th}). The R = 0.5 tests, on the other hand, showed slower growth rates than long cracks for the same ΔK for ΔK-ranges above the long-crack threshold, see Figures 44 to 46. For constant-amplitude loading, the most significant event was the growth of short cracks below the long-crack thresholds for all stress ratios considered. Growth of short cracks was recorded at ΔK values as low as 0.6 MPa-$m^{1/2}$. These low values of ΔK for short cracks were from 15 to 30 percent of their respective long-crack thresholds.

4.3 Analysis of Variation in Growth Rate Data Among Participating Laboratories

An analysis was carried out to determine whether there were any significant variations between the data obtained by the different laboratories. In considering the results of this analysis the following should be understood:

a) After data had been rejected by the non-interaction analysis, sometimes the amount of data remaining was rather sparse.

b) There were different amounts of data obtained by different laboratories and sometimes there were no data at one or more stress levels.

These observations mean that the results from the analysis should be treated with caution. Nevertheless, it was felt that any serious discrepancies between the laboratories should be detectable.

Figures 47 to 52 show mean least-square-best-fit straight lines for each participant and loading action. These lines have been plotted over the maximum range of data and they should not be extrapolated beyond the current ranges. Results are presented for a particular laboratory only where at least two stress levels were tested. In general, the agreement among the various laboratories was very good. There was a tendency in some cases for the best-fit lines from various laboratories to cross each other. This reflects the fact that usually there was a central region where the data were concentrated and regions of rather sparse data at high and low growth rates. This tended to make the results from the various participants agree in the central region. With the rather large amount of scatter, the best-fit lines could vary considerably in slope, depending upon the position of a relatively small number of data points outside the central region. In most cases, the lines from the various laboratories were grouped closely together, with only one or two sets of data showing considerable discrepancy. However, no laboratory consistently produced extreme results and the large amount of scatter made some variations between laboratories inevitable.

4.4 Fatigue Lives to Various Crack Sizes From Participating Laboratories

In the following sections, the fatigue lives to various crack sizes from the twelve participants are compared. The information on crack sizes as a function of cycles were obtained from the Short-Crack Data Charts. Several particular crack sizes were selected for comparison. These crack sizes are schematically shown to scale in Figure 53. Usually, cracks initiated at inclusion-particle clusters along the notch root that were 2 to 7 μm wide in the L-direction (see Fig. 10 and Section 6.2). A review of the data charts revealed that most participants were recording data when the cracks were about 0.02 mm in length. This particular crack size is close to the grain diameter (0.025 mm) along the notch root. In "durability" analyses, a crack size of about 0.2 mm is sometimes selected as the initial defect size. This

particular crack size was also selected for comparison. All participants were required to terminate their tests when a crack had grown completely across the sheet thickness (L = B = 2.3 mm). This crack size is very close to the initial crack size considered in "damage-tolerant" analyses. Comparisons of fatigue lives to a crack size of 0.02 and 2.3 mm were made for each participant. The fatigue lives to various crack sizes (0.02, 0.2 and 2.3 mm) were also summarized for all participants. These fatigue lives were also compared with fatigue lives to complete failure (results from Annex B).

Figures 54 to 59 show the fatigue lives to a crack length (L) of 0.02 mm for each loading action. This crack size is of the order of a grain diameter. On each figure, fatigue lives are shown for three stress levels (S_{max}). In the FALSTAFF and GAUSSIAN tests, S_{max} is the largest stress level in the complete spectrum. The number of cycles is the fatigue life to initiate and grow a crack to 0.02 mm in length for a particular test specimen. In general, there were data from about four to six different participants for each loading action, except the GAUSSIAN results where there were only two. (Note that some data points have been displaced slightly for clarity.) The agreement among the various participants was considered reasonable in view of the fact that initiation and growth of short cracks (less than 0.02 mm) must be influenced by local microstructure.

The fatigue lives to breakthrough (L = B) for all participants are shown in Figures 60 to 65 for each loading action. This crack size is close to the "damage-tolerant" defect size. Again, results are shown for the three stress levels used in the test programme. The scatter in fatigue lives to breakthrough was only about one-half of that for fatigue lives to the grain-size defect (0.02 mm). The agreement among the various participants was generally within a factor-of-3.

A summary of the fatigue lives to various crack sizes is shown in Figures 66 to 71 for the six loading actions, respectively. Again, fatigue lives are plotted against the maximum stress level. The symbols show the logarithmic average in life to a given crack size for all participants at each stress level. Results are shown for fatigue lives to crack sizes of 0.02, 0.2 and 2.3 mm. For all crack sizes, the symbols are the average of five or more tests, except the GAUSSIAN results which are the average of only three to six tests). The solid curve on each figure shows the average fatigue lives to complete failure. Under the GAUSSIAN load sequence, only one test was taken to complete failure (see solid symbol in Fig. 67). The fatigue lives to complete failure were obtained in the preliminary test programme (Annex B). As can be seen, crack growth was actually measured over about 90 percent of the total fatigue life for most loading actions. The results at a stress ratio of 0.5 (Fig. 71), however, indicated about 80 percent of the total fatigue life was crack growth from a 0.02 mm crack. These results imply that cracks initiate very early in life for the 2024-T3 aluminum alloy.

5. MODELS OF SHORT-CRACK GROWTH BEHAVIOUR

Many investigators have shown that LEFM concepts are inadequate to explain short-crack growth behaviour [1-18]. Using nonlinear fracture mechanics, some investigators have tried to explain the growth of short cracks in plates and at notches. In particular, the J-integral concept and an empirical length parameter [3,4] have been used to correlate short-crack and long-crack growth rate data. The physical intepretation of the length parameter, however, is unclear. Several other researchers [12,17] have also introduced "length" parameters into crack-growth models. These length parameters have been associated with microstructural features (or barriers to crack growth) such as grain size. Short cracks have been observed to slow down or stop at grain-boundary locations. A microstructural barrier model [17,19] will be reviewed in the next section. Many other investigators [5-11,28] have suggested that crack closure [35] may be a major factor in causing some of the differences between the growth of short and long cracks. Reference 36 has shown, on the basis of crack closure, that a large part of the short-crack effect in an aluminum alloy could be attributed to a short crack emanating from a defect "void" of incoherent inclusion particles and a breakdown of LEFM concepts. The crack-closure model will also be reviewed in subsequent sections.

5.1 Microstructure Barrier Model

The microstructural barrier model, developed by Miller and co-workers [17,19], was conceived to separate regimes of "microstructurally short cracks" and "physically short cracks." The regime of microstructurally short cracks (MSC) occurs when crack lengths are less than d, a dominant microstructural barrier size. Various researchers consider this regime to be synonymous with growth of a crack across a single grain or several grain diameters. For example, a crack may initiate at an inclusion particle on a grain boundary, as shown in Figure 72(a), propagate, slow down, and stop at the next grain boundary. With further cycling, or if the stress level is increased, this barrier can be overcome and the crack will propagate to the next barrier. However, several different microstructural barriers to crack growth may exist in a single material because of material anisotropy and texture [37].

Crack-growth rates in the MSC regime have been expressed in the form

$$\frac{da}{dN} = A_1 (\Delta\gamma)^n (d - a) \qquad \text{for } a < d \tag{5}$$

where $\Delta\gamma$ is the shear-strain range, A_1 and n are material constants. As illustrated in Figure 72(b), equation (5) exhibits a decreasing rate as the crack length increases in the range $0 < a < d$ for a constant strain range. When the crack length is equal to d, the rate is zero, and a fatigue-limit condition exist. Figure 72(b) shows the behaviour of short cracks close to fatigue limit stress levels. At stress ranges below the fatigue limit, cracks may initiate but they stop at microstructural barriers. For crack lengths greater than d, crack-growth rates increase with crack length (typical long-crack behaviour). At stress ranges above the fatigue limit, cracks will initiate and only slow down as they propagate through microstructural barriers.

The physically short crack (PSC) regime is defined for crack lengths greater than the spacing of dominant barriers. The growth rates in the PSC regime are strongly dependent upon stress level rather than on crack length. A crack-growth rate relation for this regime is of the form

$$\frac{da}{dN} = A_2 (\Delta\gamma)^m a - A_3 \quad \text{for } a > d \tag{6}$$

where A_3 represents a threshold condition, A_2 and m are material constants.

Miller [19] suggests that the complexities near microstructural barriers in the MSC and PSC regimes hinder theoretical analyses of short-crack growth behaviour based on LEFM parameters and he emphasizes the development of empirical equations, based on extensive experimental data, to determine the constants in equations (5) and (6).

Clearly, as the crack size approaches zero, a crack size must be reached below which the assumptions of the ΔK concept are violated. But for many engineering applications, a ΔK-based analysis that extends into the regime of questionable validity may still be very useful. Certainly from a structural designer's viewpoint, a single analysis methodology that is applicable to all crack sizes is very desirable. Therefore, the application of ΔK analyses to short-crack problems should be thoroughly explored.

5.2 Analytical Crack-Closure Model

A crack-closure model developed in reference 27, and applied to short cracks in references 28 and 36, is used herein to analyze crack growth and closure under constant-amplitude loading and under the two variable-amplitude load spectra. The following section includes a brief description of the closure model and of the assumptions made in the application of the model to the growth of short and long cracks.

The closure model [27] was developed for a central crack in a finite-width specimen subjected to uniform applied stress. This model was later extended to through cracks emanating from a circular hole in a finite-width specimen also subjected to uniform applied stress [28]. The model was based on the Dugdale model [38], but modified to leave plastically deformed material in the wake of the crack. The primary advantage in using this model is that the plastic-zone size and crack-surface displacements are obtained by superposition of two elastic problems--a crack in a plate subjected to a remote uniform stress and a crack in a plate subjected to a uniform stress applied over a segment of the crack surface.

Figure 73 shows a schematic of the model at maximum and minimum applied stress. The model is composed of three regions: (1) a linear-elastic region containing a circular hole with a fictitious crack of half-length $c'+\rho$, (2) a plastic region of length ρ, and (3) a residual plastic deformation region along the crack surface. The physical crack is of length $c'-r$, where r is the radius of the hole. (The model was also assumed herein to apply for a crack emanating from a semi-circular notch.) The compressive plastic zone is ω. Region 1 is treated as an elastic continuum. Regions 2 and 3 are composed of rigid-perfectly plastic (constant stress) bar elements with a flow stress, σ_0. The flow stress (σ_0) is the average between the yield stress and the ultimate strength. The shaded regions in Figures 73(a) and 73(b) indicate material that is in a plastic state. At any applied stress level, the bar elements are either intact (in the plastic zone) or broken (residual plastic deformation). The broken elements carry compressive loads only, and then only if they are in contact. The elements yield in compression when the contact stress reaches $-\sigma_0$. To account for the effects of state of stress on plastic-zone size, a constraint factor α was used to elevate the tensile flow stress for the intact elements in the plastic zone. The effective flow stress $\alpha\sigma_0$ under simulated plane-stress conditions was $1.1\sigma_0$ and under simulated plane-strain conditions was $1.73\sigma_0$ (Irwin's plane-strain constraint [39]). The plane-strain constraint factor of 1.73 was found to correlate crack-growth rate data for various stress ratios in the near threshold region and to give crack-opening stresses in agreement with experimental measurements [34].

The closure model was used to calculate crack-opening stress as a function of crack length and load history. The applied stress level at which the crack surfaces are fully open is denoted as S_0, the crack-opening stress. The crack-opening stress calculated for a through crack was also assumed to apply at each location along a surface- or corner-crack front. The crack-opening stress was used to calculate the effective stress-intensity factor range, ΔK_{eff}. In turn, the crack-growth rate was calculated using a ΔK_{eff}-against-crack-growth-rate relationship determined from the long-crack data (see Section 6.1).

In the following sections, the effect of an initial defect "void" size on the crack-closure behaviour of short cracks under constant-amplitude and spectrum loading is presented. For all loading conditions, plane-strain conditions were assumed to apply for the growth of "short" cracks. These results are used later to predict the growth rates for short cracks and the fatigue life to breakthrough.

5.2.1 Constant-Amplitude Loading

The closure model was used to study the influence of defect void size on the closure behaviour of short cracks growing from a notch, as shown in Figure 15(a). Some typical results of calculated crack-opening stresses normalized by the maximum applied stress as a function of half-crack length, a, are shown in Figure 74. The crack-growth simulation was performed under R = -1 loading ($S_{max}/\sigma_0 = 0.15$) with an initial defect (void or crack) size a_i of 3 μm, c_i of 12 μm, and for various values of h. The configuration of the assumed initial defect is shown in the insert and the initial dimensions were determined from analyses conducted in Annex B. Results shown in the figure demonstrate that the defect height had a large influence on the closure behaviour of short cracks. For h greater than about 0.4 μm, the initial defect surfaces did not close, even under compressive loading. The newly created crack surfaces, however, did close and the crack-opening stresses are shown by the lower solid curve. The crack-opening stress was initially the minimum applied stress, but rapidly rose and tended to level off as the crack grew. For $h = 0$, however, the defect surfaces make contact under the compressive loading and the contacting surfaces greatly influenced the amount of residual plastic deformation left behind as the crack grew. The

calculated crack-opening stresses stabilized very quickly at the steady-state value, as shown by the upper solid curve. These results suggest that part of the short-crack effect may be due to an initial defect height that is sufficient to prevent closure over the initial defect surfaces.

The predicted crack-growth rates for h > 0.4 μm showed a "minimum" at a half-crack length of about 20 μm (solid symbol in Fig. 74). This minimum in crack-growth rate behaviour for short cracks is illustrated in Figures 1 and 72(b). Several researchers [12,17,18] have observed and attributed this behaviour to crack-grain boundary interaction. Incidentally, the average grain size in the a-direction is about 25 μm for the 2024-T3 aluminum alloy. The minimum in the analysis, however, is caused by a decrease in the effective stress range (ΔS_{eff}) with an increase in crack length, such that the ΔK_{eff} reaches a minimum. Thus, a minimum in growth rates for short cracks may be caused by two different phenomena. One is the crack-grain boundary interaction and the other is a transient behavior of crack-opening stresses. Comparisons of predicted rates from the closure model with experimental data are made in Section 6.4.

Figure 75 shows the calculated crack-opening stresses for short cracks under the four constant-amplitude loading conditions used in the test programme. The particular values of S_{max}/σ_o used are as shown. The initial defect size (a_i,c_i) was the same as shown previously and the defect height was 0.4 μm. The high R-ratio (R = 0.5) results show that the crack is always fully open, that is, $S_o = S_{min}$. Results at R = 0 stabilized very quickly after about 20 μm of crack growth. Negative R-ratio results showed the largest transient behaviour on crack-opening stresses. Results at R = -2 had not stabilized after about 100 μm of crack growth. The results at the negative stress ratios are also strongly influenced by the maximum applied stress level [27,36].

5.2.2 FALSTAFF and GAUSSIAN Load Sequence

The closure model was also used to calculate the crack-opening stresses under the two variable-amplitude load spectra. Again, the initial defect void size (a_i,c_i,h) was the same as used for constant-amplitude loading. Figures 76 and 77 show crack-opening stresses plotted against crack depth (c) for the FALSTAFF and GAUSSIAN load sequence, respectively. Only a small part of the opening values calculated from the model is shown in the figures. The dashed lines indicate the peak stress (S_{max}) and the lowest stress (S_{min}) in the stress spectrum. The initial crack was a small surface crack located at the center of the notch. The crack propagated as a surface crack until breakthrough (a = t) and then became a through crack of length, c. The value of c at breakthrough was about 0.8 mm, as indicated, and the c/a ratio was about 0.7, see Figure 15(a) and Section 6.3.

For the FALSTAFF sequence (Fig. 76), the opening stresses started at negative values, rapidly rose, and became positive at about 25 μm of crack growth. Twenty-four applications of the FALSTAFF sequence were required to grow the crack to this length. To grow the crack to breakthrough required 16 additional FALSTAFF sequences. The opening stresses tended to steadily rise as the crack grew. This rise was primarily due to changes in the "constraint" factor (see Section 6.1). For crack lengths less than about 0.2 mm, plane-strain constraint conditions were present. For crack lengths greater than about 0.8 mm, plane-stress constraint conditions were present. Comparisons of predicted and experimental fatigue lives to breakthrough and complete rupture are presented in Section 6.5 and Annex B, respectively.

For the GAUSSIAN sequence (Fig. 77), the opening stresses showed a similar trend to that observed for the FALSTAFF sequence. Because of the compressive loading, however, the opening stresses remained negative for a longer period of crack growth than that shown in Figure 76. Only about one application of the GAUSSIAN sequence (10^6 cycles) was required to grow the crack from the initial crack size to a 2-mm through crack.

6. RESULTS AND DISCUSSION

In the following sections, the experimental data generated in the AGARD Cooperative Test Programme on initiation sites, crack shapes, short-crack growth rates, and fatigue lives to breakthrough under constant-amplitude and spectrum loading are summarized and compared with predictions made using a ΔK-based analysis and the analytical crack-closure model. The experimental data and the results from the closure model are used to make an assessment of the significance of the short-crack effect for the 2024-T3 aluminum alloy material.

6.1 Long-Crack Growth Rates and Correlation

To apply the closure model, an effective stress-intensity factor against crack-growth rate relation must be obtained. The crack-growth rates measured on long cracks in the core-programme material were correlated against ΔK_{eff} using the closure model for a wide range in constant-amplitude stress ratios. The following section describes how the ΔK_{eff}-rate relationship was obtained from the long-crack data.

Center-crack tension specimens were used to obtain crack-growth rate data on long cracks (c > 2 mm) in the 2024-T3 aluminum alloy sheet material used in this study. The data are shown in Figure 78. The symbols above a rate of 10^{-5} mm/cycle show ΔK_{eff}-rate data obtained from Hudson [32] at various R ratios ($-1 < R < 0.7$) using a crack-opening stress equation in Reference 40. Symbols below a rate of 10^{-5} mm/cycle show the results of load-reduction threshold tests conducted by E. P. Phillips (NASA Langley Research Center), as part of the cooperative test programme [34]. These results are discussed in Annex G. The effective stress-intensity factor [35] is given by

$$\Delta K_{eff} = \frac{S_{max} - S_o}{S_{max} - S_{min}} \Delta K \qquad (7)$$

where S_o was calculated from equations given in Reference 40. For these calculations, a constraint factor (α) of 1.1 was used for rates greater than 7.5E-04 mm/cycle (end of transition from flat-to-slant crack growth) and α = 1.73 (equivalent to Irwin's plane-strain condition) was used for rates lower than 9.0E-05 mm/cycle (beginning of transition from flat-to-slant crack growth). The constraint factor of 1.73 was also selected so that the calculated crack-opening stress levels would quantitatively agree with experimental measurements of crack-opening stress made near the beginning of the load-reduction threshold test [34]. For intermediate rates, α was varied linearly with the logarithm of crack-growth rate.

Instead of using an equation to relate crack-growth rate to ΔK_{eff}, a table-lookup procedure was chosen for this study. The primary advantage in using a table is that the baseline data can be described more accurately than with a multi-parameter equation, especially in the transitional regions (flat-to-slant crack growth and near threshold). The solid-line segments in Figure 78 were generated using a visual fit to the data and the end points of these segments are listed in the following table:

ΔK_{eff} MPa-$m^{1/2}$	$\frac{dc}{dN}$ mm/cycle
1.43	3.56E-07
2.42	3.05E-06
3.30	6.10E-06
4.40	1.52E-05
5.50	4.06E-05
11.0	4.32E-04
49.5	2.54E-01

In the low-growth rate regime near and at threshold, some tests [41] have indicated that the threshold develops because of a rise in crack-opening stress. This rise has not been accounted for in the analysis of the threshold test data shown in Figure 78. An extrapolation of the long-crack data (solid line) into the region below the long-crack threshold (dashed line) was used because the data did not extend to the low ΔK_{eff} values where short cracks were expected to grow. The crack-growth model required a baseline ΔK_{eff}-rate relation in the low ΔK_{eff} region in order to predict the growth of short cracks. For ΔK_{eff} values below or above the extreme values listed in the table, a power law using the first-two or last-two points, respectively, was used to obtain rates. The upper limit for the power-law relation is, of course, defined by fracture toughness. A lower limit or short-crack threshold, $(\Delta K_{eff})_{th}$, was established in Annex B and was 1.05 MPa-$m^{1/2}$.

A schematic of the assumed constraint variation and plastic-zone envelope along the crack plane is shown in Figure 79. For long crack lengths from the notch, plane-stress conditions (α = 1.1) were assumed when the crack-growth rate was higher than the rate at transition from flat-to-slant crack growth because the plastic-zone size would be of the order of the sheet thickness. For small crack lengths, and a flat crack front, plane-strain conditions (α = 1.73) were assumed because the plastic-zone size would be small compared to sheet thickness. These conditions are expected to be adequate for low applied stress levels ($S_{max} < \sigma_o/K_T$). However, for high applied stress levels that cause the notch root to yield, the constraint at the notch root is expected to be under plane-stress conditions because of the small B/w ratio, even though the growth rates for short cracks may be less than the rate at transition. In the current study, however, the constraint factor was assumed to be controlled solely by the crack-growth rate. For low growth rates and under applied tensile loading, the notch root is assumed to yield when the local stress is $1.73\sigma_o$, but under applied compressive loading, the root is assumed to yield when the local stress is $-\sigma_o$. The first assumption may cause difficulty when S_{max} is greater than σ_o/K_T.

6.2 Initiation Sites for Short Cracks

Typical initiation sites at the edge of the semi-circular notch are shown in Figure 80. The specimens were tilted at 45 degrees from the load axis so that both the fatigue surface and notch surface are visible. Pits on the notch surface show where inclusion particles were removed from a large cluster by the machining and polishing process. Crack initiation, in general, occurred at inclusion particle clusters. These cracks appear to have initiated from defects caused by the separation of the alloy matrix material from an inclusion cluster. In Figure 80(a), the size of the inclusion cluster (or initiation site) is about 7 μm wide (2a-direction) and 14 μm in depth (c-direction). Figure 80(b) shows what appears to be a crevice with inclusion particles at the base as the initiation site. Thus, the initial defect may be considered a "void." Here the initial defect void size is 4 μm wide, 18 μm deep, and several microns in height (h). Inclusion particle sizes at initiation sites ranged from 2 to 7 μm in the 2a-direction (see Figs. 5 and 80). The initiation sites were, generally, within the middle one-half of the specimen thickness and the cracks tended to grow as semi-elliptical surface cracks (see Section 4.1). Examination of the microstructure across the specimen thickness showed that the grain structure was uniform, whereas the occurrence of inclusion clusters was less probable toward the specimen surfaces. Other evidence to support initiation in the middle of the notch root is stress concentration. The stress-concentration factor at the notch is slightly higher (about 5 percent) in the middle of the specimen than on the edge of the notch [42]. Therefore, for short cracks observed in the cooperative test programme, modeling the crack as a defect growing along the specimen centerline is a reasonable assumption. Multi-crack initiation and crack interaction are not considered in the present analysis.

6.3 Crack Shapes and Predictions

To calculate the stress-intensity factor range for a surface crack, the crack dimensions a and c must be known. The replica method was used to monitor crack length in the a-direction as a function of cycles. To gain information about the growth of the crack in the depth direction, c, some specimens were statically pulled to failure early in life (see Table 7) when the crack length was a specified size. A photomicrograph of a specimen is shown in Figure 81. The initiation site at the notch edge is indicated by an arrow. The boundary between the dark region of primarily faceted fracture displaying river markings and the surrounding lighter region of dimple rupture indicates the surface-crack shape. In Figure 81, the surface crack was nearly semi-circular (c/a was about unity). Figure 82 shows the variation of c/a with crack size (a/t) for naturally initiated cracks from the cooperative test programme. Some additional data on the core-programme material for naturally initiated cracks and for cracks initiated from a small machined notch [25] are also shown. Very early in life, the cracks tended to be nearly semi-circular (c/a = 1). But the cracks tended to grow more along the bore of the notch than away from the notch (c/a < 1). At breakthrough (a/t = 1), the c/a ratio was estimated to be about 0.7. Because corner cracks (Fig. 15(b)) occurred very infrequently (see Section 4.1), they were not considered in the present analysis.

The solid curve in Figure 82 is the predicted crack shape using Equation 2(a), evaluated at $\phi = \pi/2$ (point where crack intersects notch surface) and $\phi = 0$ (maximum depth point), and the baseline crack-growth rate relationship obtained for long cracks. The initial crack size for the analysis was $a_i = 3$ μm and $c_i = 12$ μm (see Annex B). This initial crack shape and size is about the same shape and size of the inclusion-particle clusters shown in Figure 80. The prediction agreed reasonably well with the experimental data.

The dashed curve in Figure 82 shows the equation used to calculate crack depth from crack length measurements made in the cooperative test programme. For a/t ratios greater than about 0.05, the equation and the crack-growth analysis agreed quite well. For half-crack lengths less than about 20 μm, there were some large differences between the stress-intensity factors calculated for the different theoretical crack shapes (solid and dashed curves). Figure 83 compares crack shapes predicted from the analysis and calculated by Equation (1) for the same surface-crack lengths. The solid and dashed semi-elliptical shapes were from analyses and Equation (1), respectively. Figure 83(a) shows the assumed initial defect size and the shape calculated from the equation. Here the stress-intensity factor ratio (analysis to equation), at the point where the crack intersects the notch surface, was 1.55. However, the crack shape changes very rapidly and approaches a semi-circular crack, as shown in Figure 83(c). Here the half-crack length, a, was only 15 μm and the stress-intensity factor ratio (analysis to equation) was 1.07. Because the "actual" crack shapes were difficult to determine for crack lengths less than about 15 μm, Equation (1) was used to calculate crack shapes.

6.4 Short-Crack Growth Rates and Predictions

In the following, comparisons are made between measured and predicted crack-growth rates against stress-intensity factor range (ΔK) for short cracks under the cooperative programme loading conditions. Because a large amount of experimental data exist at each loading condition, only typical data from at least two participants are shown for each loading condition. (The predicted curves could not be seen if all of the data were shown.) Only the experimental data analyzed with the non-interaction criteria were used. Results for the long-crack data (see Annex G and H) are also shown for comparison. To compare the short- and long-crack growth rate data, the rate da/dN is assumed to be equivalent to dc/dN for the same ΔK value. The short cracks are growing in the a-direction while the long cracks are growing in the c-direction. This assumption also applies in predicting short-crack growth behaviour from long-crack results.

Figures 84 to 89 show comparisons for R = -2, -1, 0, 0.5, FALSTAFF, and GAUSSIAN loading, respectively. Experimental data for each stress level are denoted by a particular symbol. The solid curves show predictions from the closure model for various maximum applied stress levels. The dashed lines show long-crack data (Table G1) for all loading conditions.

Results for R = -2, Figure 84, show a strong influence of stress level (S_{max}) on the growth rates for short cracks. The short cracks grow faster at higher stress levels for the same value of ΔK. To make predictions, the initial crack size was again 3 by 12 by 0.4 μm, and an effective stress-intensity factor threshold, $(\Delta K_{eff})_{th}$, was chosen as 1.05 MPa-$m^{1/2}$. The reason for selecting this effective threshold is discussed in Annex B. The predictions from the model show a similar stress-level effect on the growth of short cracks. Although the initial crack-growth rates from the model were in qualitative agreement with the measured rates, the model predicted slower rates in the mid-range than those measured. The predicted rates approached the long-crack rates faster than in the test. As previously mentioned, plane-strain conditions ($\alpha = 1.73$) were assumed for the growth of short cracks. The actual behaviour, however, may be closer to plane stress. Strain-gauged specimens (discussed in Annex B) indicated that the notch root yielded when the normal stress (σ_{yy}) was slightly lower than the uniaxial yield stress (at about the proportional limit) of the material. Obviously, further study is needed to understand the state-of-stress behaviour of short cracks.

At 50 MPa, the predictions show that the crack nearly arrested. The minimum rate occurred at a ΔK_{eff} of 1.08 MPa-$m^{1/2}$. Another prediction was made at an applied stress level of 49 MPa. The prediction demonstrates that a short crack can initiate and grow from a defect, but as the crack-opening stresses rise (decreasing the value of ΔK_{eff}), the crack can be arrested. Here the crack was arrested at a ΔK value of about 3 MPa-$m^{1/2}$. A short-crack threshold based on ΔK would, of course, be a function of initial defect size and stress level.

The results for R = -1 loading are shown in Figure 85. A large stress-level effect was also shown for both tests and analyses. Here the predicted rates were in better agreement with the measured rates in the mid-range than those shown for R = -2. Both measured and predicted rates approached the long-crack

rates for ΔK values greater than about 10 MPa-$m^{1/2}$. For all of these conditions, the local notch-root stresses were elastic (see Table 6).

The R = 0 results, shown in Figure 86, indicated a small influence of stress level on both the measured and predicted rates. The initial rates from the model were in good agreement with measured rates. In contrast to previous behaviour, the measured rates in the mid-range were slightly slower than those predicted from the model and those measured from long-crack tests.

No stress-level effect was observed for the R = 0.5 results (Fig. 87), even though the local notch-root stresses were above the yield stress of the material. These results did show, however, that short cracks grew at substantially slower rates than those measured for long cracks at ΔK values greater than the long-crack threshold. This effect is believed to be caused by notch-root yielding under plane-stress conditions. Because the model assumes plane-strain conditions for short cracks, the notch root does not yield in the analysis (see discussion in last paragraph of Section 6.1).

The measured and predicted short-crack growth rates for FALSTAFF and GAUSSIAN loading are shown in Figures 88 and 89, respectively. Here the "average" crack-growth rate is plotted against the "maximum range" stress-intensity factor (see Section 3.5.1 and 3.5.2). The predicted crack length against cycles curve was treated identically to the experimental data. Thirty values of crack length (2a) and cycles were taken from the analysis at equal cyclic intervals between the initial crack length (6 μm) to breakthrough (2a = t or L = B). The predicted results for FALSTAFF showed a small stress-level effect and, generally, agreed with the trends in measured rates. The analyses tended to overpredict the rates for ΔK values greater than about 8 MPa-$m^{1/2}$. However, the measured and predicted rates were substantially higher than those measured for long cracks at the same ΔK. The results for the GAUSSIAN loading are shown in Figure 89. Measured and predicted rates generally covered the same range in rates for a given ΔK. The analyses, however, tended to overpredict rates for low values of ΔK and underpredict rates for high values. These trends will be further discussed in the next section.

6.5 Fatigue Life to Breakthrough and Predictions

All specimens used to obtain short-crack growth rate data were terminated when a continuous crack was all the way across the notch root; that is, the breakthrough condition. Under this condition, a surface crack or corner crack became a through crack (L = B). These data were used to verify life-prediction methodology using the closure model.

To predict fatigue life to breakthrough, an initial defect size and a ΔK_{eff}-rate relationship is needed. The initial surface-crack "void" size was the same as used in Annex B (3 by 12 by 0.4 μm) and was assumed to be located at the center of the notch. Long-crack data (Annex G) were used in Section 6.1 to obtain a ΔK_{eff}-rate relation but neglecting the long-crack thresholds. However, an effective threshold, $(\Delta K_{eff})_{th}$, was obtained from fatigue-limit data under fully-reversed loading (see Annex B).

Fatigue lives to breakthrough from all participants are shown in Figures 90 to 93 for constant-amplitude loading at negative and positive R-ratios, respectively. A symbol indicates a breakthrough and a symbol with an arrow indicates that a test was terminated without a crack. The solid curves show the predicted number of cycles to breakthrough. Because the closure model predicted considerably slower rates than those measured from short-crack tests at R = -2, the predicted lives to breakthrough were about 3 times longer than the average test lives, as shown in Figure 90. Similarly, the predicted lives at R = -1 were slightly greater than the test lives (Fig. 91). In contrast, the predicted lives for the positive R-ratio tests (Figs 92 and 93) were less than the test lives. The predictions for R = 0 were only slightly less than the average of the test data. But the predicted results for R = 0.5 were about a factor-of-2 less than the experimental results.

The fatigue lives to breakthrough for the FALSTAFF and GAUSSIAN loading conditions are shown in Figures 94 and 95, respectively. The closure model was used to predict crack growth and fatigue life to breakthrough from the same initial defect size as previously discussed. The predicted lives for the FALSTAFF loading were somewhat shorter than the test lives. Because the FALSTAFF spectrum is a high R-ratio type loading, the predicted results are similar to those shown for the high R-ratio constant-amplitude loading (Fig. 93). Predicted results for the GAUSSIAN loading, on the other hand, were in good agreement with the test data.

The comparisons shown in Figures 90 to 95 show a systematic trend in predicted and measured fatigue lives to breakthrough. The model generally overpredicted lives for negative R-ratios and slightly underpredicted lives for high positive R-ratios. This behaviour is suspected to be caused by the assumed state-of-stress or a breakdown in using the ΔK-concept. As previously mentioned, plane-strain conditions were assumed to exist for "short" cracks. The model did not account for the tensile yielding that occurred at the high R-ratio (R = 0.5) loading. (See Table 6.) From the results of strain-gauged tests (Annex B), the state-of-stress for "short" cracks is probably under plane-stress conditions. But as the crack grows away from the notch, plane-strain conditions may prevail. For long cracks, the state-of-stress may again become plane stress. Thus, the state-of-stress history from a "short" crack to a long crack is very complicated. Further study is needed to assess the variation in the state-of-stress and how to use this information in making life predictions. Also, the use of a non-linear fracture mechanics parameter, such as ΔJ or a plasticity-corrected ΔK, may improve the model predictions.

6.6 Significance of Short-Crack Effects

Because the use of fracture mechanics (ΔK-based) methodologies to characterize the growth of fatigue cracks in metals is well established in the design of aerospace structures, the significance of the short-crack effects are expressed herein in the same terminology. The experimental data generated in the AGARD Cooperative Test Programme and the analytical crack-closure model have identified several significant features of short-crack growth behaviour in 2024-T3 aluminum alloy sheet material. These features are briefly discussed in the following sections.

At stress concentrations, typical for aircraft structures, short cracks initiate early in the fatigue life, if the applied stress levels are above the fatigue limit. This means that as non-destructive inspection (NDI) techniques improve, which is inevitable, smaller crack sizes will be detected in aircraft structures. In particular, Wanhill [43] points out that as the design philosophy changes from a fail-safe approach to a damage-tolerant or durability evaluation, a better understanding of the behaviour of short cracks is required, especially in aircraft engines. The growth of these short cracks is strongly influenced by loading action and stress level. The growth differences between short and long cracks, at the same stress-intensity factor range, were more pronounced for loading actions which included compressive loading, whereas, short-crack growth behaviour in tests with only positive loading was nearly the same as for long cracks. But why do short cracks grow faster than long cracks? The answer to this question lies in several reasons: (1) the loss of similitude [16] which occurs when stress levels are too high and small-scale yielding conditions are exceeded, (2) local microstructural features are favorably oriented for rapid crack growth [6,12], and (3) the lack of crack closure in the early stages of crack growth [5-11,28]. Perhaps the most significant feature of short-crack growth behavior, observed in the test programme, was the growth of short cracks well below the long-crack thresholds. This observation should have the largest impact on design-life calculations. Long-crack data that includes a threshold clearly cannot be used in analyses that treat the early stages of crack growth because this leads to prediction of infinite life for crack sizes as much as an order-of-magnitude larger than the crack sizes actually monitored in the test programme [44]. Thus the use of long-crack thresholds in damage-tolerant and durability analyses should be thoroughly investigated.

In the future, the short-crack effect may have a large impact on design-life calculations if procedures are adopted that treat the fatigue process as entirely crack growth and the design requirements include one for total fatigue life [44]. Basing all life calculations on crack-growth analyses seems reasonable in view of test results in this study and others [45,46] in which crack growth was actually monitored over more than 90 percent of the total fatigue life. A crack-growth-based safe-life approach to design may be a viable alternative to traditional "crack initiation" safe-life analyses currently used for such structures as landing gear, helicopter rotor systems, and turbine engines. One advantage of a crack-growth-based procedure is that the measure of damage -- crack size -- is a physically measurable quantity that can be used to gain a better understanding and evaluation of life-prediction analyses. Another advantage would be the use of a single analysis procedure for all life calculations rather than one procedure for initiation and another for crack growth. Disadvantages of the crack-growth-based procedure are that generation of short-crack data is more difficult than classical fatigue testing and more complex stress analyses would be required. However, with continually improving computerized stress analyses and encouraging results from models used to predict short-crack effects, a continued exploration of crack-growth-based life design is warranted.

7. CONCLUSIONS

For short-crack tests and analyses conducted on single-edge-notched tension fatigue specimens made of 2024-T3 aluminum alloy sheet material:

Cooperative Test Programme

1. For nearly 950 crack-initiation sites, over 70 percent of the cracks initiated at inclusion-particle clusters or voids along the notch root in the middle half of the sheet thickness.

2. Short-crack growth rate data from the various participants agreed well for both constant-amplitude and spectrum load conditions. All results from participants show about the same amount of scatter in growth rate data.

3. Fatigue lives to breakthrough (crack length equals sheet thickness) from the various participants agreed well for all loading conditions.

Experimental Results

1. For all constant-amplitude loading (R = -2, -1, 0 and 0.5), short cracks grew at stress-intensity factors well below the long-crack thresholds.

2. For constant-amplitude loading at negative stress ratios (R = -2 and -1), short-crack growth rates were faster than long-crack rates at the same stress-intensity factor range. Short cracks also grew faster at higher stress levels for the same stress-intensity factor range.

3. For constant-amplitude loading at positive stress ratios (R = 0 and 0.5), short-crack growth rates were equal to or slower than long-crack rates at the same stress-intensity factor range above the long-crack threshold. No stress level effect was observed at positive stress ratios.

4. For FALSTAFF and GAUSSIAN loading, short cracks grew faster than long cracks at the same stress-intensity factor range.

5. High stress levels tended to produce more multi-cracks along the notch root than the low stress levels near the fatigue limit.

6. For all loading conditions, 80 to 90 percent of the total fatigue life was spent as crack growth from a total crack length of 20 μm along the notch root (inclusion-particle cluster sizes or initiation sites ranged from 2 to 7 μm in length).

Analytical Results

1. For most constant-amplitude loading (R = -2, -1 and 0), the "analytical crack-closure" model predicted growth rates and stress-level effects like those observed in tests. For R = 0.5, the model generally predicted higher rates than those observed in tests.

2. For FALSTAFF and GAUSSIAN loading, the "analytical crack-closure" model predicted growth rates like those observed in tests.

3. The "analytical crack-closure" model generally overpredicted the fatigue lives to breakthrough for negative stress ratios and slightly underpredicted fatigue lives for positive stress ratios. The model predicted fatigue lives for the FALSTAFF and GAUSSIAN load sequences quite well.

8. NOMENCLATURE

A_1, A_2, A_3	material constants
a	one-half surface-crack (or total corner-crack) length, m
a_i	initial one-half surface-defect (or crack) length, m
B	specimen thickness, m
c	surface-crack depth or through-crack length, m
c'	initial surface-defect (or crack) depth, m
c_i	crack length plus hole radius, m
d	dominant microstructural barrier size, m
$d_{i,j}$	horizontal distance between adjacent crack tips, m
F	boundary-correction stress-intensity factors
h	one-half surface-defect (or crack) height, m
$h_{i,j}$	vertical distance between crack planes, m
I	irregularity factor for Gaussian sequence
K	stress-intensity factor, MPa-$m^{1/2}$
K_T	stress-concentration factor
L	total length of surface or corner crack, m
m	crack-growth exponent in physical short-crack regime
N	cycles
n	crack-growth exponent in microstructural short-crack regime
Q	shape factor for surface or corner crack
R	stress ratio (S_{min}/S_{max})
r	semi-circular notch radius, m
S	applied gross stress, MPa
S_{max}	maximum applied gross stress, MPa
S_{min}	minimum applied gross stress, MPa
S_o	crack-opening stress, MPa
t	one-half specimen thickness, m
w	specimen width, m
x,y	Cartesian coordinates
α	constraint factor
ΔK	stress-intensity factor range, MPa-$m^{1/2}$
ΔK_{eff}	effective stress-intensity factor range, MPa-$m^{1/2}$
$(\Delta K_{eff})_{th}$	effective threshold stress-intensity factor range, MPa-$m^{1/2}$
ΔK_{th}	threshold stress-intensity factor range, MPa-$m^{1/2}$
$\Delta\gamma$	shear-strain range
ρ	length of tensile plastic zone, m
σ_o	flow stress (average between σ_{ys} and σ_u), MPa
σ_u	ultimate tensile strength, MPa
σ_{ys}	yield stress (0.2 percent offset), MPa
σ_{yy}	normal stress acting in y-direction, MPa
ϕ	parametric angle of ellipse
ω	length of cyclic plastic zone, m

9. REFERENCES

1. Pearson, S.: Initiation of Fatigue Cracks in Commercial Aluminum Alloys and the Subsequent Propagation of Very Short Cracks, Engineering Fracture Mechanics, Vol. 7, No. 2, 1975, pp. 235-247.

2. Kitagawa, H.; and Takahashi,S.: Applicability of Fracture Mechanics to Very Small Cracks or the Cracks in the Early Stage, Proceedings of the 2nd International Conference on Mechanical Behavior of Materials, Boston, MA, 1976, pp. 627-631.

3. El Haddad, M. H.: A Study of the Growth of Short Fatigue Cracks Based on Fracture Mechanics, Ph.D. Thesis, University of Waterloo, Waterloo, Ontario, Canada, 1978.

4. El Haddad, M. H.; Dowling, N. E.; Topper, T. H.; and Smith, K. N.: J Integral Application for Short Fatigue Cracks at Notches, International Journal of Fracture, Vol. 16, No. 1, 1980, pp. 15-30.

5. Broek, D.: The Propagation of Fatigue Cracks Emanating from Holes, National Aerospace Laboratory NLR Technical Report 72134U, 1972.

6. Morris, W. L.; James, M. R.; and Buck, O.: Growth Rate Models for Short Surface Cracks in Al 2219-T851, Metallurgical Transactions A, Vol. 12A, January 1981, pp. 57-64.

7. Hudak, S. J., Jr.: Small Crack Behavior and the Prediction of Fatigue Life, Journal of Engineering Materials and Technology, Vol. 103, 1981, pp. 26-35.

8. Nisitani, H.; and Takao,K. I.: Significance of Initiation, Propagation, and Closure of Microcracks in High Cycle Fatigue of Ductile Materials, Engineering Fracture Mechanics, Vol. 15, No. 3-4, 1981, pp. 445-456.

9. Schijve, J.: Difference Between the Growth of Small and Large Fatigue Cracks--The Relation to Threshold K-Values, Fatigue Thresholds, Vol. II, 1982, pp. 881-908. (Also: Delft University of Technology Report LR-327, 1981.)

10. Taylor, D.; and Knott, J. F.: Fatigue Crack Propagation Behavior of Short Cracks--The Effects of Microstructure, Fatigue of Engineering Materials and Structures, Vol. 4, No. 2 1981, pp. 147-155.

11. Leis, B. N.; and Forte, T. P.: Fatigue Growth of Initially Physically Short Cracks in Notched Aluminum and Steel Plates. Fracture Mechanics: Thirteenth Conference, Richard Roberts, ed., American Society for Testing and Materials, ASTM STP 743, 1981, pp. 100-124.

12. Lankford, J.: The Growth of Small Fatigue Cracks in 7075-T6 Aluminum, Fatigue of Engineering Materials and Structures, Vol. 5, No. 3, 1982, pp. 233-248.

13. Wood, H. A. and Rudd, J. L.: Evaluation of Small Cracks in Airframe Structures, AGARD Report No. 696, 1983, pp. 1.1-1.12.

14. Anstee, R. F. W. and Edwards, P. R.: A Review of Crack Growth Threshold and Crack Propagation Rates at Short Crack Lengths, AGARD Report No. 696, 1983, pp. 2.1-2.12.

15. Behavior of Short Cracks in Airframe Components, AGARD Conference Proceedings, AGARD-CP-328, 1983.

16. Leis, B. N.; Kanninen, M. F.; Hopper, A. T.; Ahmad, J.; and Broek, D.: A Critical Review of the Short Crack Problem in Fatigue, AFWAL-TR-83-4019, 1983.

17. Miller, K. J. and de los Rios, E. R. (eds.): The Behaviour of Short Fatigue Cracks, European Group on Fracture, Publication No. 1, 1986.

18. Ritchie, R. O. and Lankford, J.: Small Fatigue Cracks, The Metallurgical Society, 1986.

19. Miller, K. J.: The Behaviour of Short Fatigue Cracks and Their Initiation, Part I - A Review of Two Recent Books and Part II - A General Summary, Fatigue and Fracture of Engineering Materials and Structures, Vol. 10, No. 1 and 2, 1987.

20. Description of a Fighter Aircraft Loading Standard for Fatigue Evaluation, FALSTAFF, F+W (Switzerland), LBF (Germany), NLR (Netherlands), and IABG (Germany), March 1976.

21. van Dijk, G. M. and de Jonge, J. B.: Introduction to a Fighter Aircraft Loading Standard for Fatigue Evaluation FALSTAFF, NLR MP 75017U, May 1975.

22. Hück, M.; Schütz, W.; Fischer, R.; and Köbler, H. G.: A Standard Random Load Sequence of Gaussian Type Recommended for General Application in Fatigue Testing, LBF Report No. 2909, IABG Report No. TF-570, April 1976.

23. Gangloff, R. P.: Electrical Potential Monitoring of Crack Formation and Subcritical Growth from Small Defects, Fatigue of Engineering Materials and Structures, Vol. 4, No. 1, 1981, pp. 15-33.

24. Walker, A. C.: Continuous Fatigue Crack Inspection of Aluminum Alloy Plate Specimens Undergoing Spectrum Loading Using Ultrasonic Surface Waves, National Research Council Canada, National Aeronautical Establishment, LTR-ST-1465, July 1983.

25. Swain, M. H. and Newman, J. C., Jr.: On the Use of Marker Loads and Replicas for Measuring Growth Rates for Small Cracks, Fatigue Crack Topography, AGARD Conference Proceedings No. 376, 1984, pp. 12.1-12.17.

26. Brown, C. W. and Smith, G. C.: A Two Stage Plastic Replication Technique for Monitoring Fatigue Crack Initiation and Early Fatigue Crack Growth, Advances in Crack Length Measurement, C. J. Beevers, ed., Engineering Materials Advisory Services Ltd, 1982, pp. 41-51.

27. Newman, J. C. Jr.: A Crack-Closure Model for Predicting Fatigue Crack Growth Under Aircraft Spectrum Loading, Methods and Models for Predicting Fatigue Crack Growth Under Random Loading, J. B. Chang and C. M. Hudson, eds., American Society for Testing and Materials, ASTM STP 748, 1981, pp, 53-84.

28. Newman, J. C., Jr.: A Nonlinear Fracture Mechanics Approach to the Growth of Small Cracks, Behavior of Short Cracks in Airframe Components, AGARD Conference Proceedings No. 328, 1982, pp.6.1-6.26.

29. Lee, J. J. and Sharpe, W. N., Jr.: Short Fatigue Cracks in Notched Aluminum Specimens, Small Fatigue Cracks, R. O. Ritchie and J. Lankford, eds., The Metallurgical Society, 1986.

30. Tan, P. W.: The Boundary Force Method for Stress Analysis of Arbitrarily Shaped Plates with Notches and Cracks, Ph.D. Thesis, George Washington University, 1986.

31. Rice, R. C.; Davies, K. B.; Jaske, C. E.; and Feddersen, C. E.: Consolidation of Fatigue and Fatigue Crack Propagation Data for Design Use, NASA CR-2586, 1975.

32. Hudson, C. Michael: Effect of Stress Ratio on Fatigue-Crack Growth in 7075-T6 and 2024-T3 Aluminum Alloy Specimens, NASA TND-5390, 1969.

33. Beevers, C. J.: Advances in Crack Length Measurement, Engineering Materials Advisory Services Ltd, Warley, West Midlands, United Kingdom, 1982.

34. Phillips, E. P.: The Influence of Crack Closure on Fatigue Crack Growth Thresholds in 2024-T3 Aluminum Alloy, Mechanics of Fatigue Crack Closure, J. C. Newman, Jr. and W. Elber, eds., American Society for Testing and Materials, ASTM STP 982, 1988.

35. Elber, W.: The Significance of Fatigue Crack Closure, American Society for Testing and Materials, ASTM STP 486, 1971, pp. 230-242.

36. Newman, J. C., Jr.; Swain, M. H.; and Phillips, E. P.: An Assessment of the Small-Crack Effect for 2024-T3 Aluminum Alloy, Small Fatigue Cracks, R. O. Ritchie and J. Lankford, eds., The Metallurgical Society, 1986.

37. Miller, K. J.; Mohamed, H. J.; and de los Rios, E. R.: Fatigue Damage Accumulation Above and Below the Fatigue Limit, The Behaviour of Short Fatigue Cracks, European Group on Fracture, Publication No. 1, 1986, pp. 491-511.

38. Dugdale, D. S.: Yielding of Steel Sheets Containing Slits, Journal of Mechanics and Physics of Solids, Vol. 8, No. 2, 1960, pp. 100-104.

39. Irwin, G. R.: Plastic Zone Near a Crack and Fracture Toughness, Proceedings of the 7th Sagamore Conference, 1960, p. IV-63.

40. Newman, J. C., Jr.: A Crack-Opening Stress Equation for Fatigue Crack Growth, International Journal of Fracture, Vol. 24, 1984, R131-R135.

41. Minakawa, K. and McEvily, A. J.: On Near-Threshold Fatigue Crack Growth in Steels and Aluminum Alloys, Fatigue Thresholds, Vol I, 1982, pp. 373-390.

42. Folias, E. S.: Some Remarks on Three-Dimensional Fracture, Fracture Mechanics: Nineteenth Symposium, ASTM STP 969, T. A. Cruse, ed., American Society for Testing and Materials, Philadelphia, 1988, pp. 56-72.

43. Wanhill, R. J. H.: Short Cracks in Aerospace Structures, NLR MP 85054U, 1985. (Also in The Behaviour of Short Fatigue Cracks, European Group on Fracture, Publication No. 1, 1986.)

44. Phillips, E. P. and Newman, J. C., Jr.: Potential Impact of the Small-Crack Effect on Design-Life Calculations, VI International Congress on Experimental Mechanics, Portland, Oregon, June 5-10, 1988.

45. Potter, J. M. and Yee, B. G. W.: Use of Small Crack Data to Bring About and Quantify Improvements to Aircraft Structural Integrity, Proceedings of AGARD Specialists Meeting on Behaviour of Short Cracks in Airframe Components, AGARD-CP-328, 1983.

46. Wang, D. Y.: A Study of Small Crack Growth under Transport Spectrum Loading, Proceedings of AGARD Specialists Meeting on Behaviour of Short Cracks in Airframe Components, AGARD-CP-328, 1983.

47. Wanhill, R. J. H.: Low Stress Intensity Fatigue Crack Growth in 2024-T3 and T351, NLR MP 87001, 1987. (Also Engineering Fracture Mechanics, in press)

48. Martin, J. W.: Micromechanisms in Particle-Hardened Alloys, Cambridge University Press, Cambridge, England, 1980.

49. Yoder, G. R., Cooley, L. A. and Crooker, T. W.: On Microstructural Control of Near-Threshold Fatigue Crack Growth in 7000-Series Aluminum Alloys, NRL Memorandum Report 4787, Naval Research Laboratory, Washington, D. C., April 1982.

50. Stofanak, R. J.; Hertzberg, R. W.; Leupp, J. and Jaccard, R.: On the Cyclic Behavior of Cast and Extruded Aluminum Alloys--Part B--Fractography, Engineering Fracture Mechanics J., Vol. 17, 1983, pp. 541-554.

51. Hahn, G. T.; Sarrate, M. and Rosenfield, A. R.. Plastic Zones in Fe-3Si Steel Double-Cantilever-Beam Specimens, International Journal of Fracture, Vol. 7, 1971, pp. 435-446.

52. Hahn, G. T.; Hoagland, R. G. and Rosenfield, A. R.: Local Yielding Attending Fatigue Crack Growth, Metallurgical Transactions, Vol. 3, 1972, pp. 1189-1202.

53. Kang, T. S. and Liu, H. W.: Fatigue Crack Propagation and Cyclic Deformation at a Crack Tip, International Journal of Fracture, Vol. 10, 1974, pp. 201-222.

54. Rice, J. R.: Mechanics of Crack Tip Deformation and Extension by Fatigue, Fatigue Crack Propagation, ASTM STP 415, American Society for Testing and Materials, Philadelphia, Pennsylvania, 1967, pp. 247-309.

55. Lucas, J. P. and Gerberich, W. W.: A Proposed Criterion for Fatigue Threshold--A Dislocation Substructure Approach, Fatigue of Engineering Materials and Structures, Vol. 6, 1983, pp. 271-280.

56. Isida, M.: Stress-Intensity Factors for the Tension of an Eccentrically Cracked Strip, Trans. ASME, Series E, Journal of Applied Mechanics, Vol. 33, 1965, p. 674.

TABLE 1

Participants in Short-Crack Growth Behaviour Programme

Country	Code	Laboratory	Participants
France	F	Centre d'Essais Aeronautique de Toulouse - CEAT	A. Liberge
Germany (a)	D	Deutsche Forschungs- und Versuchsanstalt fur Luft- und Raumfahrt - DFVLR	H. Nowack
	G	Industrieanlagen Betriebsgesellschaft - IABG	J. Foth P. Heuler
Italy	I	University of Pisa	G. Cavallini R. Galatolo
Netherlands	H	Nationaal Lucht-en Ruimtevaartlaboratorium - NLR	R. Wanhill
Portugal	P	Laboratorio Nacional de Engenharia e Technologia Industrial - LNETI	M. H. Carvalho
		Centro de Mecanica e Materiais da Universidade Tecnica de Lisboa - CEMUL	M. de Freitas
Sweden	S	Aeronautical Research Institute - FFA	A. F. Blom
Turkey	T	Middle East Technical University - METU	A. Ankara C. Kaynak
United Kingdom	E	Royal Aerospace Establishment - RAE	P. R. Edwards D. S. Lock R. Cook
United States of America (b,c,d)	B	The Johns Hopkins University - JHU	W. N. Sharpe J. J. Lee J. Cieslowski
	N	National Aeronautics and Space Administration - NASA Langley Research Center	M. H. Swain E. P. Phillips J. C. Newman
	W	Air Force Wright Aeronautical Laboratory - AFWAL - FIBEC	C. Mazur J. Rudd

(a) P. Heuler, IABG, conducted long-crack tests on core-programme material under GAUSSIAN loading.
(b) F. Adams and J. M. Potter, Air Force Wright Aeronautical Laboratory, machined core-programme specimens.
(c) E. P. Phillips, NASA Langley Research Center, conducted long-crack tests on core-programme material under constant-amplitude and FALSTAFF loading.
(d) W. N. Sharpe, The Johns Hopkins University, conducted crack-closure measurements on short cracks [29].

TABLE 2

Test Conditions for Core Programme

Loading (a)	Maximum Gross Stress S_{max} (MPa)	Number of Specimens (b)	Estimated Fatigue Life, kilocycles
Constant Amplitude R = -2	75	3	20
	60	3	60
	50	3	250 (c)
Constant Amplitude R = -1	105	3	50
	80	3	150
	70	3	200 (c)
Constant Amplitude R = 0 (d)	145	3	50
	120	3	130
	110	3	500 (c)
Constant Amplitude R = 0.5 (d)	225	3	50
	205	3	130
	195	3	500 (c)
FALSTAFF (e)	275	3	300
	205	3	1000
	170	3	3500
GAUSSIAN (e) (I = 0.99)	170	3	300
	145	3	1000
	125	3	2000

(a) Test frequency: 5 to 20 Hz.
(b) Three specimens were provided, see Section 3.4.
(c) If no crack is found in one-million cycles terminate test.
(d) Guide plates should not be used for R = 0 and 0.5.
(e) Maximum stress is highest in sequence.

TABLE 3

Participant Test Matrix on Short-Crack Growth

Participant	Constant Amplitude Loading (a) R = -2 H M L	-1 H M L	0 H M L	0.5 H M L	Spectrum Loading FALSTAFF H M L	GAUSSIAN H M L
France -CEAT	X X X	X X X	X X X[b]		X X	
Germany -DFVLR		X			X X X	X X X
Germany -IABG		X X X	X X X		X X X	X X X
Italy -Pisa		X X X	X X X	X X X	X X	
Netherlands -NLR		X X X				X X X
Portugal-LNETI/CEMUL	X X X	X X X	X X X	X X X		
Sweden -FFA	X X X	X X X	X X X		X X X	
Turkey -METU	X X X	X X X	X X X	X X X		
United Kingdom -RAE	X X X	X X X	X X X	X X X	X X X	X X X
USA-JHU	X X X	X X X	X X X	X X X		
USA-NASA	X X X	X X X	X X X	X X X	X X X	
USA-AFWAL	X X X	X X X	X X X		X X X	

(a) H, M and L represent high, medium and low stress levels, respectively.
(b) Tests conducted at R = 0.1 for H, M and L stress levels.

TABLE 4

Nominal Chemical Composition of 2024-T3 Aluminum Alloy Sheet

Element	Percent
Silicon	.16
Iron	.33
Copper	4.61
Manganese	.57
Magnesium	1.51
Chromium	.02
Zinc	.06
Aluminum	Balance

TABLE 5

Average Tensile Properties of 2024-T3 Aluminum Alloy Sheet

Ultimate tensile strength, MPa	Yield stress (0.2-percent offset), MPa	Modulus of elasticity, MPa	Elongation (51-mm gage length), percent
495	355	72,000	21

(a) Average of 167 tests [32].

TABLE 6

Local Notch-Root Elastic Stresses for Core-Programme Conditions

Loading	Maximum Gross Stress S_{max} (MPa)	$\frac{K_T S_{max}}{\sigma_{ys}}$ (a)	$\frac{K_T S_{min}}{\sigma_{ys}}$
Constant Amplitude R = -2	75	0.67	-1.34
	60	0.54	-1.07
	50	0.45	-0.89
Constant Amplitude R = -1	105	0.94	-0.94
	80	0.71	-0.71
	70	0.63	-0.63
Constant Amplitude R = 0	145	1.29	0
	120	1.07	0
	110	0.98	0
Constant Amplitude R = 0.5	225	2.00	1.00
	205	1.82	0.91
	195	1.74	0.87
FALSTAFF	275	2.45	-0.66
	205	1.82	-0.49
	170	1.52	-0.40
GAUSSIAN (I = 0.99)	170	1.52	-1.52
	145	1.29	-1.29
	125	1.12	-1.12

(a) Yield stress (σ_{ys}) is 355 MPa.

TABLE 7

Participant Test Matrix on Crack Shape

Surface-Crack Length, L (mm):		
L < 0.5	0.5 < L < 1	1 < L < 2
Germany-IABG	Germany-DFVLR	France-CEAT
Netherlands-NLR	Sweden-FFA	Italy-Pisa
United Kingdom-RAE		Portugal-LNETI/CEMUL
USA-JHU		Turkey-METU
USA-NASA		USA-AFWAL

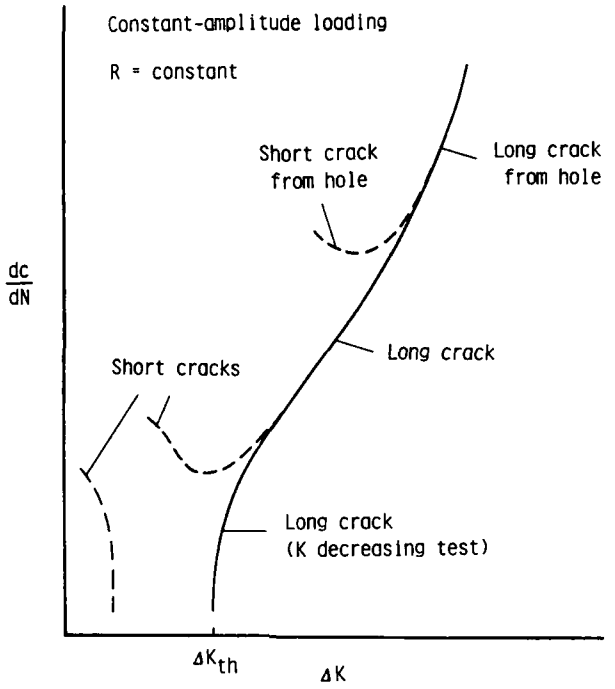

Figure 1.- Typical fatigue-crack growth rate data for short and long cracks.

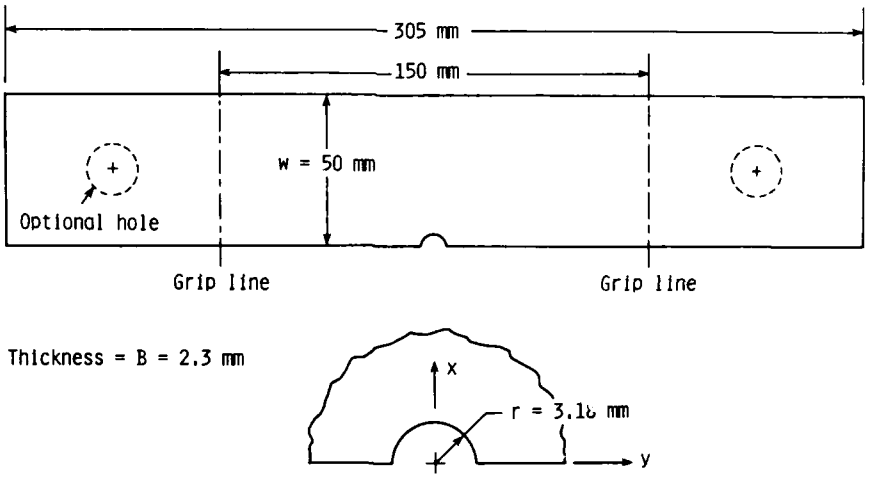

Figure 2.- Single-edge notched tension (SENT) fatigue specimen.

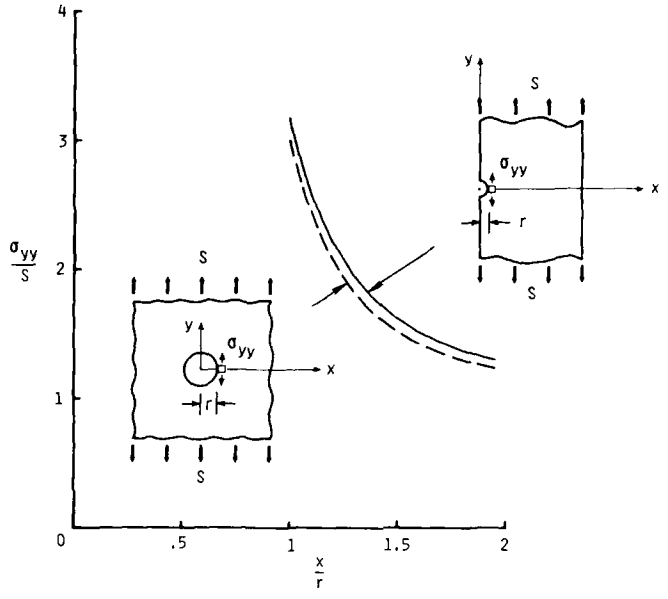

Figure 3.- Normal stress distributions for SENT specimen and for open circular hole in infinite plate.

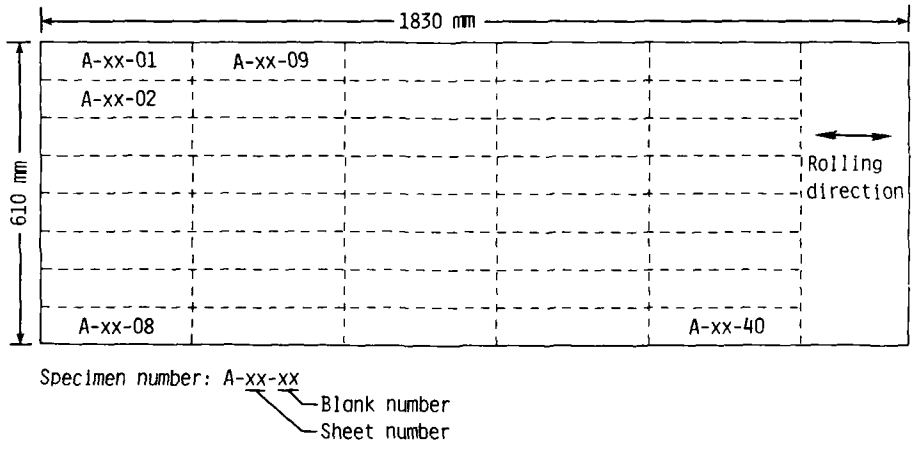

Figure 4.- Layout diagram for core-programme SENT specimens.

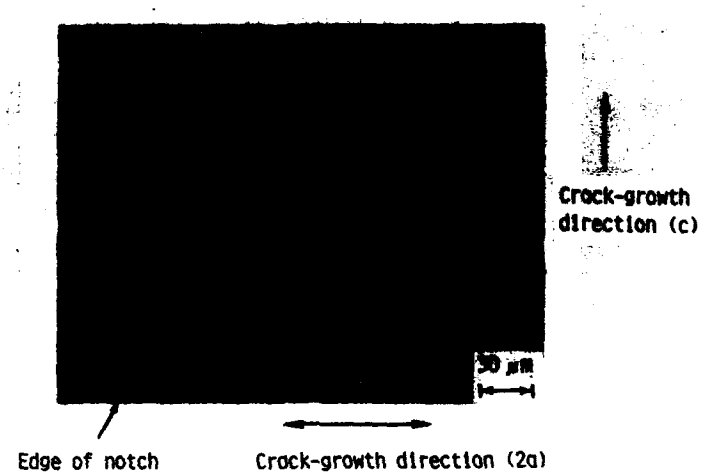

Figure 5.- Photomicrograph of section along crack-surface plane.

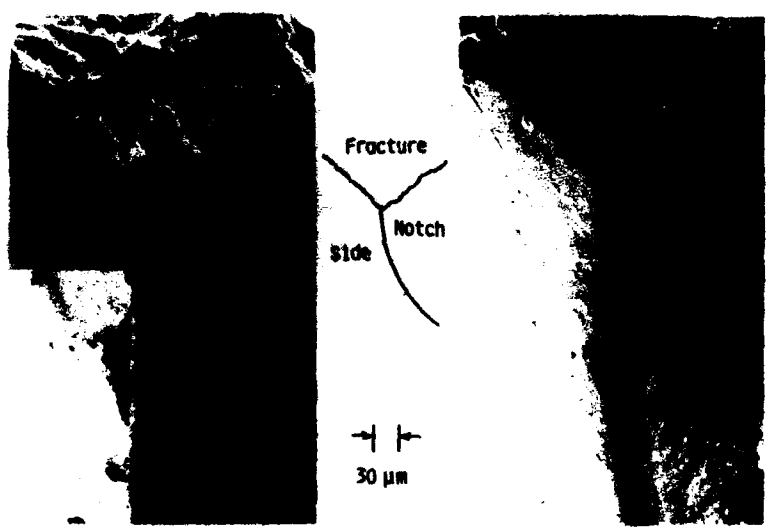

(a) One minute. (b) Five minutes.

Figure 6.- Effect of chemical polishing time on surface finish.

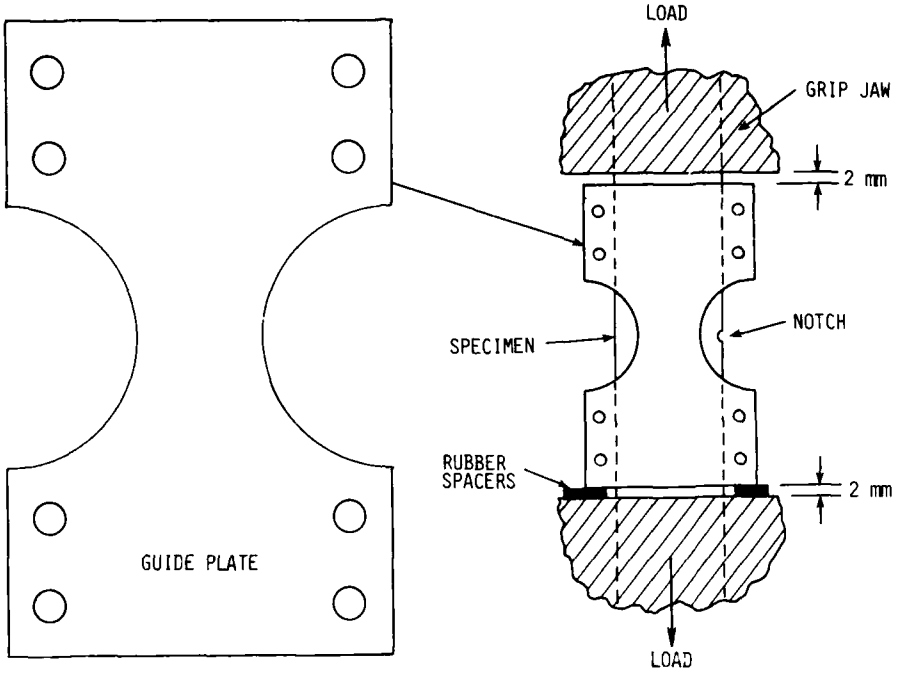

Figure 7.- Anti-buckling guide plates for compressive loads and typical test stand.

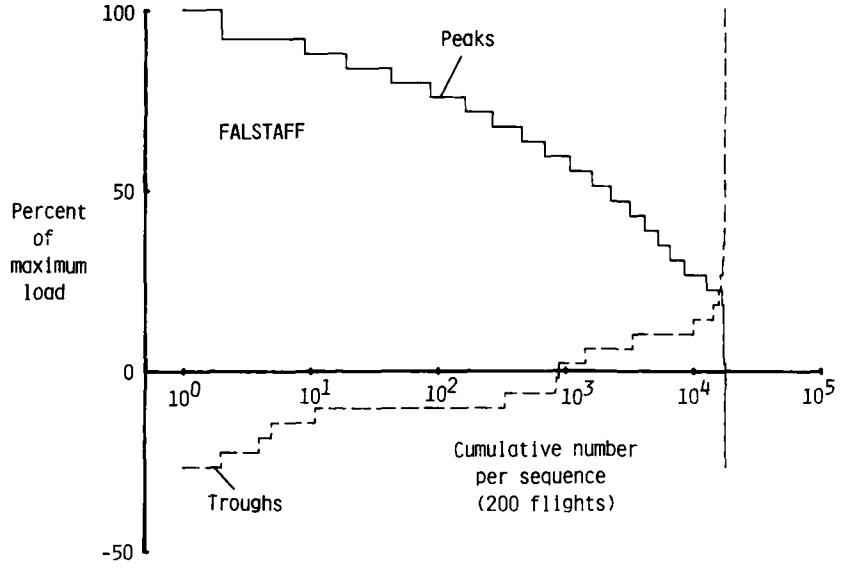

Figure 8(a).- Cumulative number of peaks and troughs in FALSTAFF sequence.

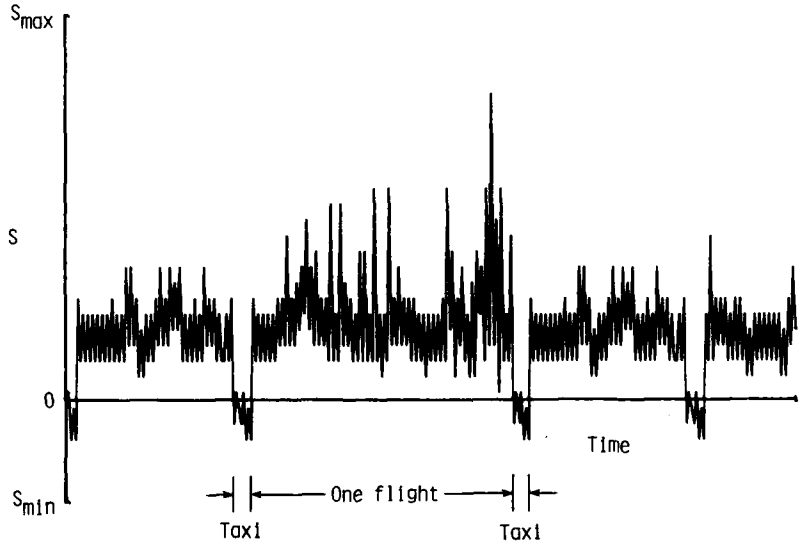

Figure 8(b).- Typical flights in FALSTAFF sequence.

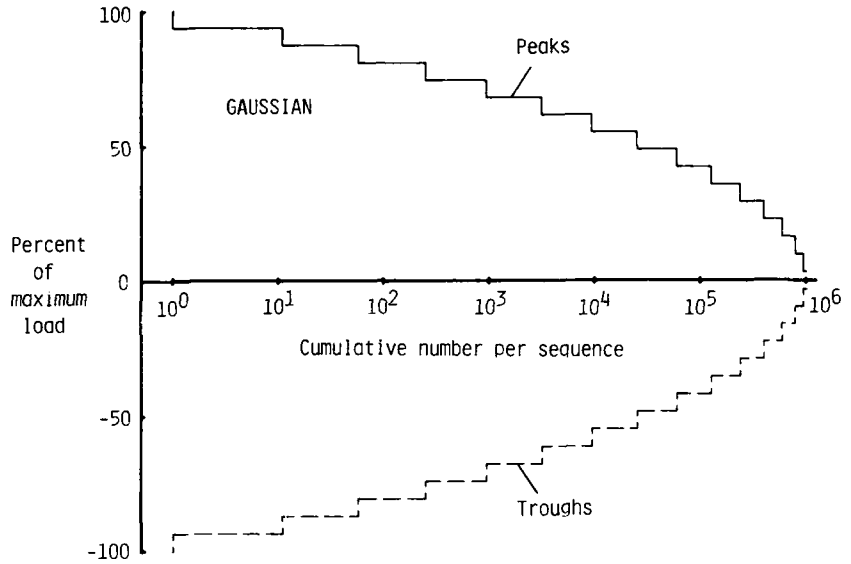

Figure 9(a).- Cumulative number of peaks and troughs in GAUSSIAN (I = 0.99) sequence.

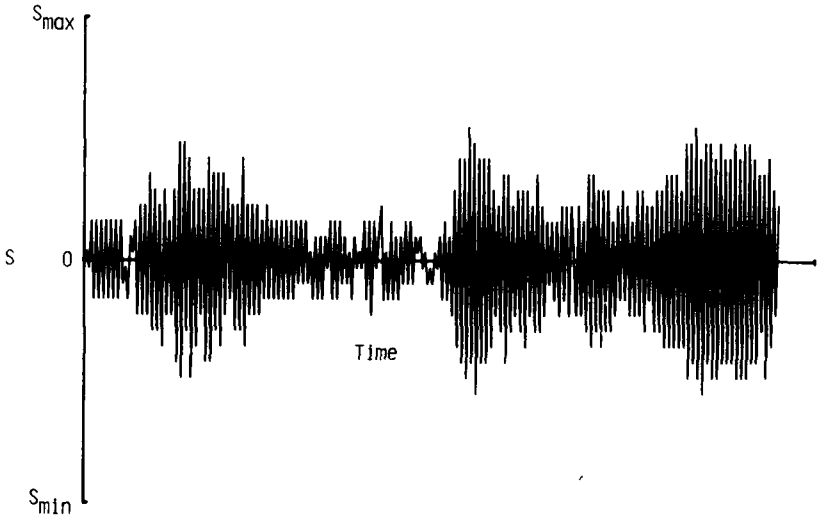

Figure 9(b).- Part of GAUSSIAN (I = 0.99) sequence.

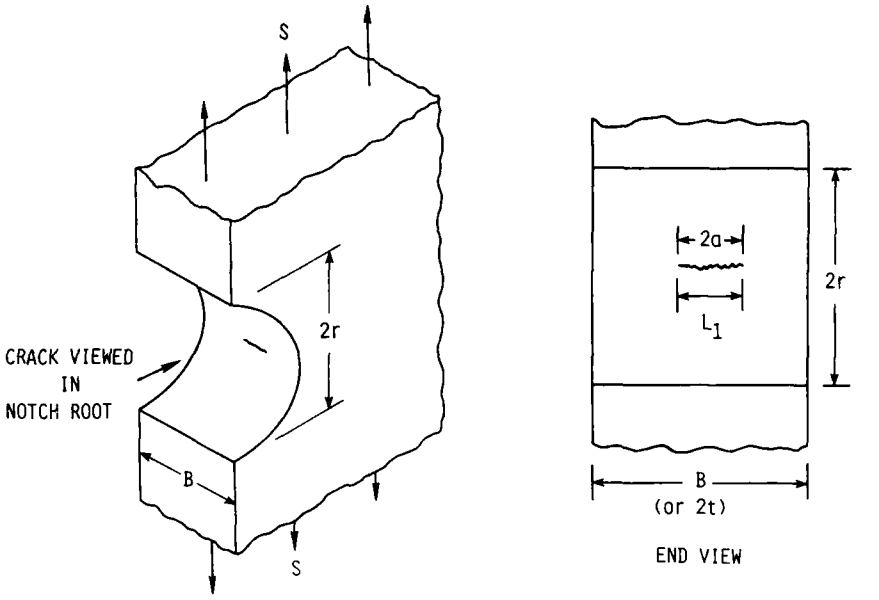

(a) Crack in notch root. (b) Crack length measurements.

Figure 10.- Notch configuration and crack-length measurement in notch root.

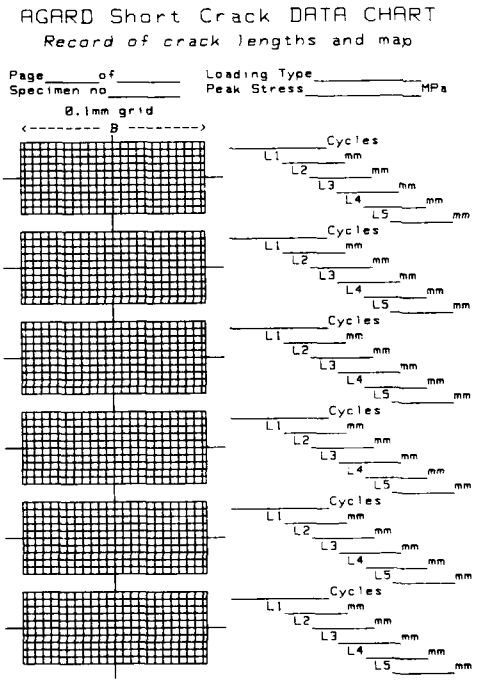

Figure 11.- Cooperative test programme short-crack Data Chart.

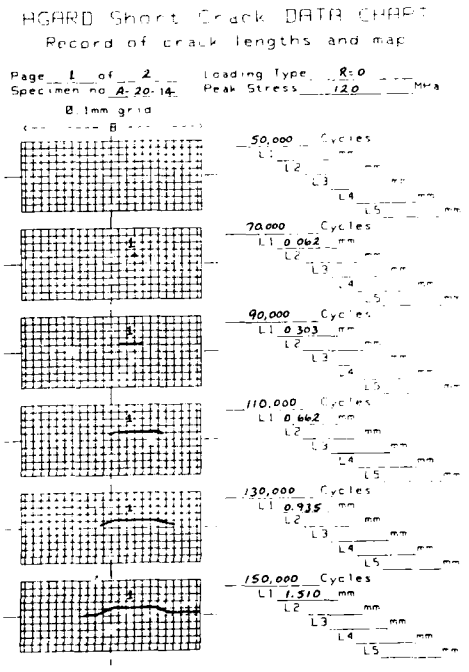

Figure 12.- Example of Data Chart for single crack.

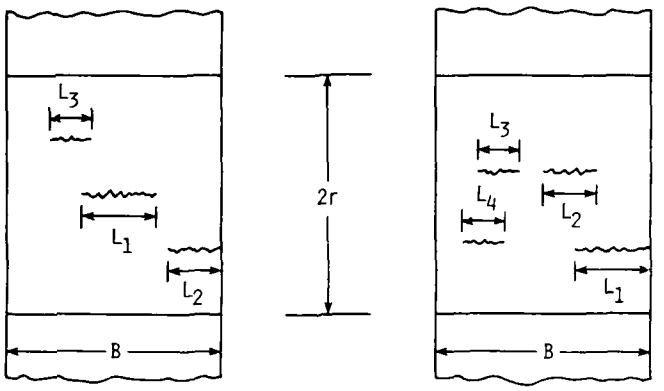

(a) Multi-cracks. (b) Multi-cracks along same plane.

Figure 13.- Multi-crack length measurements in notch root.

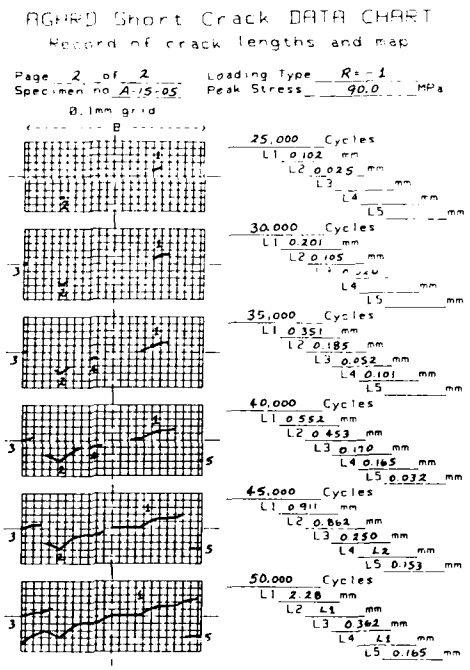

Figure 14.- Example of Data Chart for multi-cracks.

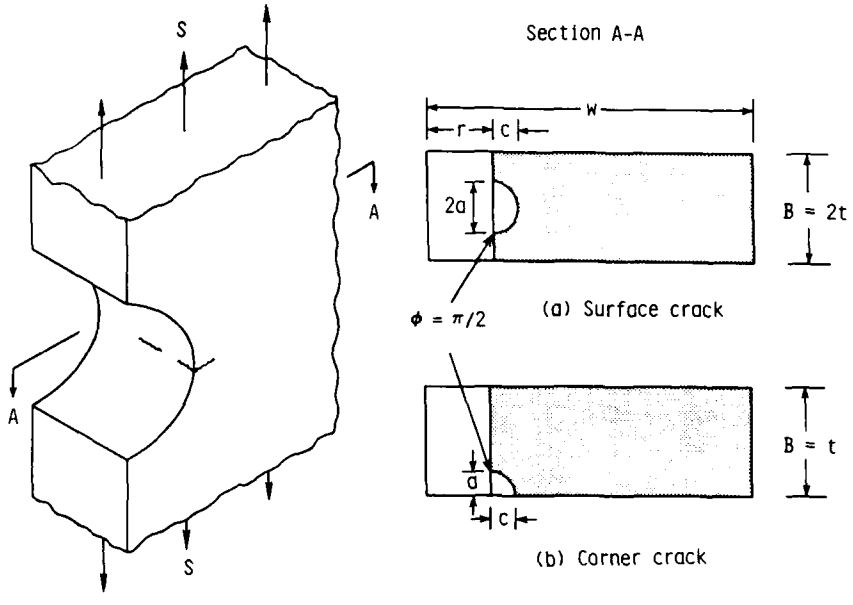

Figure 15.- Definition of dimensions for specimen, surface-crack and corner-crack configurations.

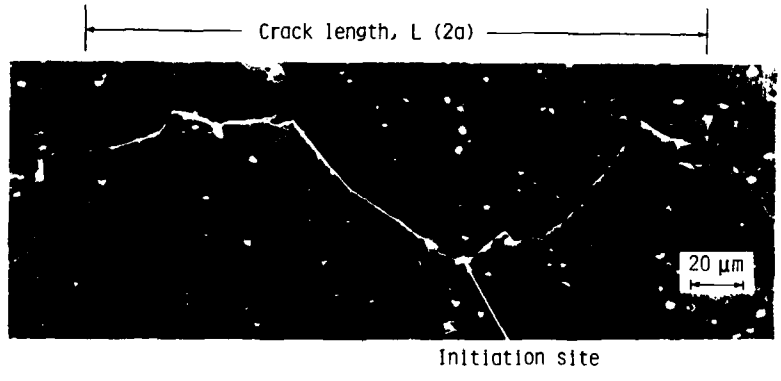

Figure 16.- Montage of photographs of surface replicas showing crack-length measurement.

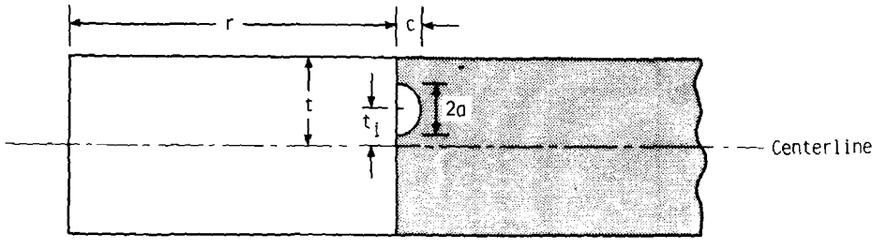

Figure 17.- Definition of crack-initiation-site parameters.

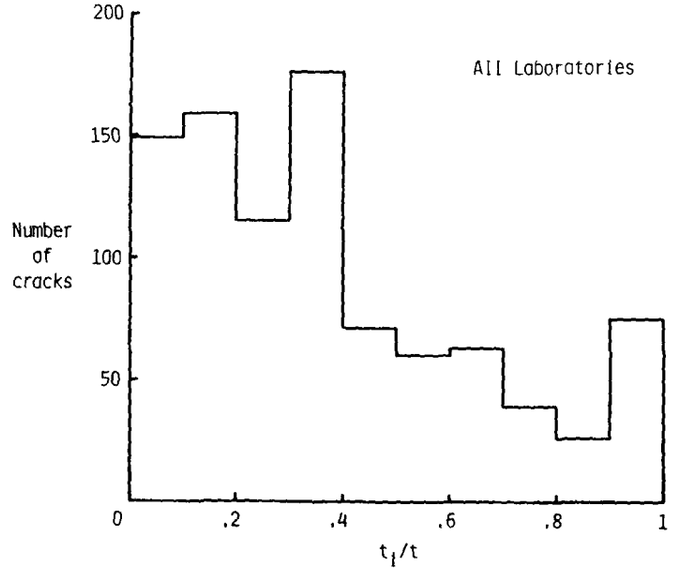

Figure 18.- Distribution of crack-initiation sites along bore of notch from all participants.

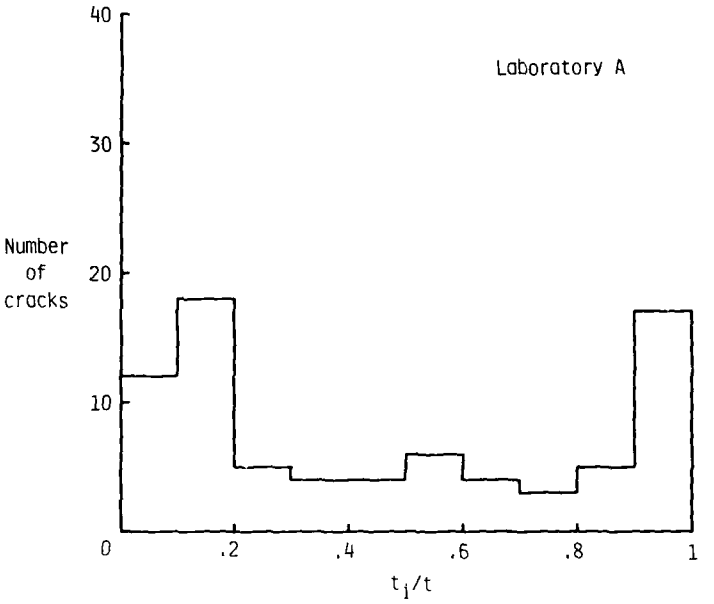

Figure 19.- *Distribution of* crack-initiation sites for laboratory with most corner cracks.

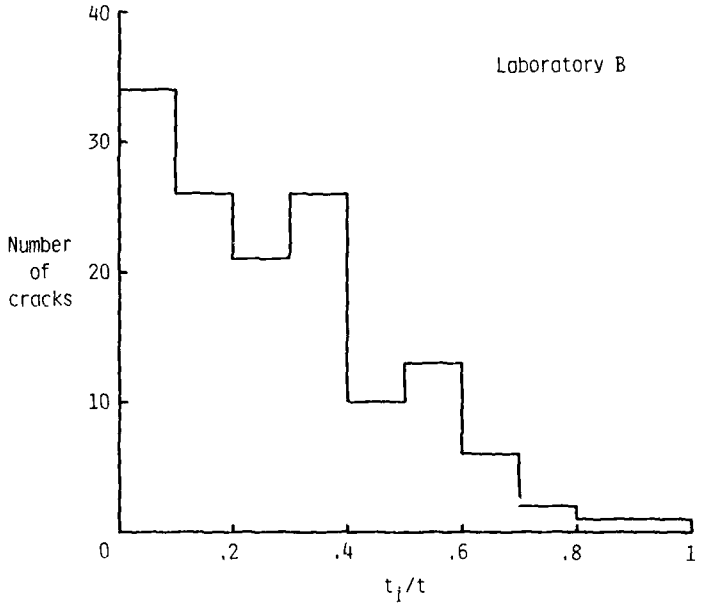

Figure 20.- Distribution of crack-initiation sites for laboratory with most surface cracks at mid-thickness.

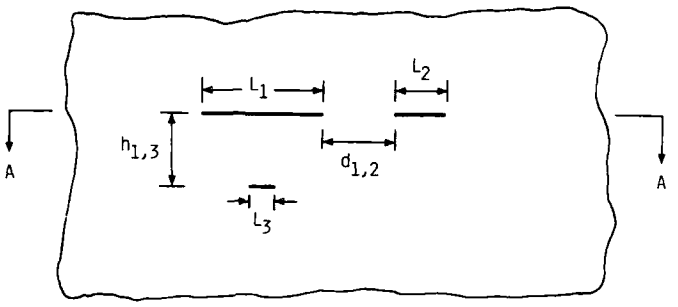

(a) Multi-cracks at notch root.

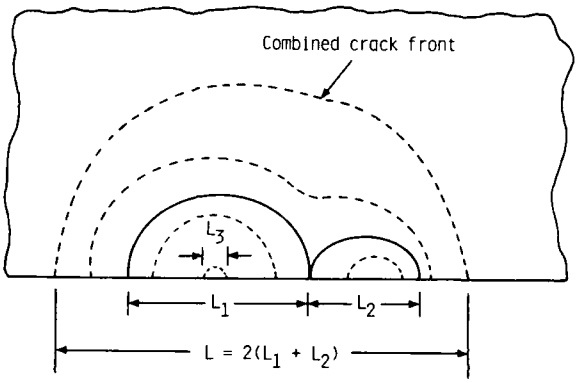

(b) Interacting surface cracks for $d_{1,2} = 0$ (section A-A).

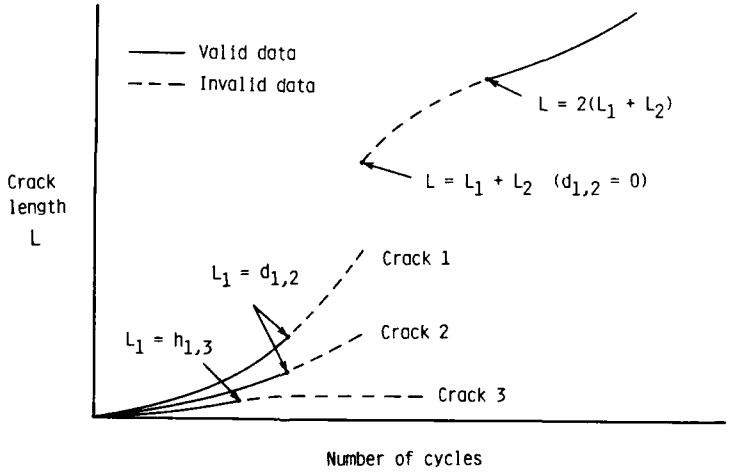

(c) Definition of valid and invalid crack-growth data.

Figure 21.- Definition of crack "non-interacting" criteria for coalescence and crack shadowing.

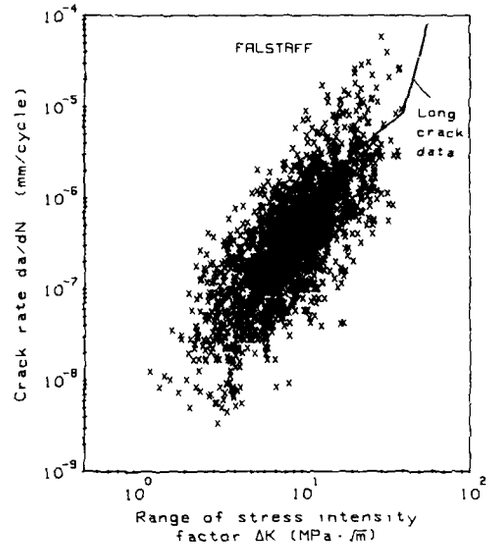

Figure 22.- All FALSTAFF results before application of "non-interaction" analysis (8 laboratories).

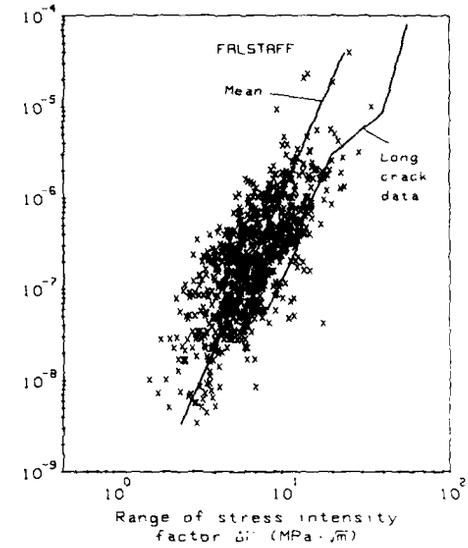

Figure 23.- All FALSTAFF results after application of "non-interaction" analysis (8 laboratories).

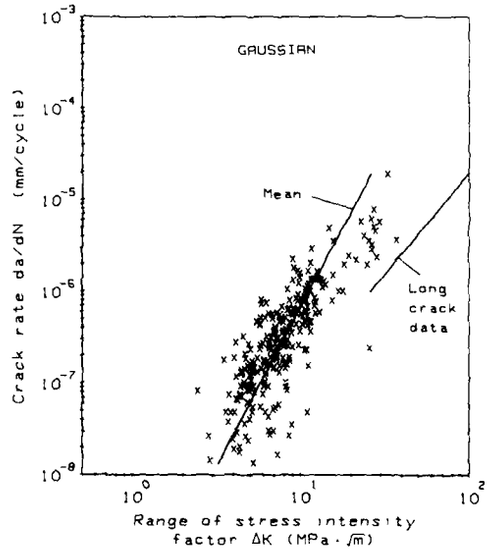

Figure 24.- All GAUSSIAN results after "non-interaction" analysis (4 laboratories).

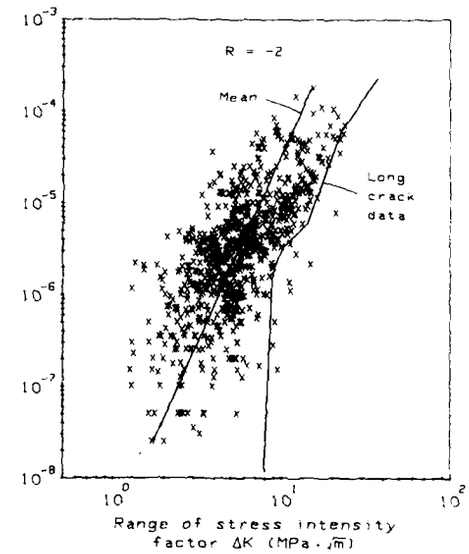

Figure 25.- All R = -2 results after "non-interaction" analysis (8 laboratories).

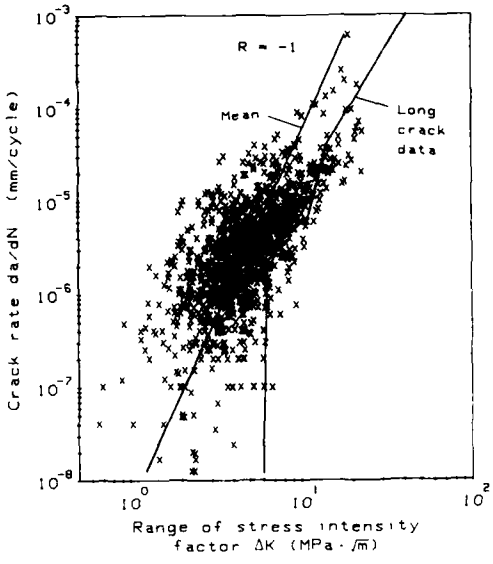

Figure 26.- All R = -1 results after "non-interaction" analysis (12 laboratories).

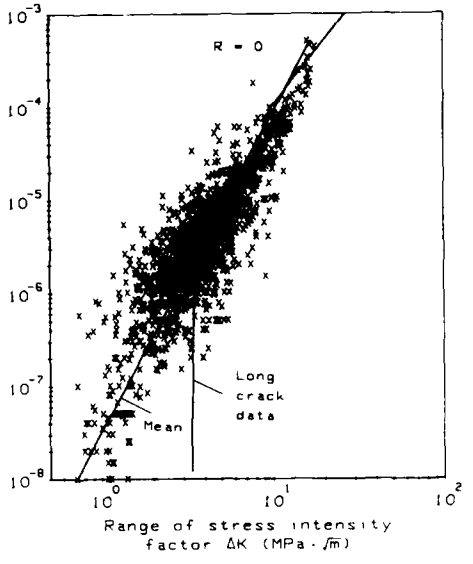

Figure 27.- All R = 0 results after "non-interaction" analysis (9 laboratories).

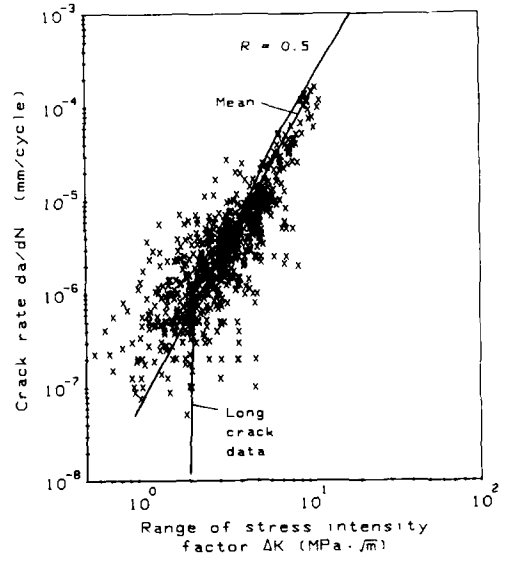

Figure 28.- All R = 0.5 results after "non-interaction" analysis (6 laboratories).

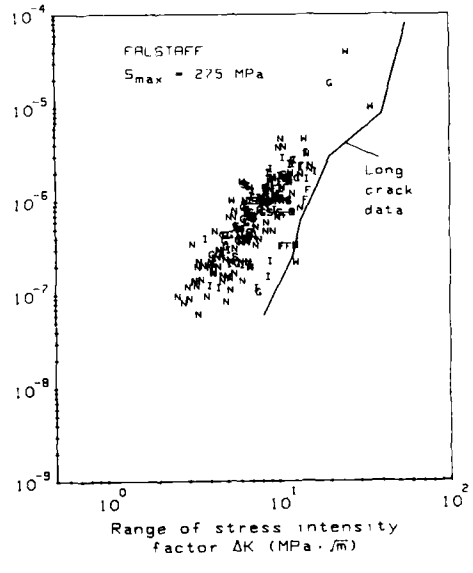

Figure 29.- FALSTAFF results at S_{max} = 275 MPa after "non-interaction" analysis.

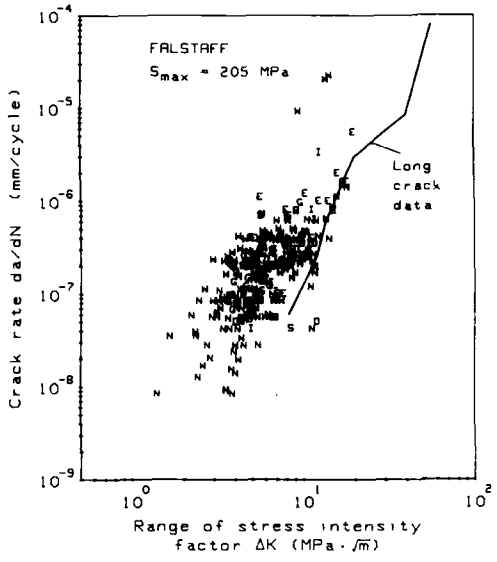

Figure 30.- FALSTAFF results at S_{max} = 205 MPa after "non-interaction" analysis.

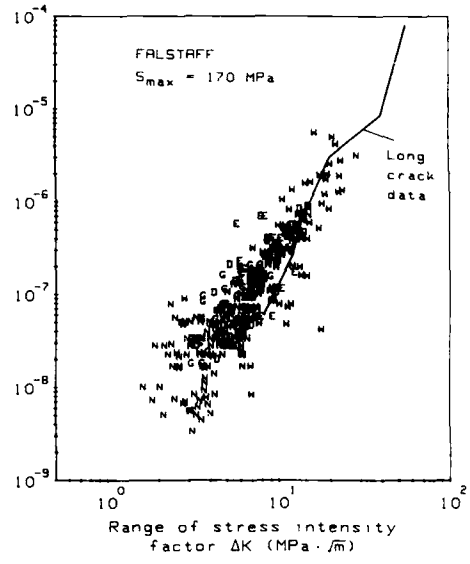

Figure 31.- FALSTAFF results at S_{max} = 170 MPa after "non-interaction" analysis.

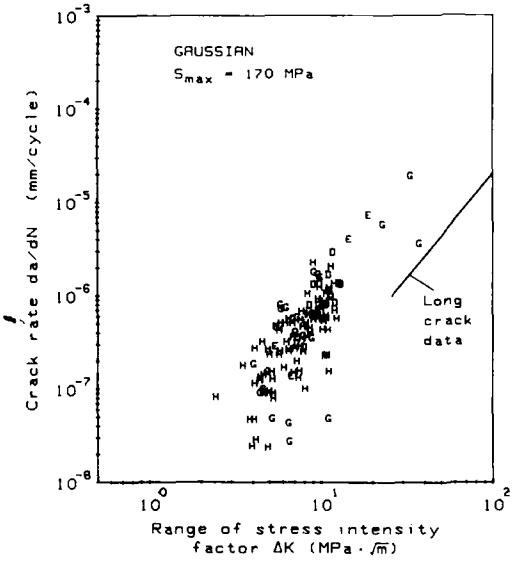

Figure 32.- GAUSSIAN results at S_{max} = 170 MPa after "non-interaction" analysis.

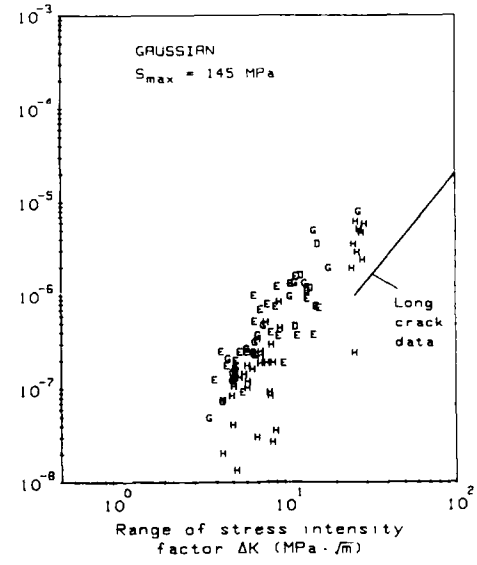

Figure 33.- GAUSSIAN results at S_{max} = 145 MPa after "non-interaction" analysis.

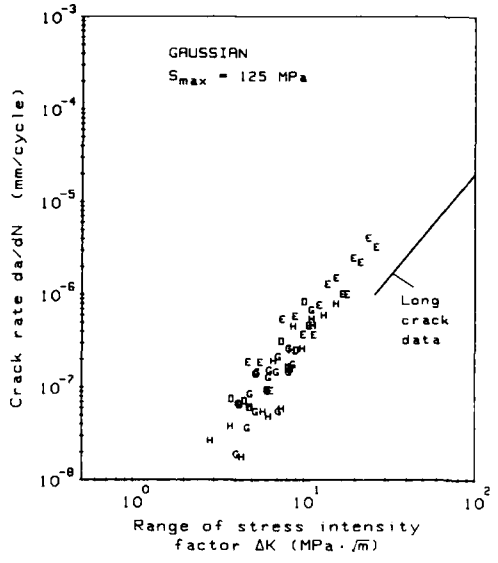

Figure 34.- GAUSSIAN results at S_{max} = 125 MPa after "non-interaction" analysis.

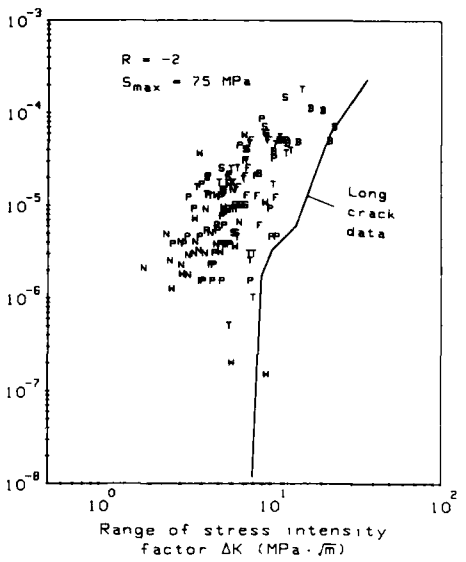

Figure 35.- Constant-amplitude (R = -2) results at S_{max} = 75 MPa after "non-interaction" analysis.

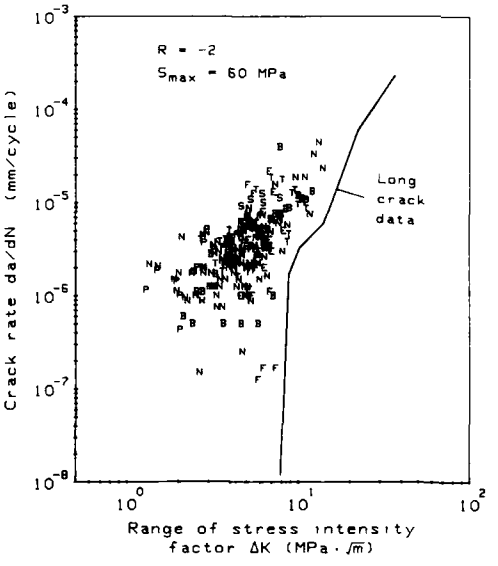

Figure 36.- Constant-amplitude (R = -2) results at S_{max} = 60 MPa after "non-interaction" analysis.

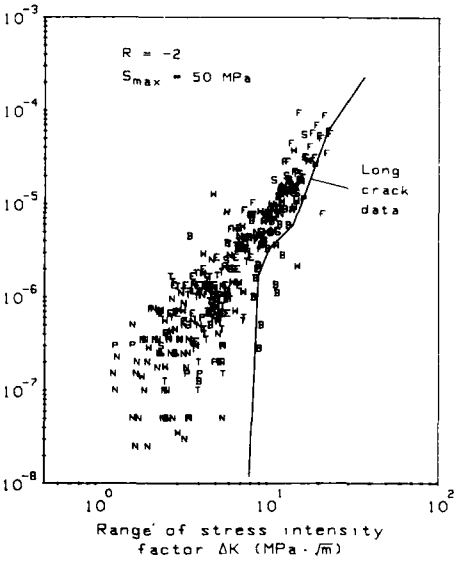

Figure 37.- Constant-amplitude (R = -2) results at S_{max} = 50 MPa after "non-interaction" analysis.

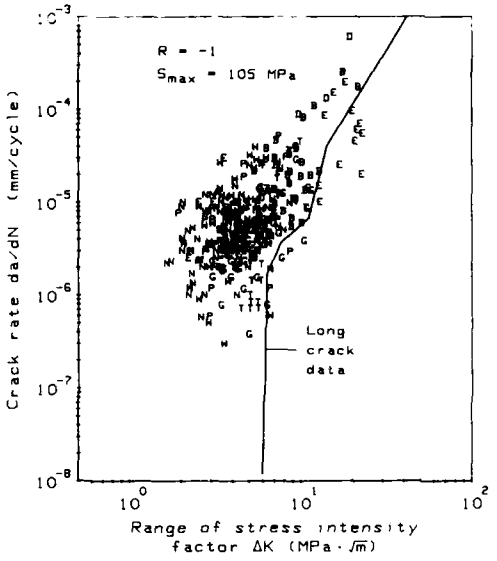

Figure 38.- Constant-amplitude (R = -1) results at S_{max} = 105 MPa after "non-interaction" analysis.

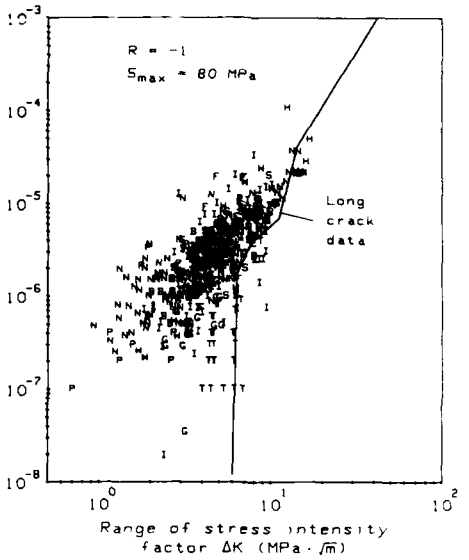

Figure 39.- Constant-amplitude (R = -1) results at S_{max} = 80 MPa after "non-interaction" analysis.

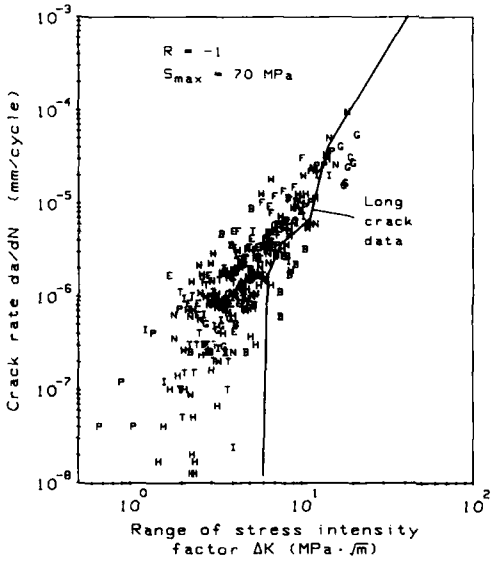

Figure 40.- Constant-amplitude (R = -1) results at S_{max} = 70 MPa after "non-interaction" analysis.

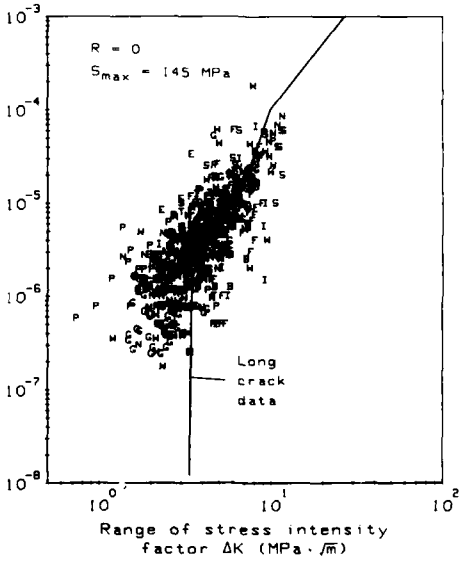

Figure 41.- Constant-amplitude (R = 0) results at S_{max} = 145 MPa after "non-interaction" analysis.

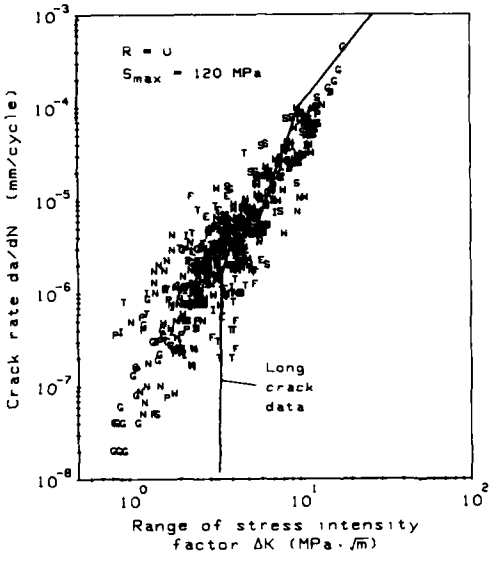

Figure 42.- Constant-amplitude (R = 0) results at S_{max} = 120 MPa after "non-interaction" analysis.

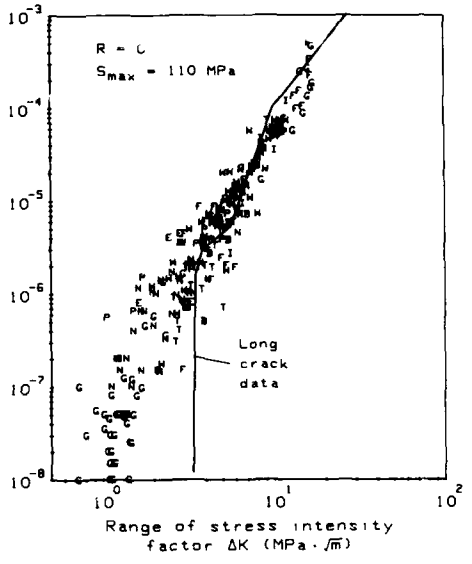

Figure 43.- Constant-amplitude (R = 0) results at S_{max} = 110 MPa after "non-interaction" analysis.

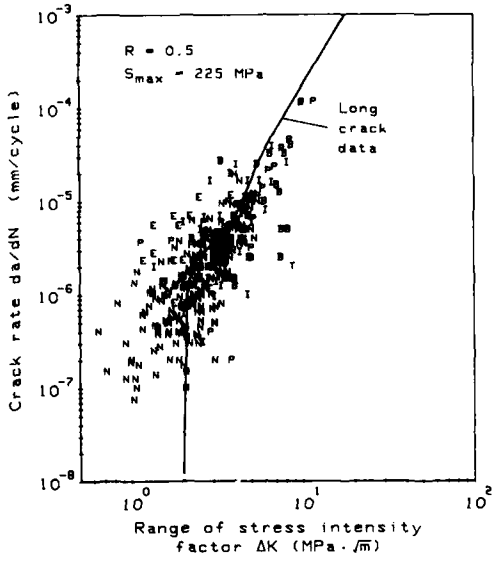

Figure 44.- Constant-amplitude (R = 0.5) results at S_{max} = 225 MPa after "non-interaction" analysis.

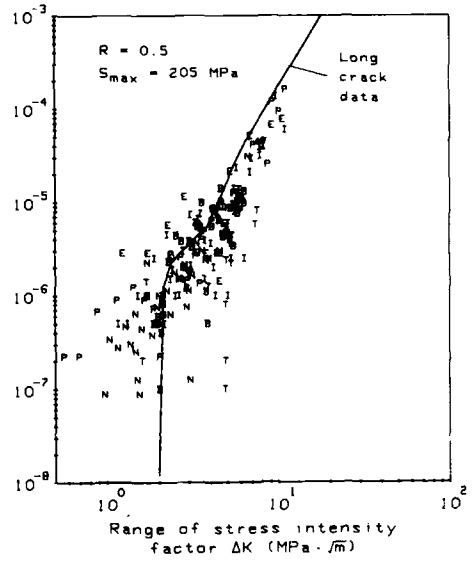

Figure 45.- Constant-amplitude (R = 0.5) results at S_{max} = 205 MPa after "non-interaction" analysis.

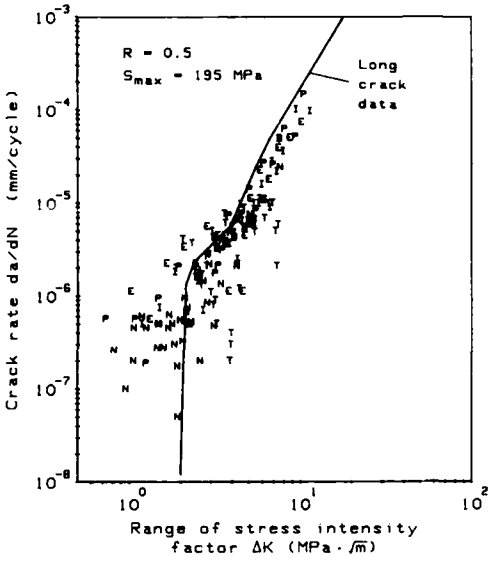

Figure 46.- Constant-amplitude (R = 0.5) results at S_{max} = 195 MPa after "non-interaction" analysis.

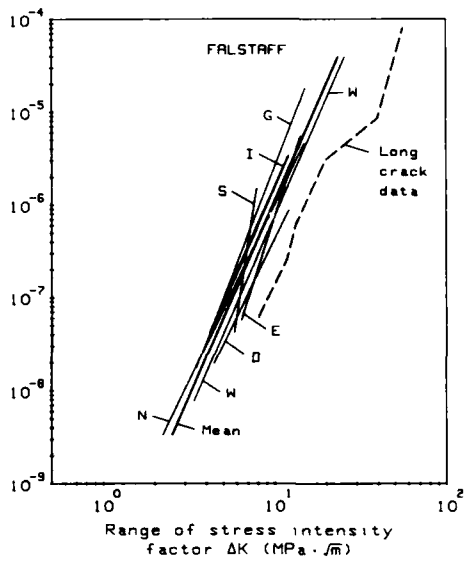

Figure 47.- Least-squares-fit straight lines for FALSTAFF short-crack data from different laboratories.

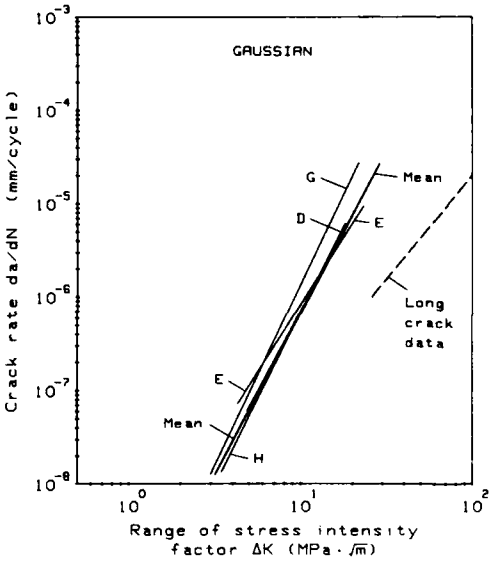

Figure 48.- Least-squares-fit straight lines for GAUSSIAN short-crack data from different laboratories.

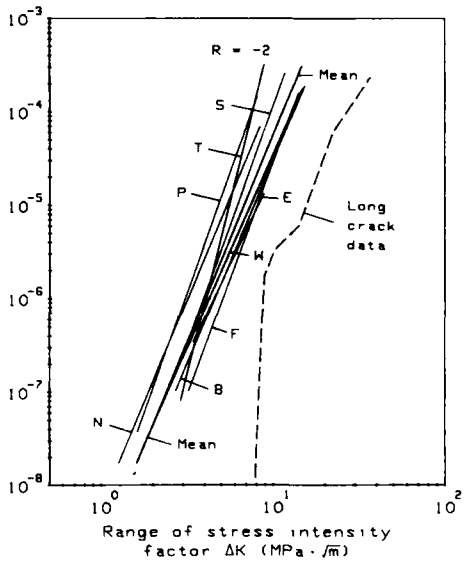

Figure 49.- Least-squares-fit straight lines for R = -2 short-crack data from different laboratories.

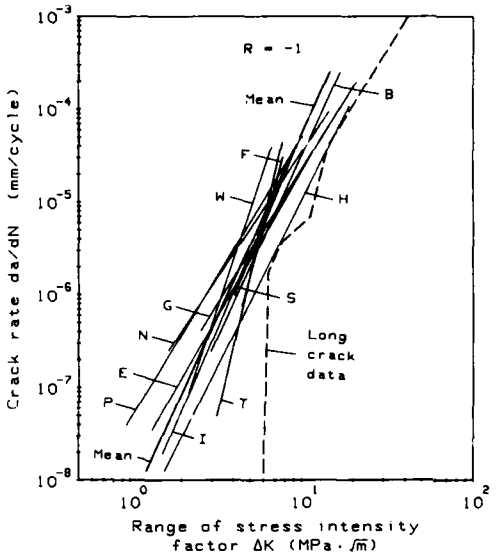

Figure 50.- Least-squares-fit straight lines for R = -1 short-crack data from different laboratories.

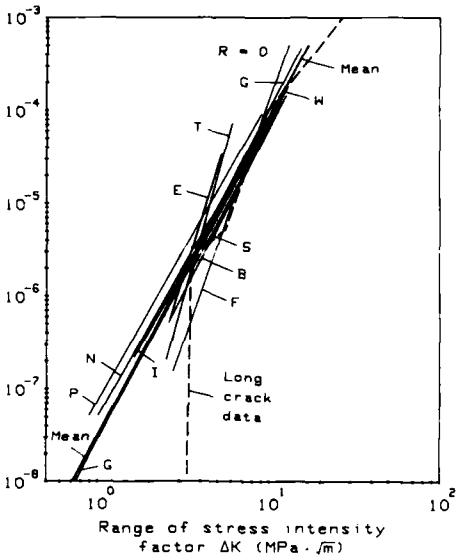

Figure 51.- Least-squares-fit straight lines for R = 0 short-crack data from different laboratories.

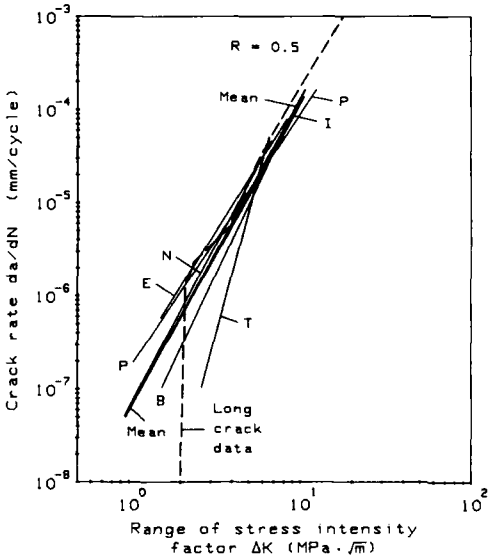

Figure 52.- Least-squares-fit straight lines for R = 0.5 short-crack data from different laboratories.

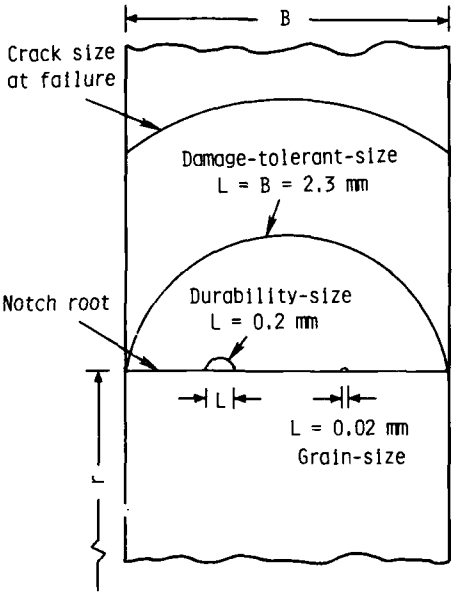

Figure 53.- Schematic of various surface cracks to define grain-size, durability-size, and damage-tolerant size defect.

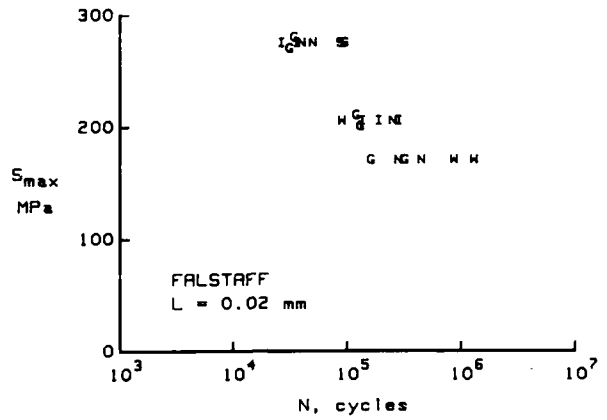

Figure 54.- Fatigue life from initiation to a grain-size defect (L = 0.02 mm) under FALSTAFF loading.

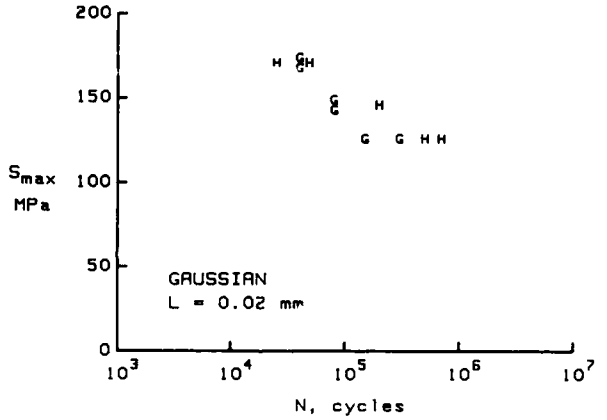

Figure 55.- Fatigue life from initiation to a grain-size defect (L = 0.02 mm) under GAUSSIAN loading.

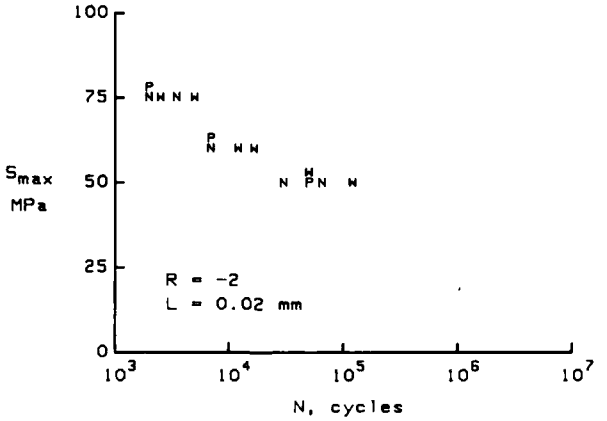

Figure 56.- Fatigue life from initiation to a grain-size defect (L = 0.02 mm) under R = -2 loading.

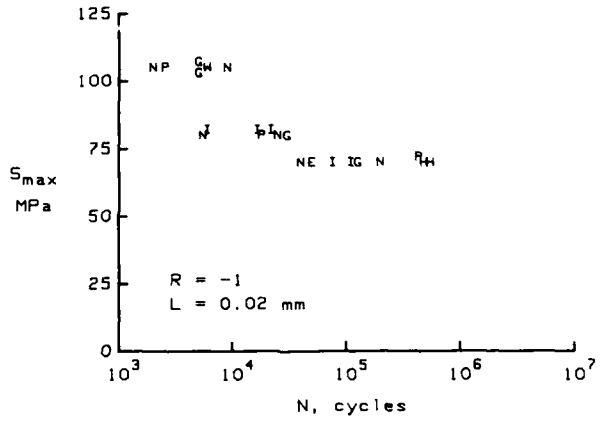

Figure 57.- Fatigue life from initiation to a grain-size defect (L = 0.02 mm) under R = -1 loading.

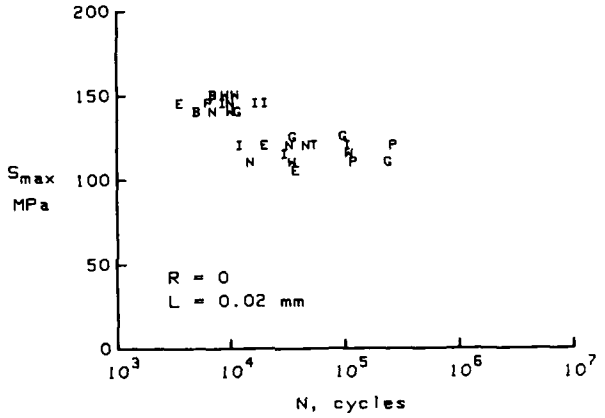

Figure 58.- Fatigue life from initiation to a grain-size defect (L = 0.02 mm) under R = 0 loading.

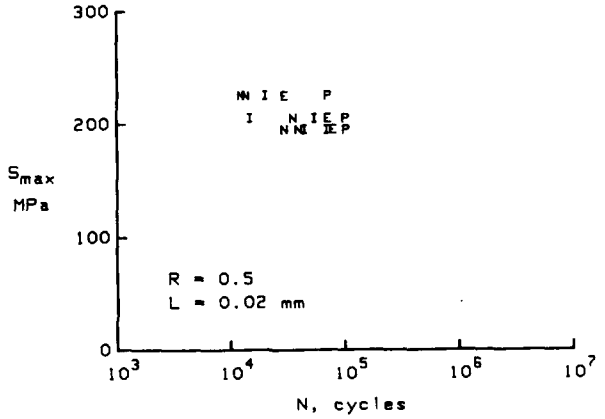

Figure 59.- Fatigue life from initiation to a grain-size defect (L = 0.02 mm) under R = 0.5 loading.

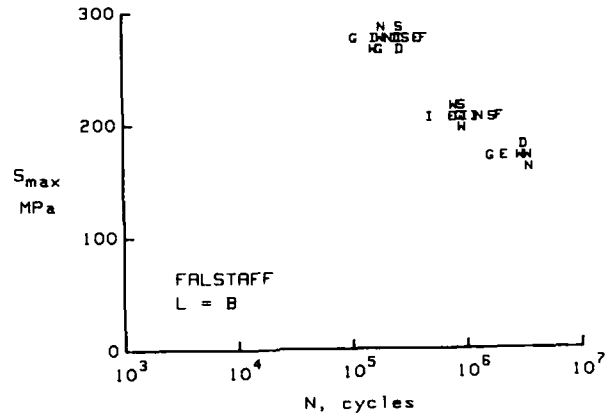

Figure 60.- Fatigue life from initiation to a damage-tolerant-size defect (L = B = 2.3 mm) under FALSTAFF loading.

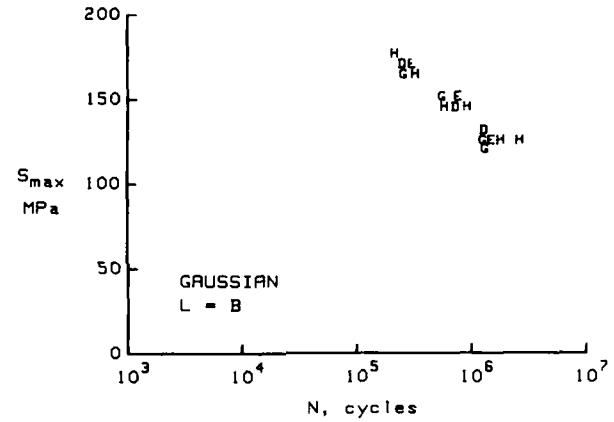

Figure 61.- Fatigue life from initiation to a damage-tolerant-size defect (L = B = 2.3 mm) under GAUSSIAN loading.

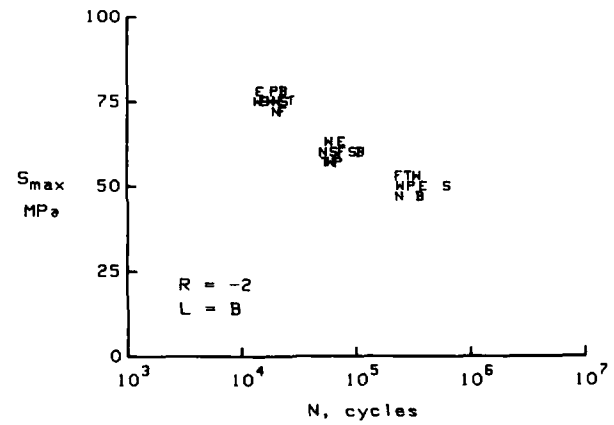

Figure 62.- Fatigue life from initiation to a damage-tolerant-size defect (L = B = 2.3 mm) under R = -2 loading.

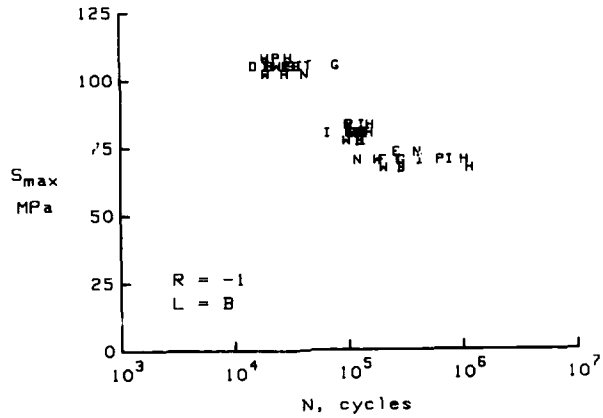

Figure 63.- Fatigue life from initiation to a damage-tolerant-size defect (L = B = 2.3 mm) under R = -1 loading.

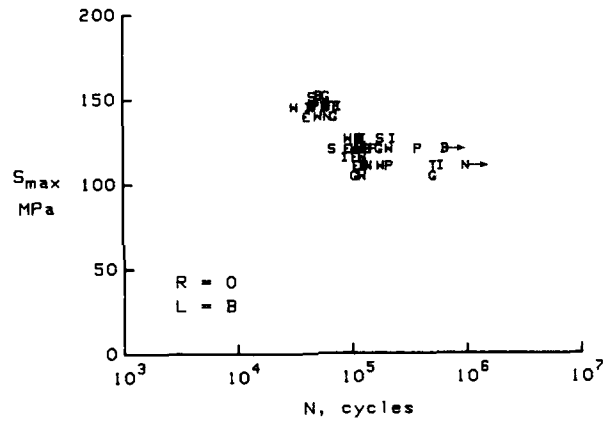

Figure 64.- Fatigue life from initiation to a damage-tolerant-size defect (L = B = 2.3 mm) under R = 0 loading.

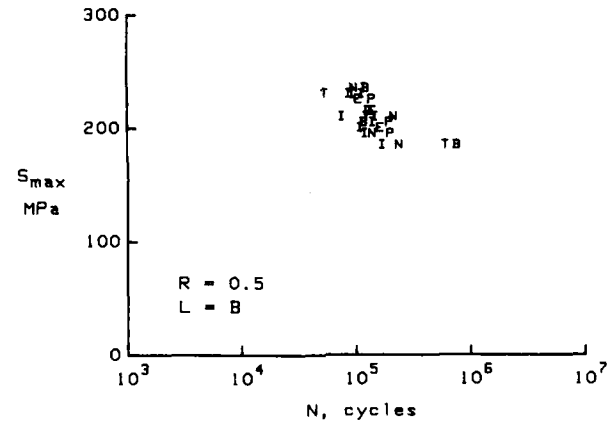

Figure 65.- Fatigue life from initiation to a damage-tolerant-size defect (L = B = 2.3 mm) under R = 0.5 loading.

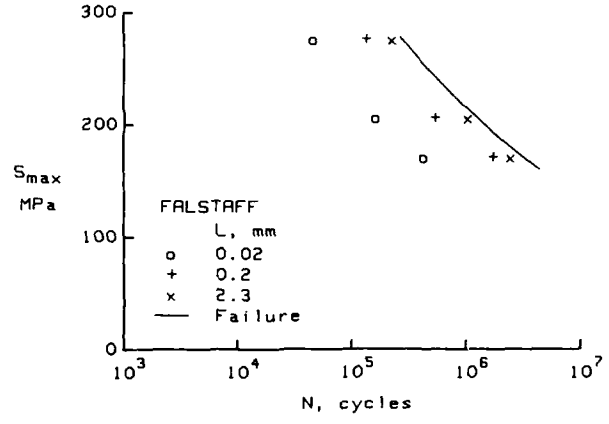

Figure 66.- Comparison of fatigue lives from initiation to various crack sizes (L) under FALSTAFF loading.

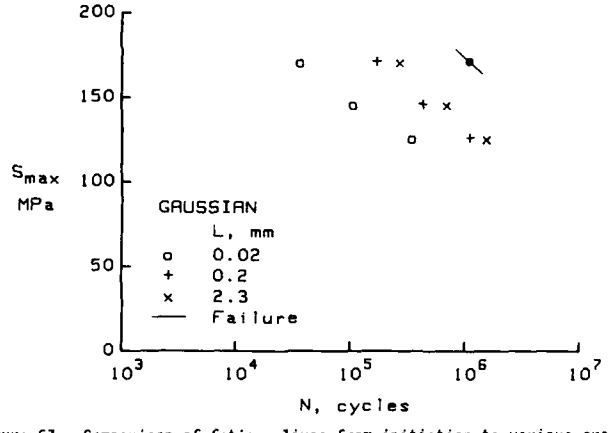

Figure 67.- Comparison of fatigue lives from initiation to various crack sizes (L) under GAUSSIAN loading.

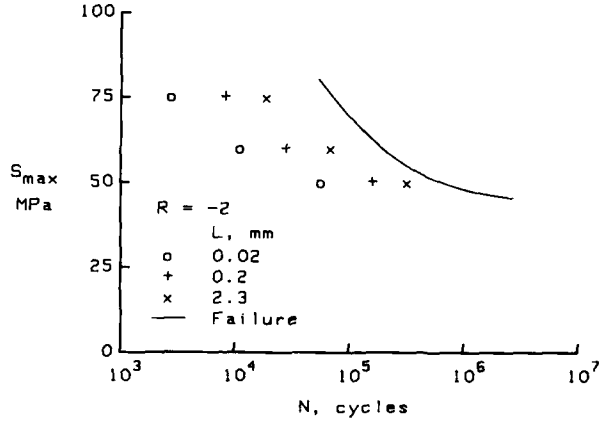

Figure 68.- Comparison of fatigue lives from initiation to various crack sizes (L) under R = -2 loading.

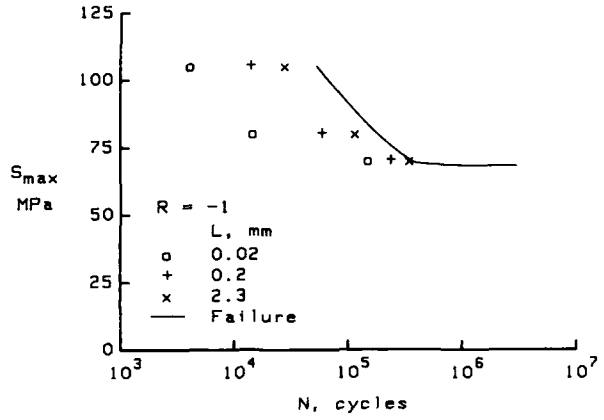

Figure 69.- Comparison of fatigue lives from initiation to various crack sizes (L) under R = -1 loading.

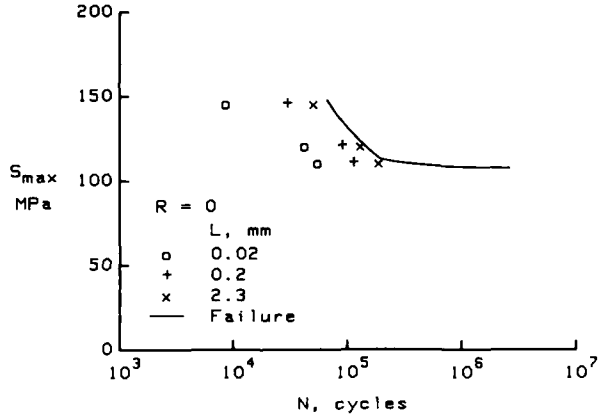

Figure 70.- Comparison of fatigue lives from initiation to various crack sizes (L) under R = 0 loading.

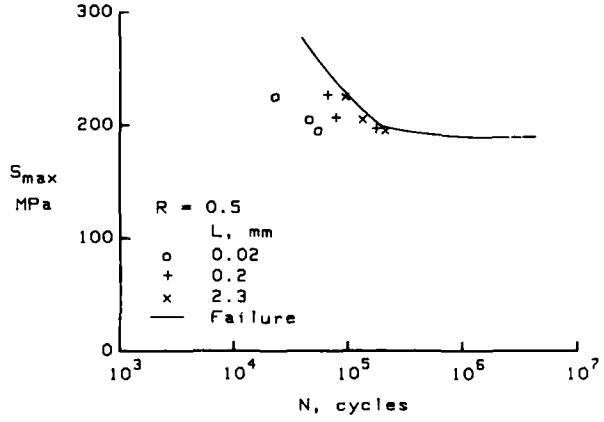

Figure 71.- Comparison of fatigue lives from initiation to various crack sizes (L) under R = 0.5 loading.

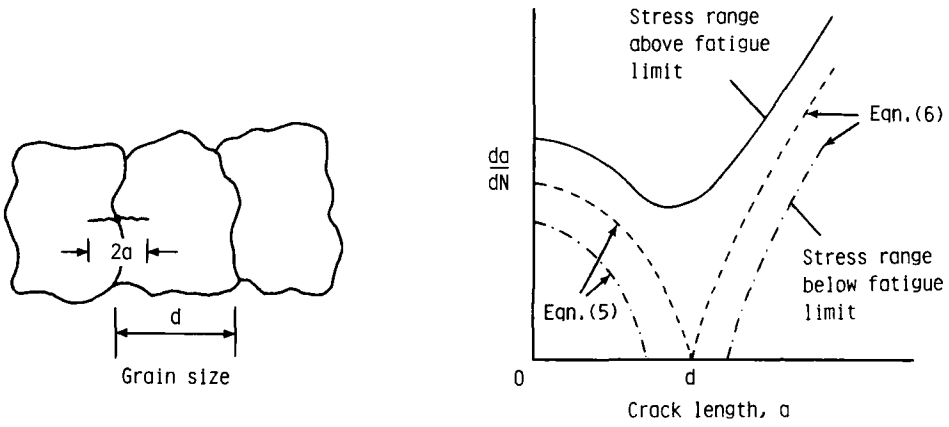

(a) Crack initiation at grain boundary.

(b) Crack-growth rate behaviour.

Figure 72.- Schematic of "micro-structural barrier" influence on crack-growth rates.

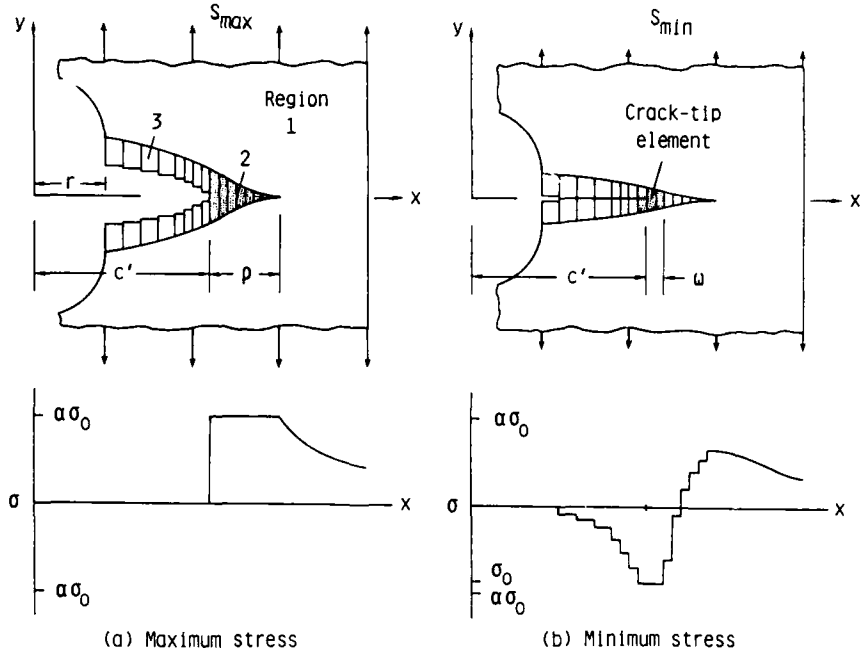

(a) Maximum stress

(b) Minimum stress

Figure 73.- Schematic of analytical crack-closure model showing crack-surface displacements and stress distributions along crack line.

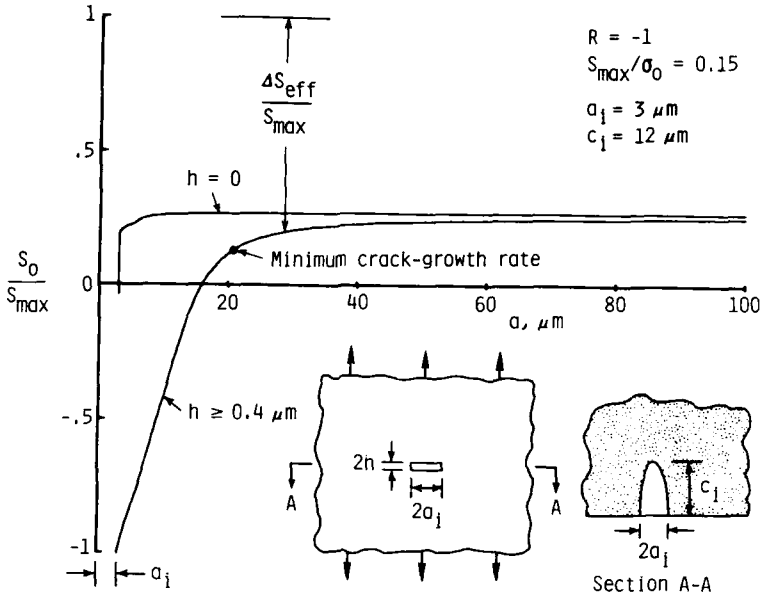

Figure 74.- Calculated crack-opening stresses for various defect void heights as a function of crack length.

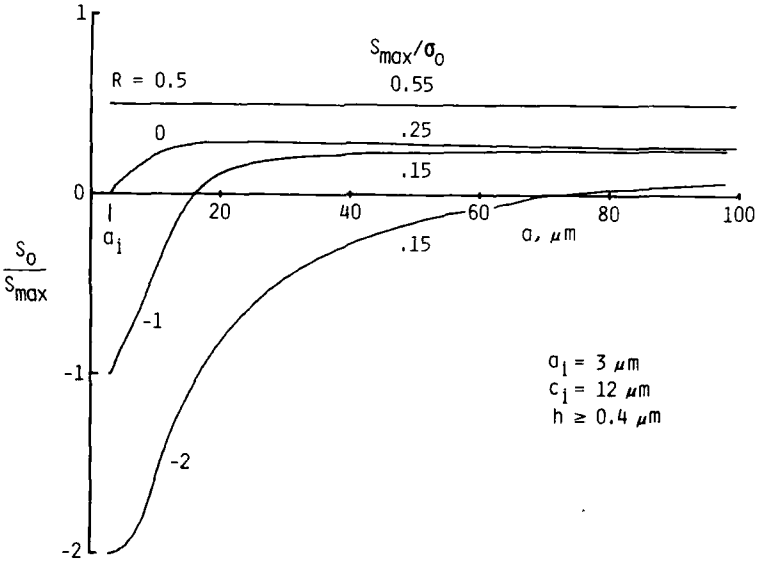

Figure 75.- Calculated crack-opening stresses for various constant-amplitude loadings as a function of crack length.

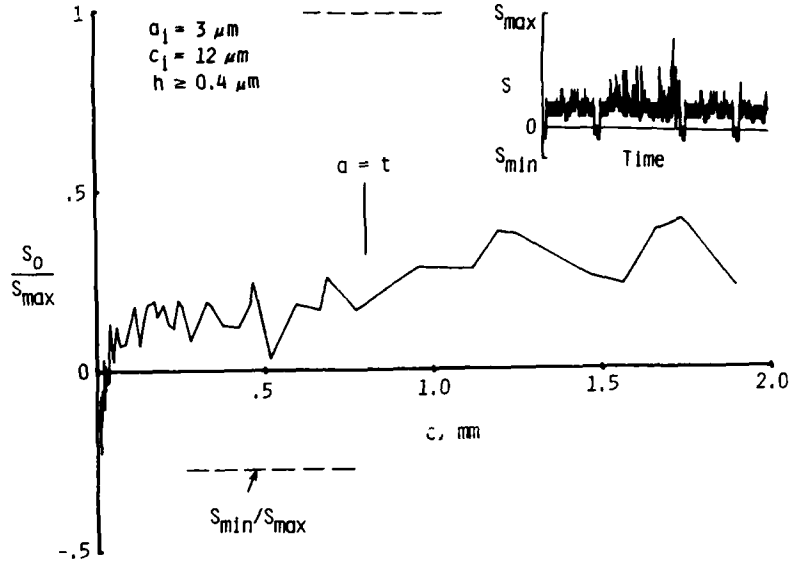

Figure 76.- Calculated crack-opening stresses for FALSTAFF loading.

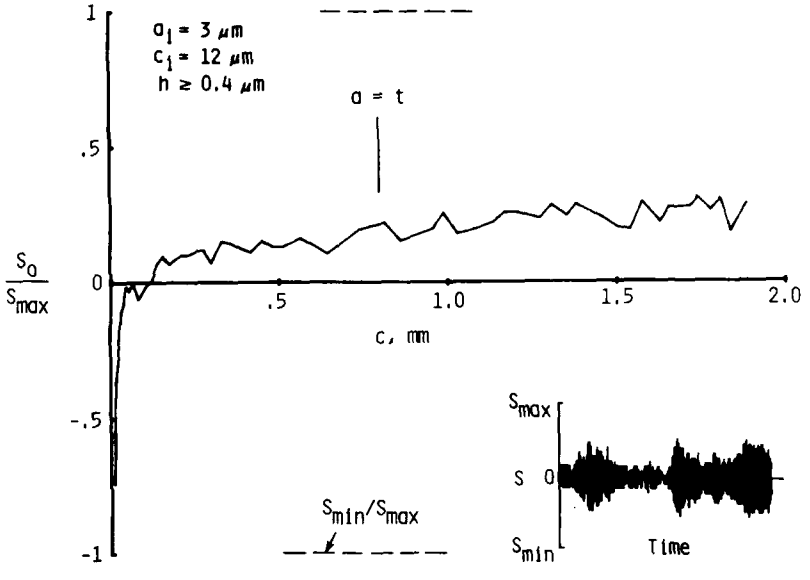

Figure 77.- Calculated crack-opening stresses for GAUSSIAN loading.

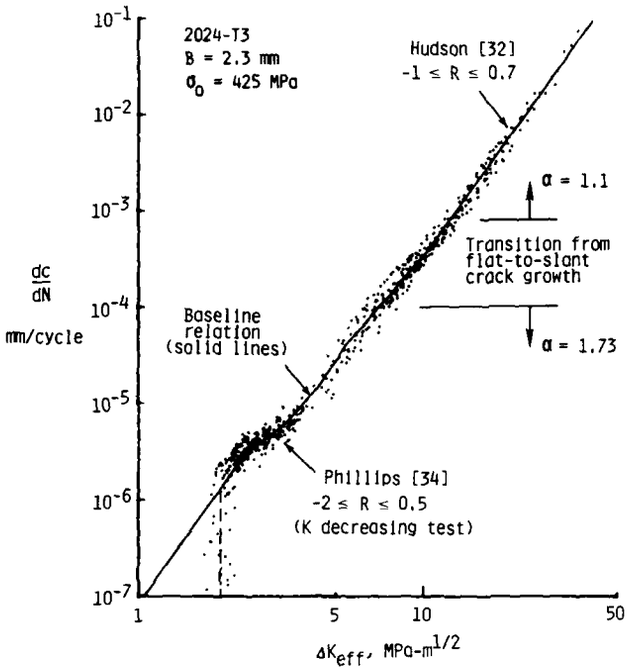

Figure 78.- Effective stress-intensity factor range against crack-growth rates for long cracks.

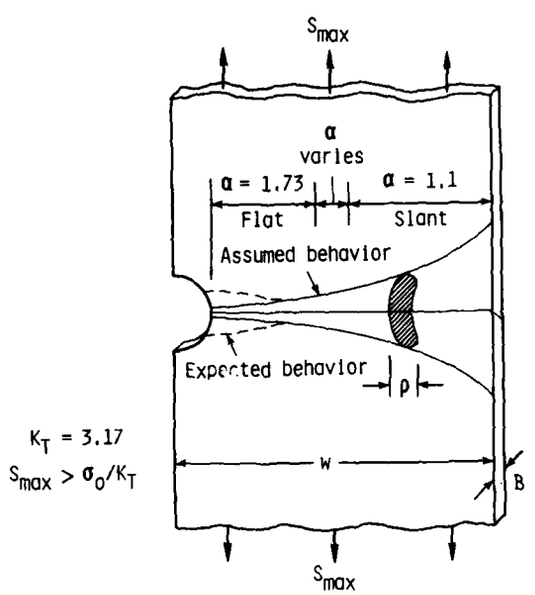

Figure 79.- Schematic of constraint variations along crack line.

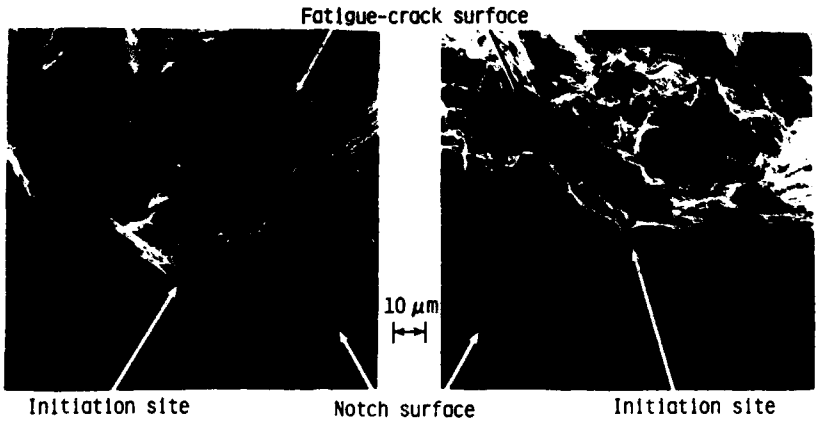

Figure 80.- Typical initiation sites at edge of notch under constant-amplitude loading (R = -1; 45 degree tilt).

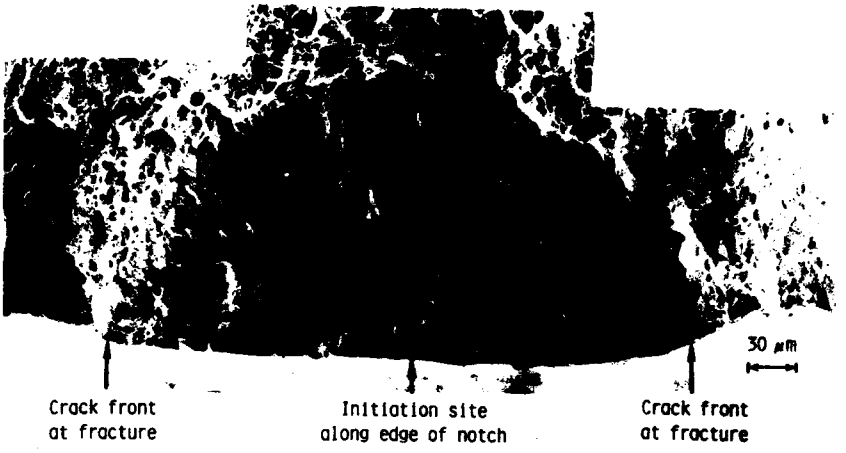

Figure 81.- Surface-crack shape early in fatigue life under constant-amplitude loading (R = -1).

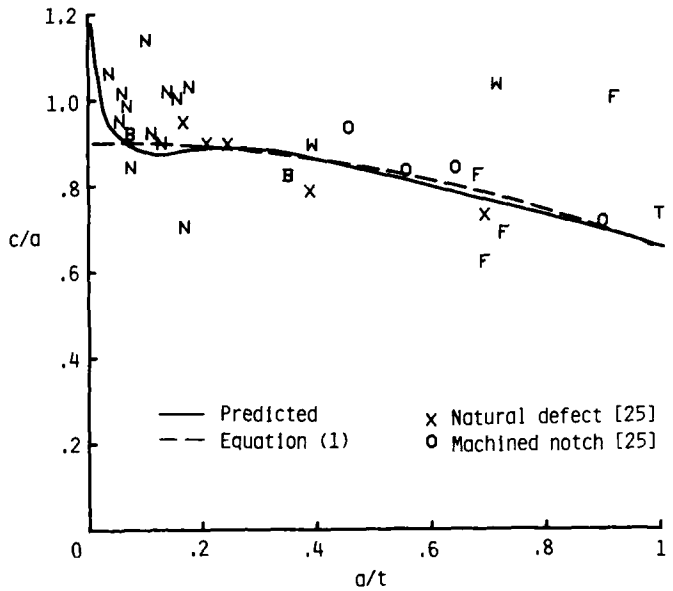

Figure 82.- Comparison of experimental and predicted surface-crack shapes.

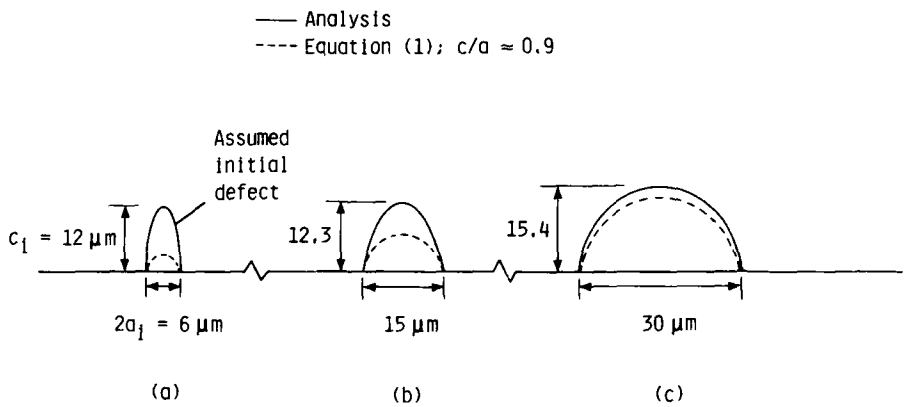

Figure 83.- Progression of crack shapes from crack-growth analysis and calculated from equation (1).

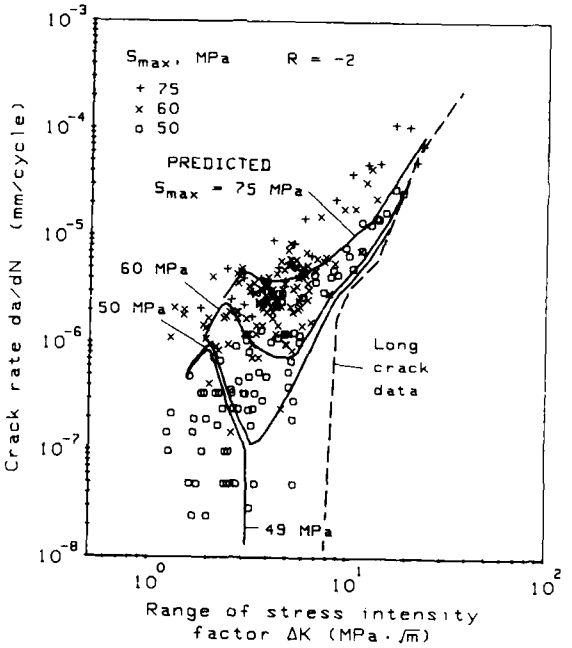

Figure 84.- Experimental and predicted crack-growth rates for short cracks under R = -2 loading.

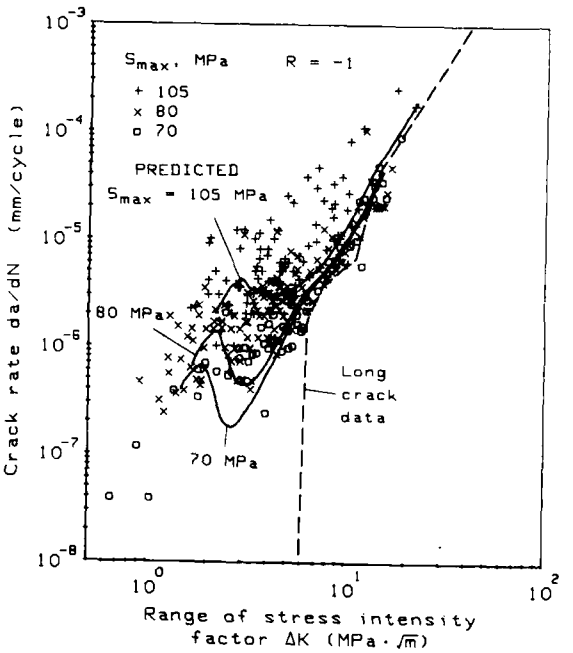

Figure 85.- Experimental and predicted crack-growth rates for short cracks under R = -1 loading.

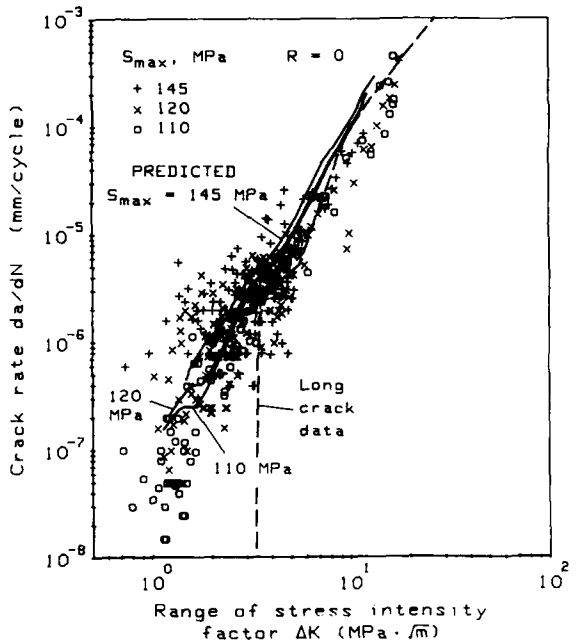

Figure 86.- Experimental and predicted crack-growth rates for short cracks under R = 0 loading.

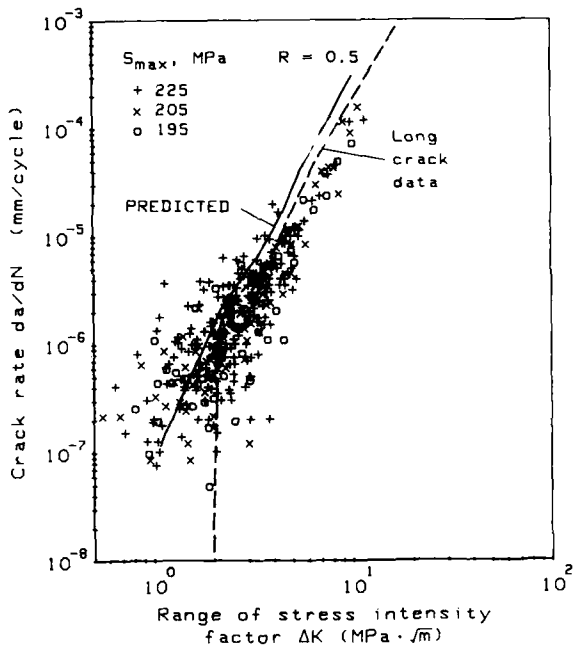

Figure 87.- Experimental and predicted crack-growth rates for short cracks under R = 0.5 loading.

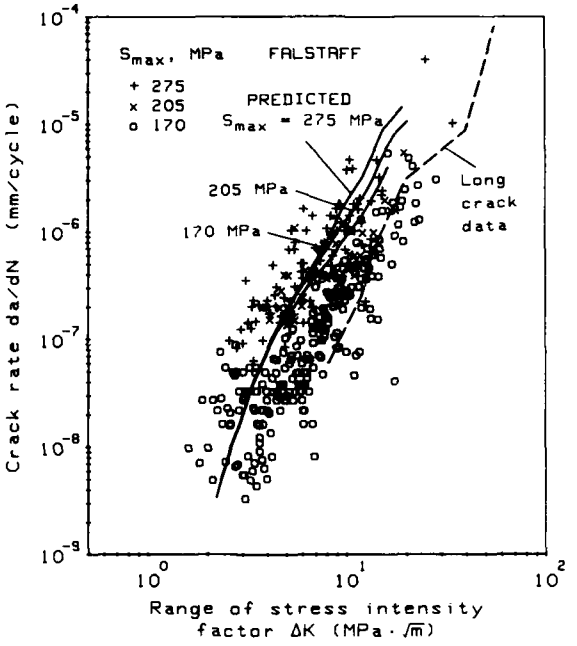

Figure 88.- Experimental and predicted crack-growth rates for short cracks under FALSTAFF loading.

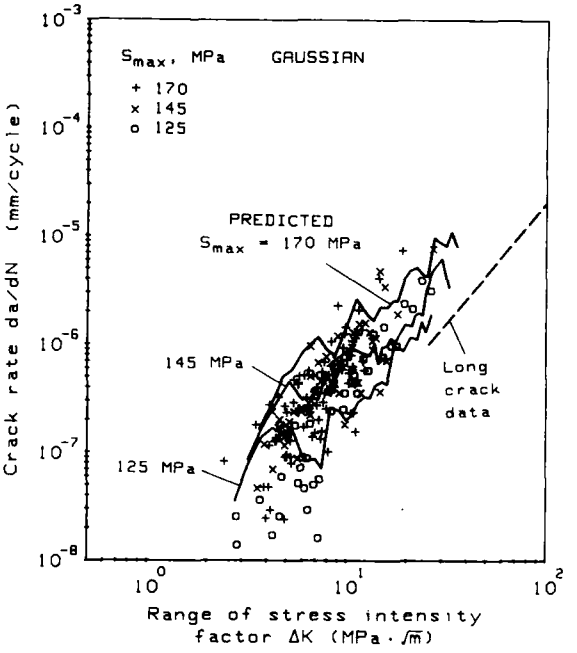

Figure 89.- Experimental and predicted crack-growth rates for short cracks under GAUSSIAN loading.

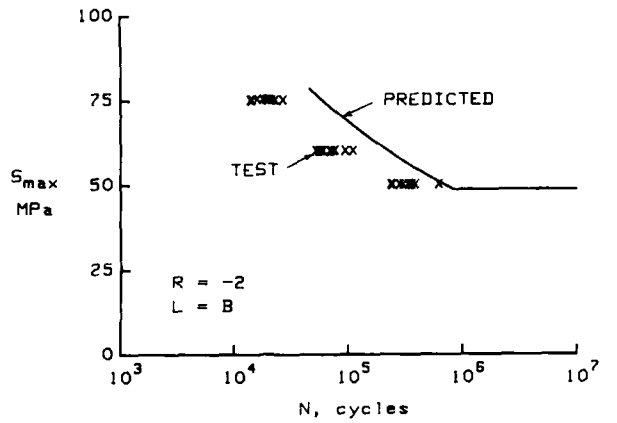

Figure 90.- Experimental and predicted fatigue life to breakthrough under constant-amplitude loading at R = -2.

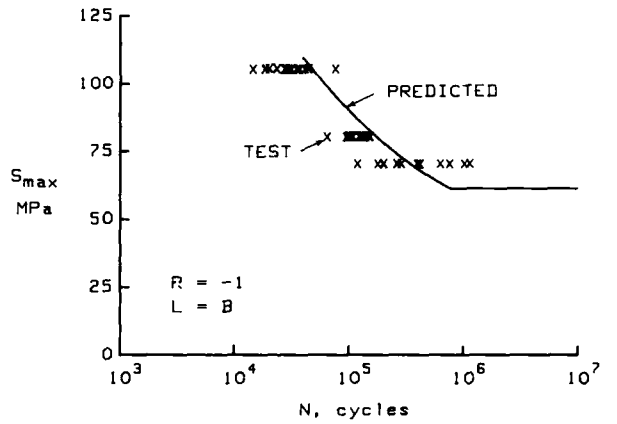

Figure 91.- Experimental and predicted fatigue life to breakthrough under constant-amplitude loading at R = -1.

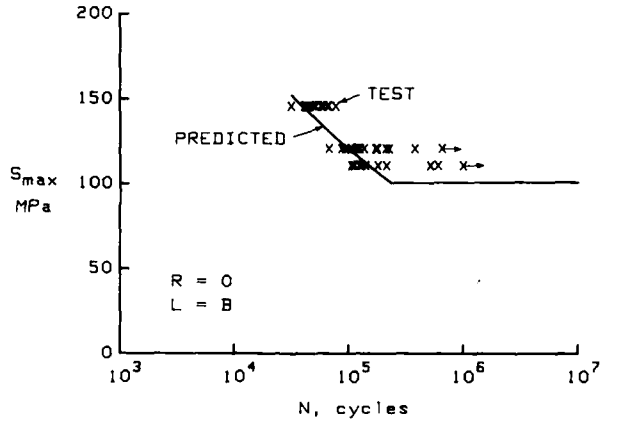

Figure 92.- Experimental and predicted fatigue life to breakthrough under constant-amplitude loading at R = 0.

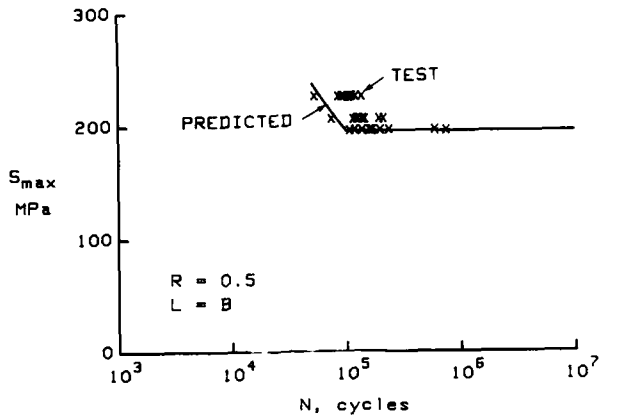

Figure 93.- Experimental and predicted fatigue life to breakthrough under constant-amplitude loading at R = 0.5.

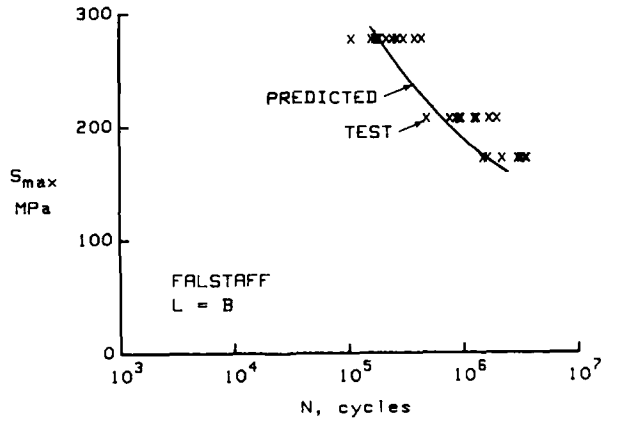

Figure 94.- Experimental and predicted fatigue life to breakthrough under FALSTAFF loading.

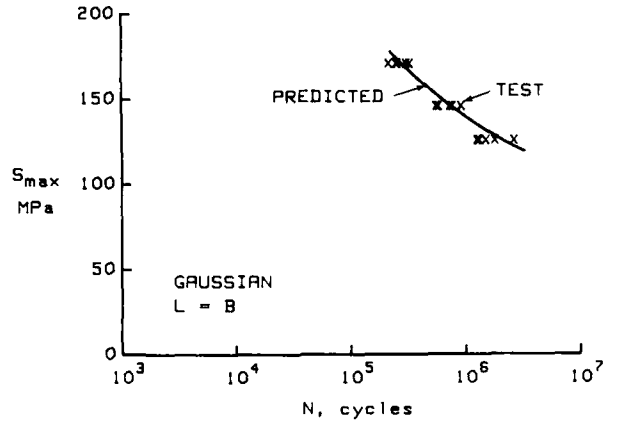

Figure 95.- Experimental and predicted fatigue life to breakthrough under GAUSSIAN loading.

ANNEX A

MICROSTRUCTURAL EXAMINATION OF CORE-PROGRAMME MATERIAL

R.J.H. Wanhill
National Aerospace Laboratory NLR
Amsterdam, The Netherlands

This annex describes the microstructure of the 2.3 mm thick 2024-T3 aluminum alloy sheet used in the core programme. The significance of microstructure for fatigue crack growth in the low stress intensity regime is briefly discussed. The results are based on an extensive compilation and analysis of data for five different batches of 2024-T3 and T351 [47].

MICROSTRUCTURAL ANALYSIS

Transmission electron microscopy of thin foils was used to derive dispersoid spacings and determine whether subgrains were present. Optical metallography was used to measure grain dimensions by the line intercept method.

Dispersoid spacings were determined from at least five sample areas per material. For each area the number of dispersoids was counted and the foil thickness determined by measuring the width of slip traces as a function of tilt angle. This enabled derivation of N_v, the number of dispersoids per unit volume. The average size of the dispersoids was also estimated. The dispersoids were approximately cylindrical with diameter $d = 0.07$ μm and length $\ell = 0.21$ μm. The long axis was aligned with the longitudinal (L) direction in the sheet. Assuming an otherwise random distribution of dispersoids, the appropriate spacing for interaction with gliding dislocations is the average distance from a dispersoid to its nearest two, three or four neighbours [47]. This mean planar distance between dispersoids can be derived from the treatment given by Martin [48]. The results for the longitudinal (L), long transverse (T) and short transverse (S) directions in the sheet are

$$\text{L direction:} \quad \lambda = [1.25/(N_v d)^{1/2}] - \ell \tag{A1}$$

$$\text{T,S directions:} \quad \lambda = [1.25/(N_v d)^{1/2}] - d \tag{A2}$$

The values for mean dispersoid spacing calculated from equations (A1) and (A2) are listed in Table A1.

No subgrains were observed in the thin foils of the core programme material. Grain size determinations were based on at least thirty separate measurements of line intercepts. Results are given in Table A1.

SIGNIFICANCE OF MICROSTRUCTURAL PARAMETERS FOR FATIGUE CRACK GROWTH

Low stress intensity constant amplitude fatigue crack growth curves for long cracks in aluminum alloys show several "knees" or transitions. This is illustrated in Figures A1 and A2. Yoder [49] and Stofanak [50] have shown for 7000 series and 6000 series aluminum alloys, respectively, that these transitions correspond to loading conditions where the monotonic or cyclic plane strain plastic zone dimensions become equal to characteristic microstructural dimensions such as dispersoid spacing, subgrain size or grain size.

A proper description of plastic-zone sizes and shapes is difficult to obtain. This is especially true for plane strain and cyclic loading conditions. Hahn et al [51,52] used an etching technique to reveal plane strain monotonic and cyclic plastic zones in the interiors of thick specimens of Fe-3Si steel. They proposed the following dimensions of the monotonic and cyclic plastic zones in the x and y directions:

Monotonic plane strain:

$$r_x = 0.03\ (K_{max}/\sigma_y)^2 \tag{A3}$$

$$r_y = 0.13\ (K_{max}/\sigma_y)^2 \tag{A4}$$

Cyclic plane strain (R = 0.1):

$$r_x^c = 0.0075\ (\Delta K/\sigma_y^c)^2 \tag{A5}$$

$$r_y^c = 0.033\ (\Delta K/\sigma_y^c)^2 \tag{A6}$$

where σ_y^c is the cyclic yield stress.

Kang and Liu [53] used a Moire grille method to measure surface plastic zone sizes for 2024-T351. By analogy with the results of Hahn et al [52] they suggested that the plane strain cyclic plastic zone is about five times smaller than the cyclic plastic zone at the specimen surface. With this assumption they obtained:

$$\text{Cyclic plane strain (R = 0.1):} \quad r_y^c = 0.036\ (\Delta K/\sigma_y^c)^2 \tag{A7}$$

which is in good agreement with equation (A6).

Kang and Liu [53] reported the monotonic and cyclic yield stresses of 2024-T351 to be 359 MPa and 462 MPa, respectively. These data and Newman's crack closure model for simulated plane strain [27] enable substituting σ_y for σ_y^c and ΔK_{eff} for ΔK in equations (A5)-(A7). The averaged results are

Cyclic plane strain:

$$r_x^c = 0.0068\ (\Delta K_{eff}/\sigma_y)^2 \tag{A8}$$

$$r_y^c = 0.0314\ (\Delta K_{eff}/\sigma_y)^2. \tag{A9}$$

Equations (A8) and (A9) apply for any R and can be used when cyclic yield stress data for particular samples of 2024-T3 and T351 are not available.

Relations for r_y and r_y^c are particularly important because they determine the maximum extent of the plastic zones. This is illustrated in Figure A3 which gives schematic drawings of the plane strain monotonic and cyclic plastic zones [51,52] with r_x, r_y, r_x^c and r_y^c determined by equations (A3), (A4), (A8) and (A9), respectively. Also shown is a first estimate of the cyclic plastic zone obtained when cyclic strain hardening (or softening) and crack closure are neglected [54]. This is a significant overestimate by more than 80 percent. Thus cyclic strain hardening and crack closure in 2024-T3 and T351 cannot be ignored.

Multilinear plots as shown in Figure A1 were fitted to the fatigue crack growth rate data. Values of ΔK at the transition points T_1, T_2 and T_3 and of ΔK_{th} were determined and are given in Table A2. Newman's crack-closure model was used to calculate $(\Delta K_{eff})_{th}$ and ΔK_{eff} at the crack growth curve transition points. These values are also listed in Table A2. Monotonic and cyclic plastic zone sizes at the crack growth curve transitions were calculated using equations (A3), (A4), (A8) and (A9) with σ_y = 359 MPa and the appropriate K_{max} and ΔK_{eff} values. These results are given in Table A3.

As previously stated there was no evidence of subgrains in this material. However, during fatigue cycling a dislocation cell structure develops in the cyclic plastic zone. The cell walls are thought to be effective barriers to localised slip at intermediate crack growth rates when the cyclic plastic zone dimensions are significantly less than the dislocation cell size. These microstructural barriers have little influence at high crack growth rates ($da/dN > 10^{-7}$ m/cycle) where crack growth occurs by multiple slip during each cycle. Using a model developed by Lucas and Gerberich [55] the effective dislocation cell size was estimated to be 0.64-1.67 μm.

Comparison of monotonic and cyclic plastic zone dimensions with the microstructural dimensions previously discussed suggests the following correlations at the crack growth curve transition points:

T_1: cyclic plastic zone dimensions ≈ mean planar distance between dispersoids

T_2: cyclic plastic zone dimensions ≈ subgrain and dislocation cell sizes

T_3: monotonic plastic zone dimensions ≈ grain dimensions

The transitions are also associated with changes in fracture surface topography. Between ΔK_{th} and T_2 the fracture surfaces are faceted. Above T_2 there is a gradual change to continuum mode fracture characterized by fatigue striations. Also, the fracture surface roughness just above T_1 is significantly greater than the roughness below T_1 and the roughness at and above T_2.

SUMMARY

An overview of the low stress intensity fatigue crack growth characteristics of long cracks in 2024-T3 and T351 is given in Figure A4. This overview and detailed microstructural and fractographic observations have been used to explain the shape of the low stress intensity fatigue crack growth curve for long cracks and the transitions T_1, T_2 and T_3 [47].

Table A1. Characteristic microstructural dimensions for the core-programme material.

Mean Planar Distance Between Dispersoids (μm)		Subgrain size (μm)	Grain Dimensions (μm)	
L[a]	0.65 ± 0.12	(b)	L	108 ± 45
T[a]	0.43 ± 0.07	(b)	T	59 ± 23
S[a]	0.43 ± 0.07	(b)	S	29 ± 7

(a) L = longitudinal, T = long transverse, and S = short transverse.
(b) Not observed.

Table A2. Stress intensity factor range at crack growth transitions and threshold.

R	ΔK_{th} [a]	ΔK at transition			$(\Delta K_{eff})_{th}$	ΔK_{eff} at transition		
		T_1	T_2	T_3		T_1	T_2	T_3
-2	8.29	9.28	15.0	23.3	2.50	2.80	4.53	7.04
-1	5.90	6.50	11.9	14.4	2.42	2.67	4.88	5.90
0	3.35	3.65	6.07	8.57	2.51	2.74	4.55	6.43
.5	1.98	2.23	4.10	6.40	1.94	2.19	4.02	6.27

(a) Stress intensity factors ranges given in MPa-$m^{1/2}$.

Table A3. Estimates of plane strain monotonic and cyclic plastic zone sizes (mm) at crack growth transitions.

(a) Monotonic plastic zone size

R	T_1		T_2		T_3	
	r_x	r_y	r_x	r_y	r_x	r_y
-2	2.23	9.65	5.82	25.2	14.0	60.8
-1	2.46	10.7	8.24	35.7	12.1	52.2
0	3.10	13.4	8.58	37.2	17.1	74.1
.5	4.63	20.1	15.7	67.8	38.1	165.0

(b) Cyclic plastic zone size

R	T_1		T_2		T_3	
	r_x^c	r_y^c	r_x^c	r_y^c	r_x^c	r_y^c
-2	0.41	1.91	1.08	5.00	2.61	12.1
-1	0.38	1.74	1.26	5.80	1.84	8.48
0	0.40	1.83	1.09	5.04	2.18	10.1
.5	0.25	1.17	0.85	3.94	2.07	9.58

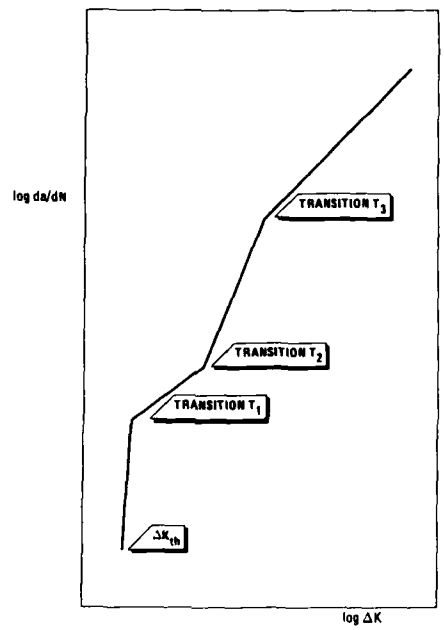

Figure A1.- Schematic constant amplitude fatigue crack growth plot for aluminium alloys.

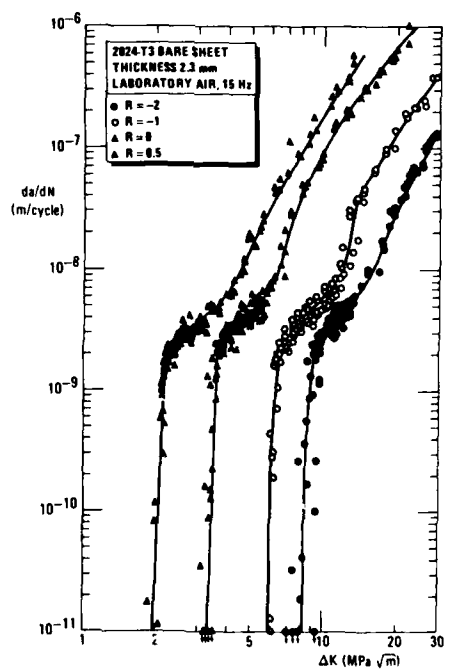

Figure A2.- Constant amplitude fatigue crack growth rates for 2.3 mm thick 2024-T3 sheet.

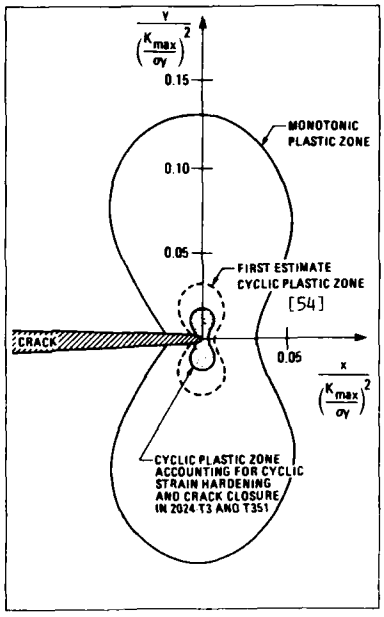

Figure A3.- Schematic drawing of plastic zones for constant amplitude cyclic loading with R = 0.

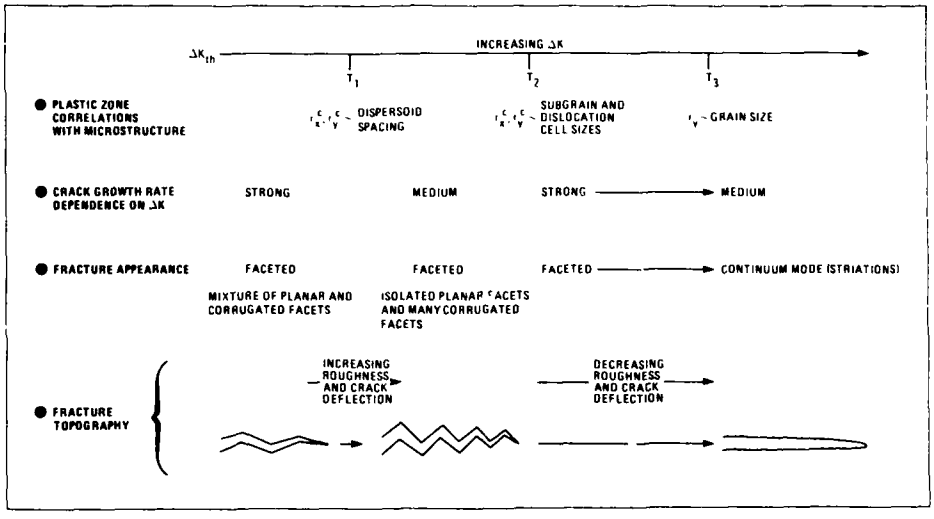

Figure A4.- Low stress intensity factor fatigue crack growth characteristics of 2024-T3 and T351.

ANNEX B

PRELIMINARY FATIGUE TESTS ON SHORT-CRACK SPECIMENS

J. C. Newman, Jr. and E. P. Phillips
NASA Langley Research Center
Hampton, Virginia, USA

and

M. H. Swain
Planning Research Corporation
Hampton, Virginia, USA

The objective of the preliminary fatigue tests was to determine the stress levels to be used by the participants in the Cooperative Test Programme (see Table 2). As previously mentioned, the United States Air Force Wright-Patterson Aeronautical Laboratory machined about 700 single-edge-notched tension (SENT) specimens from material supplied by the NASA Langley Research Center. In addition, NASA Langley machined about 50 SENT specimens from the same material. Comparison of fatigue tests conducted on the two sets of specimens indicated a large difference in fatigue behaviour under constant-amplitude loading. A recovery programme was initiated to resolve this difference before the specimens were distributed to participants. The following sections describe the recovery programme and the preliminary fatigue tests and analyses conducted to determine stress levels for constant-amplitude, FALSTAFF, and GAUSSIAN loading.

Recovery Programme.- In the original programme, all specimens were to be chemically polished for one minute to remove machining marks and to debur the edges of the notch (see Section 3.2). While Wright-Patterson was machining the core-programme specimens, Langley was testing specimens under constant-amplitude loading. Figure B1 shows a comparison of fatigue lives for the one-minute polished Langley (L-1) and Wright-Patterson (WP-1) specimens. A large difference in fatigue life was observed at $R = 0$ conditions, but a small difference was shown at $R = -1$ conditions. The solid curves show the results of a crack-propagation analysis using a small initial surface crack located at the center of the notch, as shown in Figure 15(a). The size of the crack was selected to fit the fatigue life of the Wright-Patterson specimens at $R = -1$. At $R = 0$, the solid curve was predicted using the same initial crack size.

On the basis of the test results, a machining residual-stress problem was suspected. To determine the problem and to eliminate the suspected residual stresses, three small test programmes were initiated. First, several Langley and Wright-Patterson (one-minute polished) specimens were strain gauged along the notch root to determine the notch-root strains during yielding. Second, a cyclic preload-shakedown procedure was applied to several specimens, prior to fatigue testing. The cyclic preload caused the notch root to yield. And third, several specimens were chemically polished for either three or five minutes.

The results from the strain-gauged specimens indicated that the Wright-Patterson specimens had a residual-compressive stress of 70 to 95 MPa, whereas the Langley specimens had a residual-compressive stress of about 15 MPa. These results were consistent with the fatigue lives shown in Figure B1. Strain-gauged specimens (five-minute polish) indicated that the notch root would yield when the normal stress was slightly lower than the uniaxial yield stress of the material (at about the proportional limit). The experimental evaluation of the stress concentration (K_T) indicated a value of 3.21 ± 0.1 (about 1.3 percent higher than the analytical evaluation). The gauges had about a 1-mm gauge length and were located across the middle half of the notch root.

The cyclic preload-shakedown procedure was composed of 30 cycles and was designed to yield the notch root under tension and compression loading ($R = -1$), thereby relieving the residual stresses. The maximum stress on the first cycle was 135 MPa and the initial yield-zone size was about 0.5 mm at the notch root. On each successive cycle, the maximum stress was reduced by 1 percent. During the last few cycles, the stress range at the notch root was well below the elastic limit.

Figure B2 compares the fatigue lives for the Langley one-minute polished (L-1) specimens, the Wright-Patterson (WP) specimens that were polished for either one-, three-, or five-minutes, and the preloaded (WP-P) specimens. The dashed line shows the level of preload. Results were obtained at only one stress level for each R ratio. Again, the lower solid curve was a crack-propagation analysis fit to the $R = -1$ Wright-Patterson specimen data. The upper solid curve was predicted using the same initial crack size. For $R = 0$, the five-minute polished and preloaded specimens gave the shortest fatigue lives and they agreed very well with the predicted results. At $R = -1$, however, the fatigue lives for the one- and five-minute polished specimens agreed. The preload specimens gave a much longer life than expected. The preload, however, was substantially higher than the test load. There may have been some retardation behaviour for short cracks that initiated under the preload cycles. There was very little difference between the preload and the maximum test load for the $R = 0$ condition. On the basis of these limited tests and analyses, the five-minute chemical polishing procedure (see Section 3.2) was selected for the core programme.

Fatigue Tests Under Core-Programme Conditions.- Preliminary fatigue tests were conducted on the five-minute polished SENT specimens (see Figure 6(b)) under the loading conditions selected for the core programme. A crack-propagation analysis using the closure model (see Section 5.2) was also employed to establish the stress levels and fatigue life to breakthrough in Table 2.

Figure B3 shows the results of fatigue tests conducted at $R = -1$ for various stress levels. For all the tests, the notch-root stresses were elastic (see Table 6). A symbol indicates a failure and a symbol with an arrow indicates that the test was terminated prior to failure. To predict fatigue life, a ΔK_{eff}-rate relation (see Section 6.1), an initial defect (or crack) size, and an effective stress-intensity factor threshold are needed. The initial defect size and threshold value were obtained by

matching calculated fatigue lives to the experimental data. Because the inclusion clusters near the notch surface were elongated in the c-direction (see Figs. 5 and 80), the initial crack aspect ratio $(a/c)_i$ was chosen as 0.25. Also, the defect height was chosen as 0.4 μm or greater. Calculations of fatigue life were then made for various initial surface-crack half-lengths in the a-direction. The computed results for a_i = 3 μm with a $(\Delta K_{eff})_{th}$ of 1.05 MPa-$m^{1/2}$ agreed reasonably well with the test data. The threshold value was selected so that the calculated life would match the fatigue limit. These values were chosen as the initial conditions and were used to make life predictions for other core-programme loadings.

Other fatigue tests were conducted under constant-amplitude loading at stress ratios of 0.5, 0 and -2. Figures B4 and B5 show the experimental results and the predictions of fatigue life made for each stress ratio. The predicted fatigue life and fatigue limit agreed well with the test data for each stress ratio.

A limited number of fatigue tests were also conducted under spectrum loading using the FALSTAFF and GAUSSIAN load spectra. Specimens that had been prepared using both the one- and five-minute polishing procedures were tested. Because the maximum applied stress levels in most of the spectrum tests were such that the notch root would yield, any residual stress differences between the one- and five-minute polished specimens should be minimized.

The results for the FALSTAFF tests are shown in Figure B6. A typical load sequence for the spectrum is shown in the insert. The maximum and minimum stresses to be applied in the spectrum are shown as indicated. Again, using the same initial conditions, the closure model was used to predict fatigue lives. The predicted lives were somewhat less than the test lives for both the one- and five-minute polished specimens. The ratio of predicted to test life ranged from 0.4 to 0.9. The short life predictions may have been due to the use of an improper "constraint" factor for short cracks (see Section 6.1). As previously discussed, the model uses a constraint factor of 1.73 for short cracks (growth rates less than 9.0 × 10^{-5} mm/cycle). However, the notch root was probably under a state of plane stress because the sheet material would not have been thick enough to develop plane-strain conditions. Crack-growth delay under spectrum loading for plane-stress conditions (α = 1.1) would have been greater than that under α = 1.73 conditions, and thus the predicted lives would have been greater than those shown in Figure B6.

The GAUSSIAN test results are shown in Figure B7. These tests were conducted by P. R. Edwards at the Royal Aircraft Establishment using specimens prepared at NASA Langley. Again, a typical load sequence for the spectrum (R = -1) is shown in the insert. The maximum and minimum applied stresses that would occur during the one-million cycle spectrum are indicated. Most of the tests were terminated when a crack had penetrated the sheet thickness (2a = B). One test was taken to complete failure (solid symbol). The closure model was then used to predict crack growth and fatigue life from the same initial defect size as used previously. The dashed curve shows the predicted life to breakthrough (2a = B). These results were in good agreement with both the one- and five-minute polished specimen results. The solid curve shows the predicted cycles to failure. Again, the predicted life agreed well with the single total-life test result.

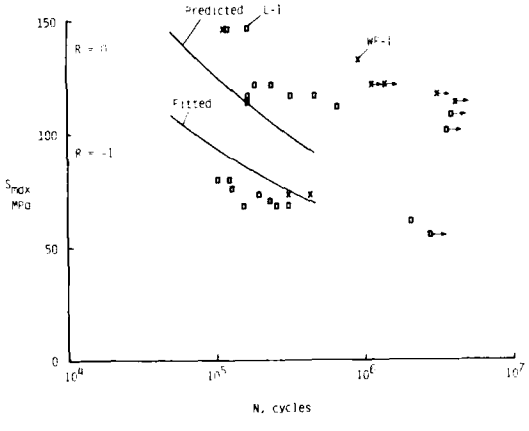

Figure B1.- Comparison of fatigue life for one-minute polished specimens from NASA Langley and Wright-Patterson Air Force Base.

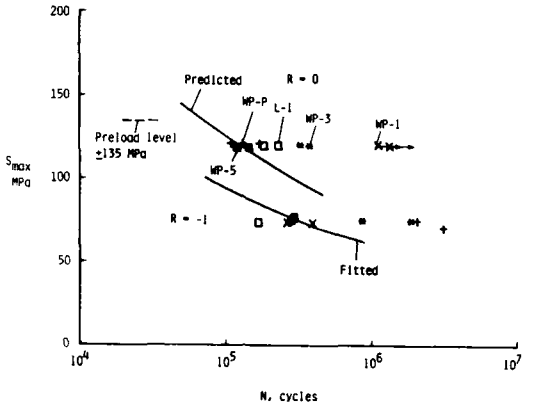

Figure B2.- Influence of polishing and cyclic preload on fatigue life under constant-amplitude loading at two R-ratios.

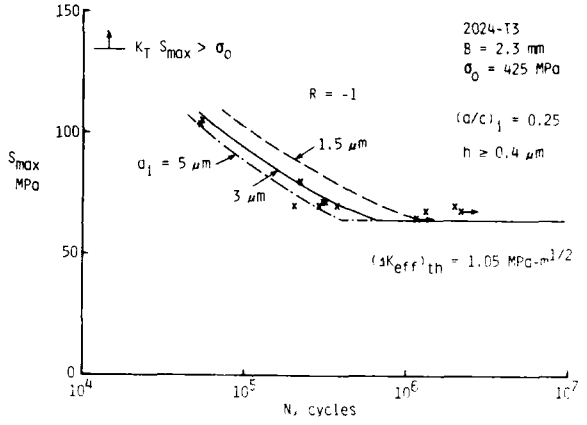

Figure B3.- Experimental and calculated fatigue life for various initial defect sizes under R = -1 loading.

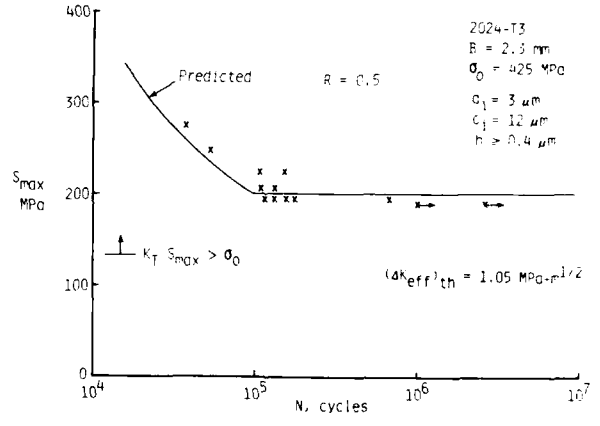

Figure B4.- Experimental and predicted fatigue life under R = 0.5 loading.

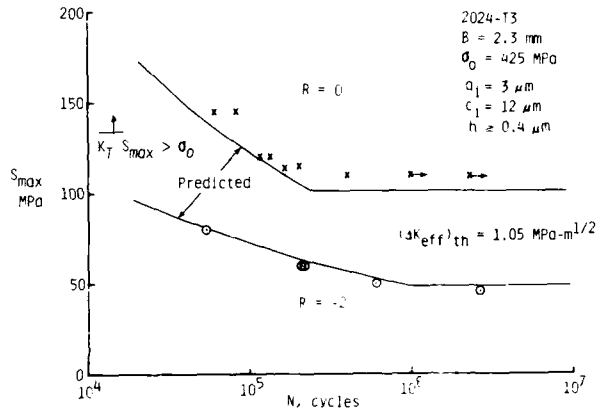

Figure B5.- Experimental and predicted fatigue life under R = 0 and R = -2 loading.

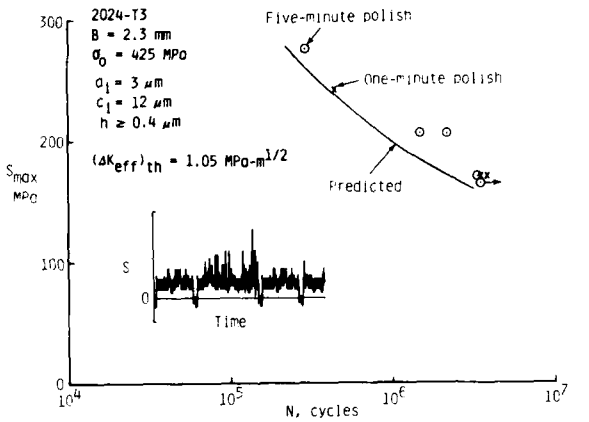

Figure B6.- Experimental and predicted fatigue life under FALSTAFF loading.

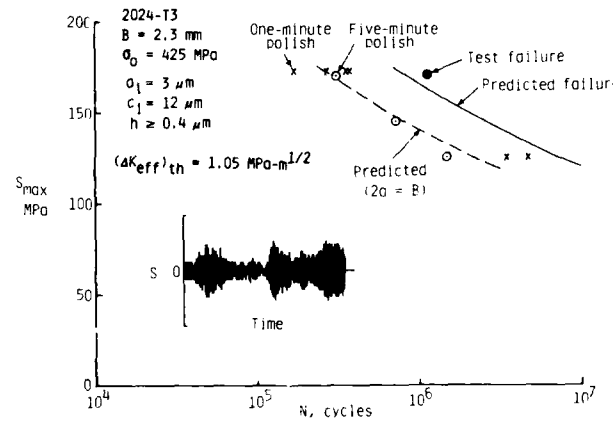

Figure B7.- Experimental and predicted fatigue life to breakthrough and failure under GAUSSIAN loading.

ANNEX C

ALIGNMENT VERIFICATION PROCEDURES

P. R. Edwards
Royal Aircraft Establishment
Farnborough, Hants, England

and

E. P. Phillips and J. C. Newman, Jr.
NASA Langley Research Center
Hampton, Virginia, USA

Each laboratory was required to align their test machines and gripping fixtures to produce a nearly uniform tensile stress field on an un-notched sheet specimen. The blank specimens (50 mm wide by 305 mm long by 2.3 mm thick) supplied by the coordinators were strain gauged as shown in Figure C1. Strain gauge readings were taken at all gauges (n = 1 through 10). The alignment verification procedures are as follows:

1. Zero all strain gauges while specimen is in a free-supported condition.

2. Put strain-gauged specimen in the test machine so that specimen "front" face (face 1) is in contact with "reference jaw" (standard position of specimen), tighten grips, and at zero load measure strains on all gauges. (ε_{nS0} is strain at gauge n, standard position, zero load).

3. With specimen in machine and at a tensile load of 10 kN measure strains (specimen in standard position). (Strain = ε_{nS10})

4. Remove specimen from machine. Put specimen in machine so that specimen "back" face (face 2) is in contact with "reference jaw" (reverse position of specimen), tighten grips, and at zero load measure strains on all gauges. (Strain = ε_{nR0})

5. With specimen in machine and at tensile load of 10 kN measure strains (specimen in reverse position). (ε_{nR10} is strain at gauge n, reverse position, 10 kN load).

The total range of bending strain at any position n is given by the difference between ε_{nS} and ε_{nR}. For example, at the center of the specimen (point A) and at a load of 10 kN, the bending strain range is given by

$$\varepsilon_{1S10} - \varepsilon_{1R10} \quad \text{and} \quad \varepsilon_{2R10} - \varepsilon_{2S10}$$

Bending strains are calculated at the three positions on the vertical axis of the specimen A through C. The final values should be the averages of those obtained from opposite gauges, that is, 1 and 2, 3 and 4, and 5 and 6.

The resulting values of bending strain at C, A, and B should be plotted as in Figure C2. The average strains, ε_L and ε_r, as defined in Figure C2 represent strains from lateral and rotational misalignment, respectively. Lateral and rotational misalignment are defined in Figure C3. The jaws of the machine should be aligned such that the lateral and rotational strains at both zero load and a load equal to 10 kN are:

$$\varepsilon_L < 20 \text{ microstrain}$$
$$\varepsilon_r < 10 \text{ microstrain} \qquad \text{Criterion 1}$$

The tensile strain range at point D, ε_{STD}, for the "standard" position is given by

$$\varepsilon_{STE} = \frac{\varepsilon_{7S10} + \varepsilon_{8S10} - \varepsilon_{7S0} - \varepsilon_{8S0}}{2}$$

and the tensile strain range at point E, ε_{STE}, is given by

$$\varepsilon_{STE} = \frac{\varepsilon_{9S10} + \varepsilon_{10S10} - \varepsilon_{9S0} - \varepsilon_{10S0}}{2}$$

The following criterion should be aimed for:

$$0.95 < \frac{\varepsilon_{STD}}{\varepsilon_{STE}} < 1.05 \text{ and } 0.95 < \frac{\varepsilon_{RTD}}{\varepsilon_{RTE}} < 1.05 \qquad \text{Criterion 2}$$

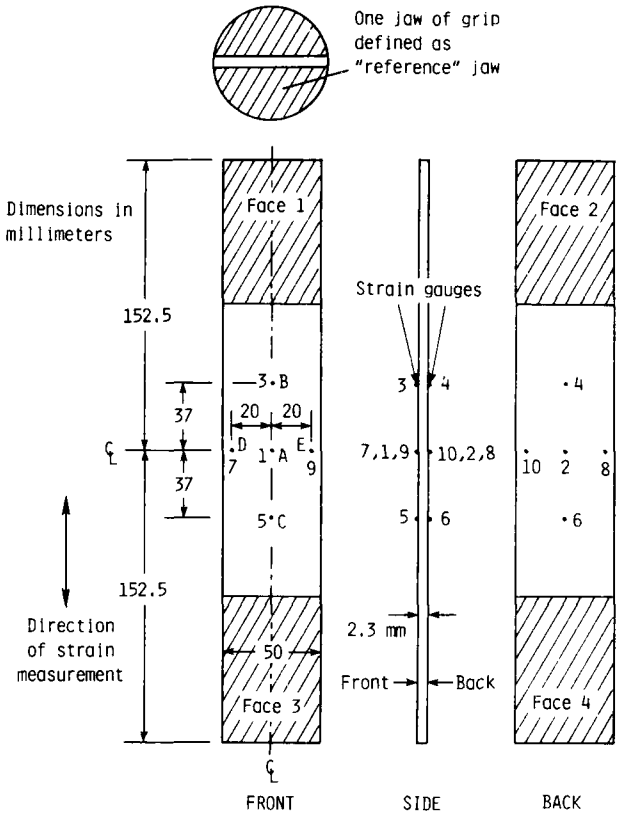

Figure C1.- Strain-gauged specimen for alignment checks.

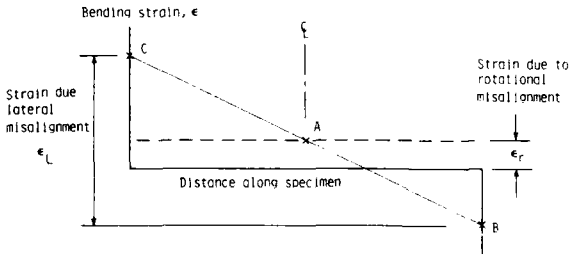

Figure C2.- Idealized plot of measured bending strains at points A, B, and C to determine rotational and lateral misalignment.

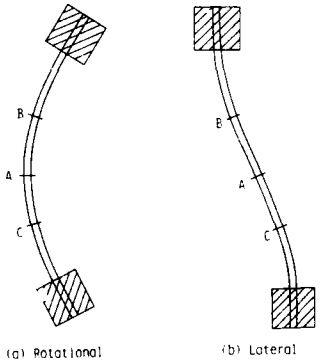

Figure C3.- Forms of misalignment.

ANNEX D

ON-LINE SPECTRUM LOADING ACCURACY VERIFICATION

P. R. Edwards
Royal Aerospace Establishment
Farnborough, Hants
England

Eight laboratories carrying out variable-amplitude load tests using the FALSTAFF spectrum were visited by one of the coordinators (P. R. Edwards) and measurements were taken to assess the accuracy with which the loading sequences were being applied.

The measurements were taken on a portable "Rainflow" counting device which had a resolution of 64 levels. Thus the device was able to measure 64 × 64 triangular Rainflow matrices. All measurements were made on an alignment specimen with central strain gauges on each side of the specimen because these measurements would be more convincing than any taken from the load cell of the servohydraulic fatigue machine. The assessment of the accuracy of loading and whether the actual sequence of loads was correct was done initially by a comparison of Rainflow matrices. However, it was found that all of the conclusions that could be drawn from such comparisons could equally be drawn from simple measurements of peaks and troughs. These measurements were extracted from the Rainflow matrix and are presented herein.

Initially, it was intended that on-line measurements be taken on both the GAUSSIAN and FALSTAFF loading sequences. However, the GAUSSIAN sequence proved very difficult to check. Whereas the FALSTAFF sequence was only 35,966 half-cycles, the GAUSSIAN sequence was just over 1 million cycles. This meant that several runs through the FALSTAFF sequence could be carried out in the course of one day, whereas each run through the GAUSSIAN sequence took a complete day. This meant that there was no time for trial runs, but perhaps more importantly strain-gauge drift, which was normally insignificant over the time that the FALSTAFF sequence was used, compromised the integrity of the much longer GAUSSIAN measurements. Therefore, it was decided that on-line measurements would be taken only on the FALSTAFF sequence. Having proved the capability of a particular machine to apply random loading accurately it was judged sufficient to carry out an off-line verification of the GAUSSIAN sequence. Note that the levels in FALSTAFF are given by the even class numbers. This verification was made in the form of a peak and trough count, and a detailed comparison of the first hundred and last hundred points of the sequence.

The first two columns of Tables D1 and D2 show the results of an off-line peak and trough count, respectively, for the FALSTAFF sequence. Note that the levels in FALSTAFF are given by the even class numbers. The subsequent columns give the on-line measurement results from the various laboratories. The laboratories that carried out variable-amplitude loading are referred to in this Annex as Laboratory 1 to 8 (these numbers are randomly selected and have no reference to any other table in this report). To a minor extent the measurements were affected by the fact that several laboratories were unable to carry out a complete pass through FALSTAFF stopping exactly on 35,966 half-cycles. As a result, occasionally the number of half-cycles recorded was not quite correct for a full pass through FALSTAFF. In these tables, it should be understood that the counting device was set up so that the alternate counting levels straddled the normal 32 FALSTAFF levels. Thus the actual FALSTAFF levels are at half the counting levels, so that counting level 64 represents FALSTAFF level 32 and counting level 2 represents FALSTAFF level 1. It follows that if any counts fall into the adjacent box then they are in error by at least one-quarter of a FALSTAFF interval. The results obtained were variable. In some cases good results were found, but others highlighted specific problems that could have caused significant deviations in fatigue life. All laboratories were presented with the measurements at the time they were taken, so that if there were any problems they could be resolved before testing started. The results from the various laboratories are as follows:

Laboratory 1: As can be seen from a comparison of columns 2 and 3, the results showed what appeared to be a scaling or truncation error. The highest loads recorded were in fact at FALSTAFF level 30, which should have been level 32. The numbers actually recorded, however, suggested that the actual sequence of numbers was accurate.

Laboratory 2: Produced a good set of results with a very small proportion of cycles outside the one-quarter of a FALSTAFF interval.

Laboratory 3: Good set of results.

Laboratory 4: Produced measurements with some wrong values in the various classes of peaks and troughs. This was found to be due to an automatic control system which was malfunctioning at the time. After the fault was repaired, a subsequent set of measurements was taken and produced very good results.

Laboratory 5: Good set of results, but slight truncation on compressive side.

Laboratory 6: Good set of results.

Laboratory 7: Produced results rather similar to those of Laboratory 1 with scaling and truncation errors. This was attributed to excessive bending in the specimen. This laboratory was having considerable problems meeting the requirements defined in Annex C for specimen alignment. On changing the type of machine grips the problem was cured.

Laboratory 8: Good set of results, but slight truncation on compressive side.

In conclusion, all laboratories eventually proved their ability to apply variable-amplitude loading accurately but the results emphasize the need for regular independent checks on loading accuracy in fatigue-testing programmes.

Table D1.- Measured Peak Counts from Laboratories using FALSTAFF.

Class	FALSTAFF (a)	Laboratory							
		1	2	3	4	5	6	7	8
1	0	0	0	0	0	0	0	0	0
2	0	0	0	0	0	0	0	0	0
3	0	0	0	0	0	0	0	0	0
4	0	0	0	0	0	0	0	0	0
5	0	0	0	0	0	0	0	0	0
6	0	0	0	0	0	0	0	0	0
7	0	0	0	0	0	0	0	0	0
8	0	0	0	0	0	0	0	0	0
9	0	0	0	0	0	0	0	0	0
10	0	0	0	0	0	0	0	0	0
11	0	0	0	0	0	0	0	0	0
12	0	0	0	0	0	0	0	0	0
13	0	0	1	0	0	0	0	0	0
14	155	0	154	156	155	155	155	155	58
15	0	155	22	2	0	0	0	0	98
16	445	3	417	444	443	444	445	447	432
17	0	442	0	0	0	1	0	0	12
18	0	0	0	0	0	0	0	0	0
19	0	0	0	0	0	0	0	0	0
20	0	0	0	0	0	0	0	0	0
21	0	0	1	0	0	0	0	1	0
22	43	43	42	43	38	43	43	42	43
23	0	0	0	0	0	0	0	324	0
24	493	493	494	493	529	493	493	170	493
25	0	155	3	0	18	0	0	4048	0
26	4058	3903	4051	4058	4301	4058	4058	12	4058
27	0	1568	4	0	7	0	0	4149	0
28	4145	2577	4140	4145	4323	4145	4145	0	4145
29	0	1987	10	0	2	0	0	1999	0
30	1999	33	1991	1999	1884	1999	1999	0	1999
31	0	1261	5	0	2	0	0	1282	0
32	1282	122	1277	1282	1310	1282	1282	0	1282
33	0	1029	0	0	1	0	0	1153	0
34	1151	622	1151	1152	1113	1151	1151	0	1151
35	0	365	0	0	0	0	0	990	0
36	987	887	987	987	914	987	987	0	987
37	0	67	1	0	1	0	0	956	0
38	954	638	942	954	860	954	954	0	954
39	0	3	11	0	1	0	0	644	0
40	640	532	610	640	595	640	640	3	640
41	0	32	34	0	9	0	0	531	0
42	533	372	528	533	485	533	532	17	533
43	0	148	4	0	3	0	0	387	0
44	404	85	400	404	358	404	397	44	404
45	0	191	1	0	1	0	7	189	0
46	233	2	229	233	210	233	198	119	234
47	0	104	4	0	0	0	35	75	0
48	193	0	170	193	177	193	134	81	193
49	0	76	23	0	0	0	59	23	0
50	104	2	79	93	97	104	25	68	104
51	0	43	25	11	1	0	79	8	0
52	76	9	52	76	66	76	9	43	76
53	0	15	24	0	0	0	67	2	0
54	45	10	15	45	42	45	1	22	45
55	0	0	30	0	0	0	44	2	0
56	24	7	23	2	20	24	0	8	24
57	0	0	1	23	0	0	24	0	0
58	10	0	10	9	7	10	0	7	10
59	0	0	0	1	0	0	10	0	0
60	7	2	4	6	7	7	0	0	7
61	0	0	3	0	0	0	7	0	0
62	0	0	0	0	0	0	0	1	0
63	0	0	0	2	0	0	0	0	0
64	2	0	2	0	2	2	2	0	2
SUM	17983	17983	17975	17986	17982	17983	17983	18002	17984

(a) FALSTAFF levels are given by even class numbers.

Table D2.- Measured Trough Counts from Laboratories using FALSTAFF.

Class	FALSTAFF (a)	Laboratory							
		1	2	3	4	5	6	7	8
1	0	1	0	0	0	0	1	0	0
2	2	0	2	1	2	3	2	0	0
3	0	2	0	1	0	0	0	1	2
4	2	0	2	1	2	2	2	0	0
5	0	2	0	1	0	0	0	2	2
6	1	0	1	1	1	1	1	0	0
7	0	1	0	1	0	0	0	1	1
8	6	3	6	5	6	6	6	0	0
9	0	3	2	2	0	0	0	6	6
10	327	327	325	327	327	327	327	308	145
11	0	9	4	2	0	0	12	18	182
12	508	498	498	505	505	506	495	294	19
13	0	0	0	1	0	1	1	218	489
14	36	36	35	36	30	36	35	25	34
15	0	134	2	0	0	0	1	11	2
16	543	409	542	543	500	543	542	538	543
17	0	1773	2	1	0	0	1	7	0
18	1941	245	1939	1943	1974	1941	1940	1943	1941
19	0	6634	5	8	0	0	1	0	0
20	6711	1275	6704	6701	6044	6711	6710	6716	6711
21	0	3112	3	1	0	0	0	0	0
22	4387	637	4384	4385	4413	4387	4387	4391	4387
23	0	808	0	7	32	0	0	0	0
24	1445	622	1445	1438	1329	1445	1445	1446	1445
25	0	94	2	0	51	0	0	0	0
26	716	511	714	716	618	716	716	716	716
27	0	18	0	0	5	0	0	1	0
28	511	309	511	511	457	511	511	511	511
29	0	94	0	0	6	0	0	18	0
30	327	140	327	327	305	327	327	309	327
31	0	110	1	0	0	0	0	100	0
32	234	25	233	235	217	234	234	136	234
33	0	68	0	0	0	0	0	108	0
34	135	1	135	135	125	135	135	27	135
35	0	37	1	0	0	0	0	62	0
36	69	3	68	69	56	69	69	7	69
37	0	20	1	0	0	0	0	37	0
38	37	8	35	37	36	37	37	0	37
39	0	4	1	0	0	0	0	23	0
40	23	4	22	23	21	23	23	0	23
41	0	0	2	0	0	0	0	12	0
42	12	3	11	9	12	12	12	0	12
43	0	0	1	3	0	0	0	4	1
44	4	2	3	3	3	4	3	0	4
45	0	0	0	1	0	0	1	3	0
46	3	1	3	2	2	3	0	0	3
47	0	0	0	1	0	0	3	2	0
48	2	0	2	0	2	2	0	0	2
49	0	0	0	2	0	0	2	1	0
50	1	0	1	0	1	1	0	0	1
51	0	0	0	1	0	0	1	0	0
52	0	0	0	0	0	0	0	0	0
53	0	0	0	0	0	0	0	0	0
54	0	0	0	0	0	0	0	0	0
55	0	0	0	0	0	0	0	0	0
56	0	0	0	0	0	0	0	0	0
57	0	0	0	0	0	0	0	0	0
58	0	0	0	0	0	0	0	0	0
59	0	0	0	0	0	0	0	0	0
60	0	0	0	0	0	0	0	0	0
61	0	0	0	0	0	0	0	0	0
62	0	0	0	0	0	0	0	0	0
63	0	0	0	0	0	0	0	0	0
64	0	0	0	0	0	0	0	0	0
SUM	17983	17983	17975	17986	17982	17983	17983	18002	17984

(a) FALSTAFF levels are given by even class numbers.

ANNEX E

SUGGESTED PLASTIC-REPLICA METHOD

M. H. Swain
Planning Research Corporation
Hampton, Virginia, USA

Cleaning and Etching of Notch Surface.- The participants received the specimens in the chemically-polished condition with the specimen number inscribed at each end. Prior to testing, the notch area was cleaned with acetone and then ethanol was applied with a swab. The notch surface could be etched by swabbing with Keller's etchant for 25 seconds. The specimen was rinsed in distilled water, then ethanol, and dried. Etching removed a very thin layer of material and revealed the grain structure. Some participants found that the grain structure and other metallurgical features showed best without the etching process.

Plastic-Replica Preparation.- For those participants who had not used the replica method to measure crack lengths, they should acquaint themselves with the method by measuring cracks of known length on an aluminum alloy material [26]. Some replica material (acetyl cellulose) was provided to the participants. The participants, however, could use any replica material of their choice.

A replica of the notch surface was made after each cyclic interval. The cyclic interval was selected so that about 25 to 30 replicas were taken during a test. A test was completed when the crack had grown across the full sheet thickness. At each cyclic interval, the specimen was held under a constant applied tensile stress ($S = 0.8\ S_{max}$ for constant-amplitude loading) while the replica was taken. (See Section 3.4.2 for the applied stress levels used for the FALSTAFF and GAUSSIAN load sequences.)

Prior to making each replica, the notch surface was cleaned with acetone (applied with a swab). The acetyl cellulose replica film (about 0.04 mm thick and cut into pieces about 7 mm by 25 mm) was held in place loosely against the notch surface using a rod that was slightly less than the diameter of the notch. The replica film was centered over the notch with the long dimension of the film lying along the circumference of the notch. A few drops of acetone were allowed to flow between the film and the notch surface. The film was then touched lightly to the specimen surface where it adhered and was left to dry for at least five minutes. (Best results are achieved by applying minimum pressure necessary to cause adherence.) While the replica was in place on the specimen, the replica was inspected for bubbles and other artifacts using a low power microscope. Any defective replicas, such as those containing bubbles, were discarded and a new replica was made. Once dry, the replica was removed from the specimen by grasping the film at one end with tweezers and peeling slowly (peel from top of notch to bottom of notch or vice-versa). One of the top corners of the finished replica film was clipped away with scissors to aid in orienting the replica for analysis in the scanning-electron microscope (SEM) or optical microscope. Each replica was stored in a container, labelled with the specimen number and the number of cycles accumulated on the specimen.

For observation in the SEM, the replicas were gripped at each end in a sample holder and coated with a thin layer of sputtered Au-Pd (approximate thickness of the coating layer is 300 Angstroms). Beam energy was lowered to about 10 keV to minimize replica heating. The replica could be tilted 45 degrees about the horizontal axis (that is, about the crack growth direction) to increase the signal level. Magnification in the direction of crack growth would not be affected. At magnifications over 1000 times, care was taken not to focus the beam in one location for extended periods because the replica would be thermally damaged. Analysis of the replicas from the last replica to those made early in life permitted easy location of the crack. Patterns in the grain structure and inclusion particles were used to locate the crack on the earlier replicas. Occasionally, a replica was twisted or had unusually large curvature making crack length measurements less accurate. For this reason, the position of the crack tip from each replica was marked on a montage of micrographs made from a relatively flat replica that had one of the largest crack lengths. After drying, the replica material would shrink. The shrinkage, however, is uniform and consistent. Thus, crack lengths measured from the replicas were smaller than the actual crack lengths (about 9 percent) for the 0.04 mm thick material.

For observation in an optical microscope, coating of the replicas with a thin layer of sputtered Au-Pd was optional. If the replicas were not coated, then both faces of the replica would be observed under the microscope. A slight bubble pattern might be observed on the face away from the face containing the crack impression. Experience had shown that it was possible to read an uncoated replica because the bubble pattern would be slightly out of focus.

ANNEX F

APPROXIMATE STRESS-INTENSITY FACTORS FOR A SURFACE CRACK AND THROUGH CRACK AT A SEMI-CIRCULAR NOTCH

J. C. Newman, Jr.
NASA Langley Research Center
Hampton, Virginia, USA

An approximate stress-intensity factor equation for a semi-elliptical surface crack located at the center of a semi-circular edge notch (Fig. 15(a)) subjected to remote uniform stress [25] is

$$K = S\sqrt{\pi a/Q}\, F_{sn}\left(\frac{a}{c}, \frac{a}{t}, \frac{r}{t}, \frac{c}{w}, \phi\right) \tag{F-1}$$

for $0.2 \le a/c \le 2$, $a/t \le 1$, $0.5 \le r/t \le 3$, $(r + c)/w \le 0.5$, $r/w = 1/16$, and $-\pi/2 \le \phi \le \pi/2$. (Note that here t is defined as one-half of the full sheet thickness.) The shape factor, Q, is given by

$$Q = 1 + 1.464\left(\frac{a}{c}\right)^{1.65} \qquad \text{for } \frac{a}{c} \le 1 \tag{F-2a}$$

$$Q = 1 + 1.464\left(\frac{c}{a}\right)^{1.65} \qquad \text{for } \frac{a}{c} > 1 \tag{F-2b}$$

and

$$F_{sn} = \left[M_1 + M_2\left(\frac{a}{t}\right)^2 + M_3\left(\frac{a}{t}\right)^4\right] g_1\, g_2\, g_3\, g_4\, f_\phi\, f_w \tag{F-3}$$

For $a/c \le 1$:

$$M_1 = 1 \tag{F-4}$$

$$M_2 = \frac{0.05}{0.11 + \left(\frac{a}{c}\right)^{3/2}} \tag{F-5}$$

$$M_3 = \frac{0.29}{0.23 + \left(\frac{a}{c}\right)^{3/2}} \tag{F-6}$$

$$g_1 = 1 - \frac{\left(\frac{a}{t}\right)^4 2.6 - 2\left(\frac{a}{t}\right)^{1/2}}{1 + 4\,\frac{a}{c}} \left|\cos\phi\right| \tag{F-7}$$

$$g_2 = \frac{1 + 0.358\lambda + 1.425\lambda^2 - 1.578\lambda^3 + 2.156\lambda^4}{1 + 0.08\lambda^2} \tag{F-8}$$

$$\lambda = \frac{1}{1 + \frac{c}{r}\cos(0.9\phi)} \tag{F-9}$$

$$g_3 = 1 + 0.1(1 - \cos\phi)^2\left(1 - \frac{a}{t}\right)^{10} \tag{F-10}$$

$$g_4 = 1.14 - 0.1/\left(1 + \frac{c}{r}\right)^{1/2} \tag{F-11}$$

The finite-width correction, f_w, was

$$f_w = 1 - 0.2\gamma + 9.4\gamma^2 - 19.4\gamma^3 + 27.1\gamma^4 \tag{F-12}$$

where

$$\gamma = (c + r)/w$$

The function f_ϕ is given by

$$f_\phi = \left[\left(\frac{a}{c}\right)^2 \cos^2 \phi + \sin^2 \phi\right]^{1/4} \tag{F-13}$$

For a/c > 1:

$$M_1 = \left(\frac{c}{a}\right)^{1/2} \tag{F-14}$$

The functions M_2, M_3, g_1, g_2, λ, g_3, g_4, and f_w are given by Equations (F-5) through (F-12), respectively, and f_ϕ is given by

$$f_\phi = \left[\left(\frac{c}{a}\right)^2 \sin^2 \phi + \cos^2 \phi\right]^{1/4} \tag{F-15}$$

When the surface-crack half-length, a, reaches one-half sheet thickness, t, the crack is assumed to be a through crack of length, c. The stress-intensity factors for a through crack emanating from a semi-circular notch subjected to remote uniform stress [30] are then used. An equation fit to these results is

$$K = S\sqrt{\pi c}\, F_n\left(\frac{c}{w}, \frac{r}{w}\right) \tag{F-16}$$

for r/w = 1/16 and (c + r)/w < 0.8. The boundary correction factor, F_n, is

$$F_n = f_1\, g_4\, f_w \tag{F-17}$$

where g_4 and f_w are given by Equations (F-11) and (F-12), respectively. The function f_1 is given by

$$f_1 = 1 + 0.358\lambda + 1.425\lambda^2 - 1.578\lambda^3 + 2.156\lambda^4 \tag{F-18}$$

where

$$\lambda = \frac{1}{1 + \frac{c}{r}} .$$

ANNEX G

LONG-CRACK GROWTH RATE DATA
-Constant Amplitude and FALSTAFF Loading-

E. P. Phillips
NASA Langley Research Center
Hampton, Virginia, USA

This annex describes test procedures and presents the results from the tests for conventional, long-crack growth rate data. These data were used for comparisons with the short-crack growth rate data. Data were generated in tests with constant stress ratio load sequences (R = -2, -1, 0, and 0.5) and with the FALSTAFF load sequence [34]. Results for long-crack tests with the GAUSSIAN load sequence (conducted by P. Heuler, Industrieanlagen Betriebsgesellschaft, West Germany) are discussed in Annex H. The constant stress ratio tests included decreasing, increasing, and constant load amplitude sequences. All cracks exceeded 6 mm in length when data were taken.

MATERIALS AND SPECIMENS

All tests were conducted on center-cracked specimens of 2024-T3 aluminum alloy sheet taken from a large stock of this material held at the NASA Langley Research Center for fatigue research programs. The baseline long-crack growth rate data for this AGARD program were generated using 50 mm wide, center-cracked specimens which were cut from some of the same sheets that were used to make the edge-notched, short-crack specimens. At growth rates below about 10^{-5} mm/cycle, the baseline data were supplemented by data generated using 76 mm wide specimens made from sheets other than those used for the short-crack program. At growth rates above about 10^{-5} mm/cycle, the baseline data were supplemented by data generated using 305 mm wide specimens made from sheets other than those used for the other two specimen sizes. The results from the 305 mm specimens were published in 1969 in Reference 32. All specimen configurations are shown in Figure G1.

TEST PROCEDURES

The test procedures described in this section apply to the tests of the 50 mm and 76 mm specimens. These specimens were tested using the same testing machines and procedures. Test procedures for the 305 mm specimens are described in Reference 32.

In all tests, cracks were initiated and grown about 2 mm at each end of the central slot before growth rate data were recorded. The same test stress ratio or FALSTAFF load sequence was used for the crack initiation and crack growth. Crack length measurements were made using a 60X microscope mounted on a micrometer slide that had a reading scale marked in increments of 2.5 μm. In the FALSTAFF tests, crack length measurements were always made at the end of a complete pass through the load sequence. Servo-hydraulic fatigue testing machines with load cells calibrated for a 9 kN range were used in the constant stress ratio tests and a 44 kN range was used in the FALSTAFF tests. The cyclic frequency was 30 Hz in the constant stress ratio tests and 12 Hz in the FALSTAFF tests. In tests involving compressive loading, freely-sliding antibuckling plates were placed around the thin specimens. All tests were conducted in ambient laboratory air.

Constant Stress Ratio Load Sequences

Growth rates below about 10^{-5} mm/cycle were generally determined in decreasing load amplitude tests. Low growth rates were achieved using a manually-controlled, discrete-step load-shedding method. In this method, the crack is grown a prescribed incremental length at each of a succession of progressively lower alternating loads. The reduction of the maximum and minimum loads for each growth increment is a fixed percentage of the loads for the just-completed growth increment. In the current work, the tests were run using a load reduction step of 6 percent and a crack growth increment of 0.5 mm. This resulted in a rate of reduction of ΔK that was within the guidelines recommended in the recently revised ASTM Standard E-647--Standard Test Method for the Measurement of Fatigue Crack Growth Rates. (The revision of Standard E-647 was approved by ASTM in 1986 but has not yet appeared in The Annual Book of ASTM Standards.) The load reduction procedure was continued until no crack growth was observed in 10^6 cycles. After the no-growth condition was achieved, some of the tests were continued as increasing-load tests. However, no increasing-load data were generated in the steep portion of the growth rate curves near threshold because the load had to be raised by about 15 percent to restart the crack growth after it stopped.

Growth rates above about 10^{-5} mm/cycle were generally determined in increasing load amplitude tests. Increasing load amplitude tests were used instead of constant load amplitude tests in order to generate data over a wide range of growth rates using a single, narrow specimen. The procedure was similar to that used for the decreasing-load tests in that the loads were increased in steps of up to 6 percent and the crack growth increment at each load was 0.5 mm. Occasionally, the test loads were held constant over several crack growth increments.

FALSTAFF Load Sequences

Three 50 mm specimens were tested using the FALSTAFF load sequence. In the test used to generate data at the high end of the growth rate range, the load spectrum remained the same throughout the test. In the test used to generate the mid-range rates, all loads in the spectrum were reduced by 6 percent after every 0.5 mm of crack growth. In the test for the lowest rates, all loads in the spectrum were reduced by 12 percent after every 0.5 mm of crack growth. The 12 percent load reduction steps were used to try to achieve very low rates in a reasonable testing time. The machine running time between the two lowest rate data points was 170 hours.

DATA ANALYSIS

The crack length against cycles data were analyzed and interpreted in terms of growth rates and ΔK. The methods used to analyze data from the 50 mm and 76 mm specimens and the 305 mm specimens were somewhat different as described herein.

Data From 50 mm and 76 mm Specimens

Growth rates were calculated from the crack length against cycles data for each crack tip using the secant (point-to-point) method. Stress-intensity factors were computed using empirical equations developed by J. C. Newman, Jr. of NASA Langley Research Center to represent the solutions obtained by Isida [56] for an eccentric crack in a strip under tension. The equations are given below:

$$K_{I,A} = S \{\pi a \sec[(\pi a/2b_1)(1-0.22(e/b)^3]\}^{1/2}$$

$$K_{I,B} = S \{\pi a \sec[(\pi a/2b_1)(1-0.37(e/b)^{0.5}+0.1(a/b_1)^{15})]\}^{1/2}$$

where $K_{I,A}$ and $K_{I,B}$ are the stress-intensity factors at the two crack tips in the center-cracked specimen. S is the applied gross-section stress, a is half the total crack length, b_1 is the distance from the center of the crack to the nearest edge of the specimen, e is the distance from the center of the crack to the centerline of the specimen, and b is half the width of the specimen. The definitions of the symbols are illustrated in Figure G2. The empirical equations fit Isida's solutions to within 3 percent for values of $a/b < 0.9$. For cracks symmetrical about the specimen centerline, which was generally the case in the current work, the empirical equations gave values that were within 0.1 percent of those given by the equations in ASTM Standard E-647. The full stress range was used to calculate ΔK for negative stress ratios. For the FALSTAFF tests, the stress range from maximum peak to minimum trough was used to calculate ΔK.

Data From 305 mm Specimens

Growth rates were calculated from the crack half-length against cycles data using a graphical method in reference 32. Stress intensity factors were calculated using the equation below:

$$\Delta K = \Delta S \{\pi a \sec(\pi a/2b)\}^{1/2}$$

where the symbols have the same definitions as given in the previous section. The full stress range was used to calculate ΔK for negative stress ratios. Note that the method of calculating ΔK is different from that used in reference 32.

RESULTS AND DISCUSSION

Constant Stress Ratio Tests

The data from all the constant stress ratio tests are plotted in Figure G3. A piece-wise-linear line has been visually fitted through the data for each stress ratio. The lines are defined by the points listed in Table G1. In Figure G4, the data from only the 50 mm specimens are plotted along with the same piece-wise-linear lines shown in Figure G3. From Figure G4, it appears that the rates from the 50 mm specimens are a little higher than the rates from the 305 mm specimens at the high growth rate end of the curve. Overall, however, the data from the 50 mm specimens agree well with the data from the other specimens and, therefore it seems reasonable to use all the data to define the long-crack behavior. To facilitate comparisons between the long-crack data and the short-crack data, scatter bands that include more than 95 percent of the data have been defined for each stress ratio. These scatter-band lines can be easily reproduced on plots of the short-crack data. The scatter-band lines were defined by translating the piece-wise-linear lines in Figure G3 in the ΔK direction by factors of 1.15 and 1/1.15. Figures G5 through G8 show the data with the scatter-band lines.

FALSTAFF Tests

The data from the FALSTAFF tests are shown in Figure G9. Again, a piece-wise-linear line has been visually fitted through the data and the points defining the line are given in Table G1. During the FALSTAFF tests, an attempt was made to validate the load shedding procedure by obtaining corroborating data in increasing-load tests. In the test using the 6 percent step load-shedding procedure, four data points were obtained in increasing-load testing at the end of the test. The locations of the increasing-load data are shown by the arrows in Figure G10. The increasing-load data points agree well with the decreasing-load data. In the test using the 12 percent step load-shedding procedure, however, some of the data were significantly different from that obtained in the other tests, and consequently some data were censored from the data population. The censored data are identified in Figure G10. The accuracy of the remaining data at the low rates is open to question because no increasing-load data were obtained in that test. An attempt was made to obtain increasing-load data but the specimen was severely overloaded (due to an electrical power outage) before any data were obtained.

Table G1.- Points Used to Define Piece-Wise-Linear Lines Drawn Through Long-Crack Growth Rate Data.

Stress Ratio R	Point	ΔK MPa-$m^{1/2}$	$\frac{da}{dN}$ mm/cycle
-2	1	7.9	1.20E-08
	2	8.9	1.70E-06
	3	10.3	3.30E-06
	4	14.2	6.00E-06
	5	22.5	6.00E-05
	6	37.0	2.30E-04
-1	1	6.0	1.20E-08
	2	6.4	1.70E-06
	3	7.7	3.70E-06
	4	11.2	6.80E-06
	5	14.3	4.00E-05
	6	42.0	1.00E-03
0	1	3.35	1.20E-08
	2	3.5	1.60E-06
	3	3.9	3.00E-06
	4	5.6	5.20E-06
	5	10.0	1.00E-04
	6	27.0	1.00E-03
0.5	1	2.0	1.20E-08
	2	2.15	1.30E-06
	3	2.4	2.30E-06
	4	3.9	5.60E-06
	5	5.5	2.40E-05
	6	6.7	5.00E-05
	7	18.0	1.00E-03
FALSTAFF	1	8.2	6.00E-08
	2	12.0	2.50E-07
	3	13.5	6.00E-07
	4	20.0	3.00E-06
	5	40.0	8.50E-06
	6	56.0	8.00E-05
GAUSSIAN[a]	1	26.0	1.00E-06
	2	100.0	.00E-05

(a) P. Heuler, Industrieanlagen Betriebsgesellschaft, Germany (see Annex H).

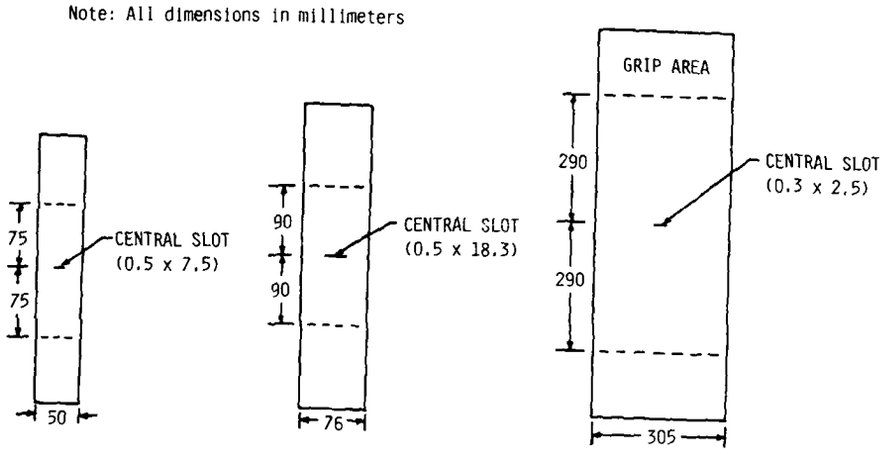

Figure G1.- Long-crack specimen configurations. (Material for all specimens was 2.3 mm thick 2024-T3 aluminium alloy.)

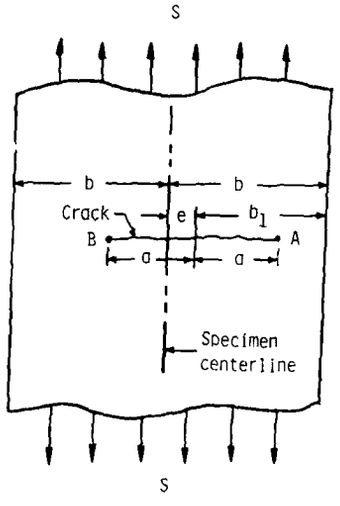

Figure G2.- Definition of symbols used in equations to calculate stress-intensity factors for center-cracked specimens.

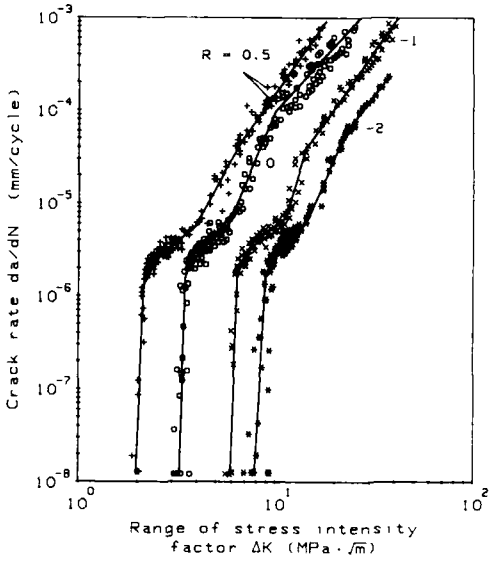

Figure G3.- Long-crack growth rate data from constant stress ratio tests.

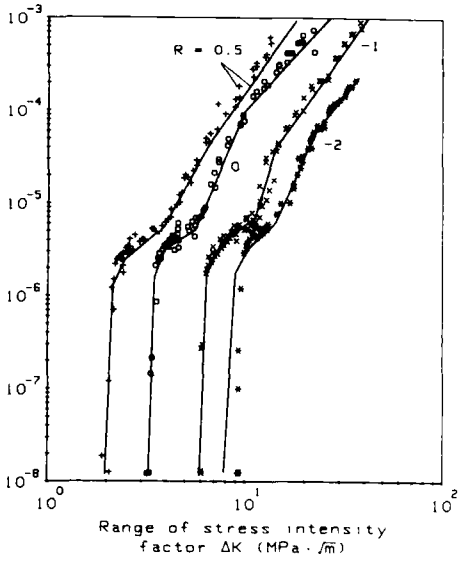

Figure G4.- Long-crack growth rate data from constant stress ratio tests on 50 mm wide specimens.

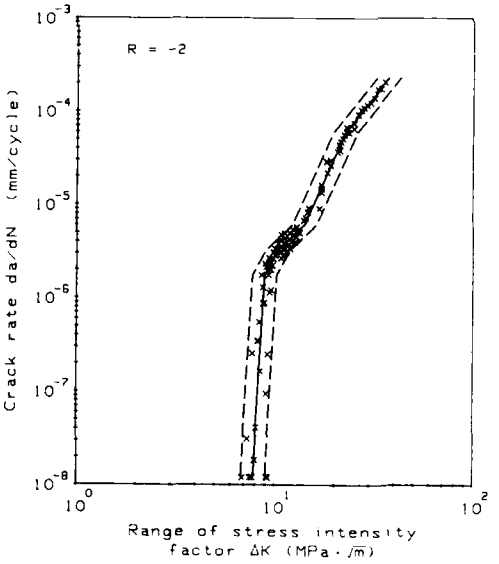

Figure G5.- Long-crack growth rate data from R = -2 tests.

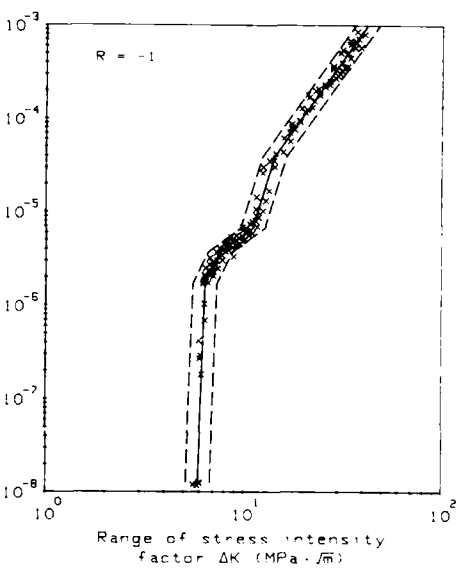

Figure G6.- Long-crack growth rate data from R = -1 tests.

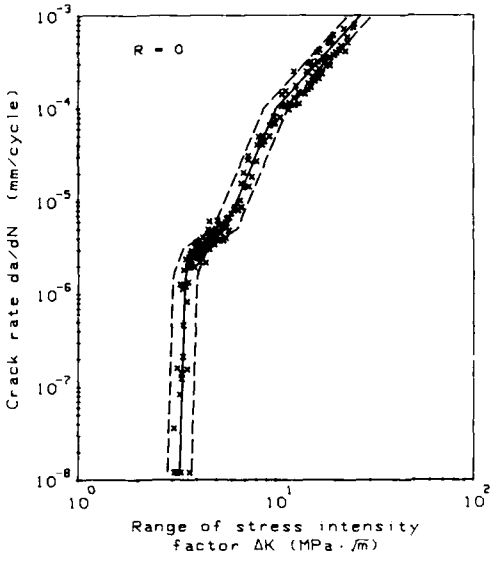

Figure G7.- Long-crack growth rate data from R = 0 tests.

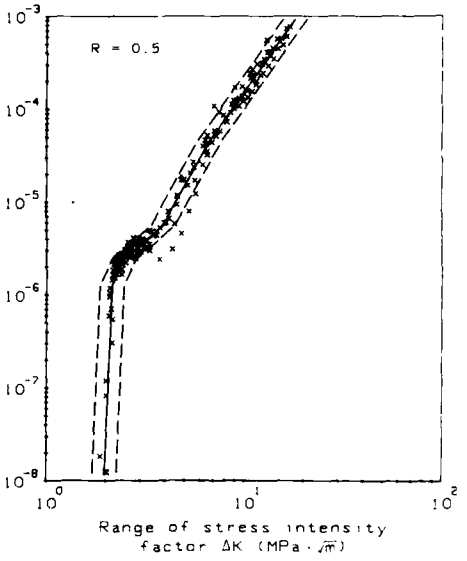

Figure G8.- Long-crack growth rate data from R = 0.5 tests.

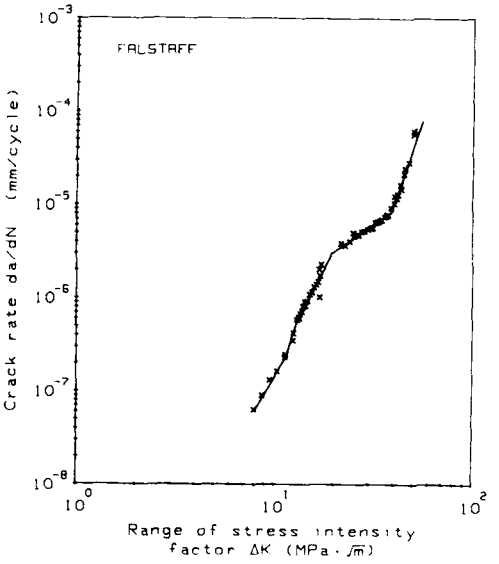

Figure G9.- Long-crack growth rate data from FALSTAFF spectrum tests on 50 mm wide specimens.

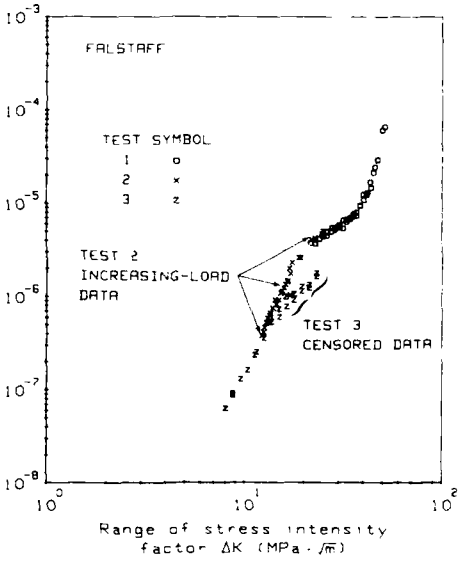

Figure G10.- Increasing-load, decreasing-load and censored growth rate data from FALSTAFF spectrum tests.

ANNEX H

LONG-CRACK GROWTH RATE DATA
-GAUSSIAN Loading-

P. Heuler
IABG, Ottobrunn
Germany

Conventional long-crack growth rate data under GAUSSIAN loading were generated at IABG within the AGARD short crack program on 2024-T3 sheet specimens. Test procedures and results are briefly reviewed in the following.

SPECIMENS

Tests were carried out on 50 mm wide center-cracked specimens of 2024-T3 aluminum alloy sheet obtained from NASA Langley Research Center. A central slot of 0.4 by 3 mm was used as the crack starter. Specimen dimensions are shown in Figure G1(a).

TEST PROCEDURES

Cracks were initiated and grown a minimum of 1.5 mm at each end by use of a load-shedding procedure (2 tests) and GAUSSIAN loading (1 test) before growth rate data were recorded. Crack length measurements were made using two resistance foils (type RUMUL) bonded on both sides at opposite crack ends. Nominal output of these foils corresponds to a crack length of 20 mm. The two signals were continuously recorded on a line-writer device. A servohydraulic fatigue testing machine was used with a load cell calibrated for a 120 kN range. The cyclic frequency was about 13 Hz with smaller frequencies for high load amplitudes. Because the tests involved fully reversed loading (R ≈ -1), freely-sliding antibuckling plates were mounted to the specimens. The tests were conducted in laboratory air. In order to achieve reasonable low growth rates, all loads in the spectrum were reduced by 10 MPa in two steps. Due to the large block size of 10^6 cycles, these load-reduction steps had to be applied within the loading sequence, that means eventually before the maximum load level had occurred. Due to some limitations, only crack growth rates down to about 10^{-6} mm/cycle could be determined.

DATA ANALYSIS

Because the cracks, in general, were symmetrical to the centerline of the specimens, the equation used to calculate the stress-intensity factor was

$$\Delta K = \Delta S \sqrt{\{\pi a \sec(\pi a/2b)\}}$$

Crack length against cycles data were digitised from the continuous plot using intervals of 50,000 cycles. When faster crack growth with higher rates was encountered, smaller intervals of 20,000 cycles were used. Crack growth rates were calculated from these crack length against cycles data by use of the secant (point-to-point) method.

The full stress range was considered from the maximum peak to the minimum trough of the GAUSSIAN sequence for calculation of ΔK applying the respective load (gross stress) level.

RESULTS AND DISCUSSION

Data from the GAUSSIAN tests are shown in Figures H1 to H4. Figure H1 shows results where the highest stress in the spectrum was held constant at 176 MPa. Figures H2 and H3 show results of load-reduction tests. Figure H4 summarises the results obtained from all three tests. The large scatter in crack growth data can be attributed to the occurrence of high load amplitudes within the GAUSSIAN sequence which introduce load-interaction effects that are more distinct for thin-sheet specimens. The number of cycles covered by the results shown in Figures H1 to H4 range from 1×10^6 to 3×10^6 cycles. Load-interaction effects due to the reduction of the overall load level during the tests should not cause much of the scatter, because some of the readings directly following the load reduction have been removed from the plots, for example, data obtained from crack increments roughly the size of the plane-stress monotonic plastic zone of the previous overloads.

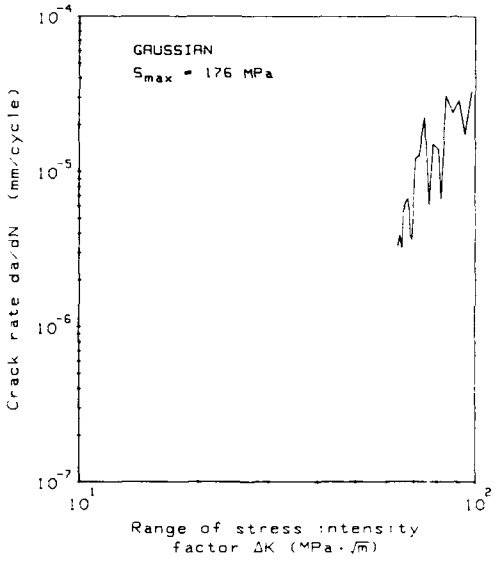

Figure H1.- Long-crack growth rate data from GAUSSIAN loading with S_{max} = 176 MPa.

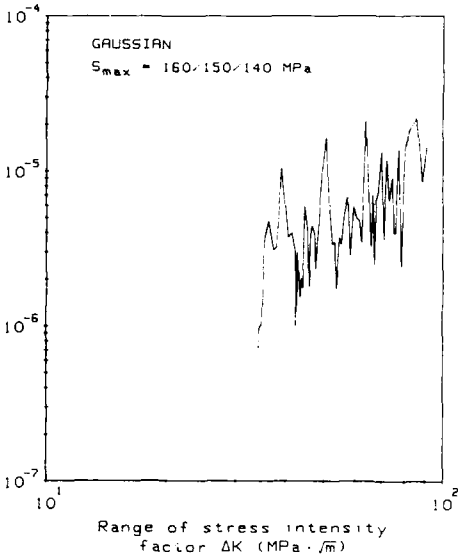

Figure H2.- Long-crack growth rate data from decreasing GAUSSIAN loading with S_{max} = 180, 170 and 160 MPa.

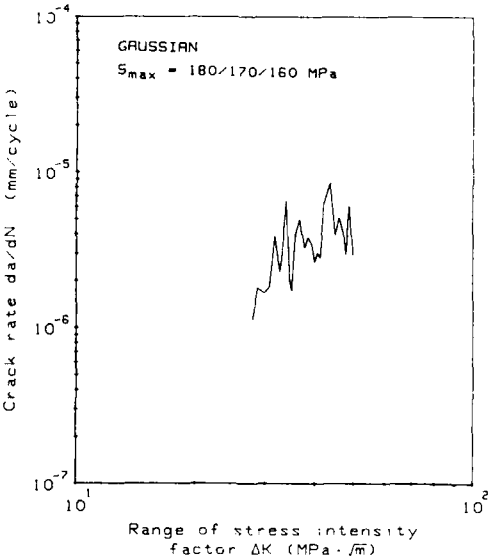

Figure H3.- Long-crack growth rate data from decreasing GAUSSIAN loading with S_{max} = 160, 150 and 140 MPa.

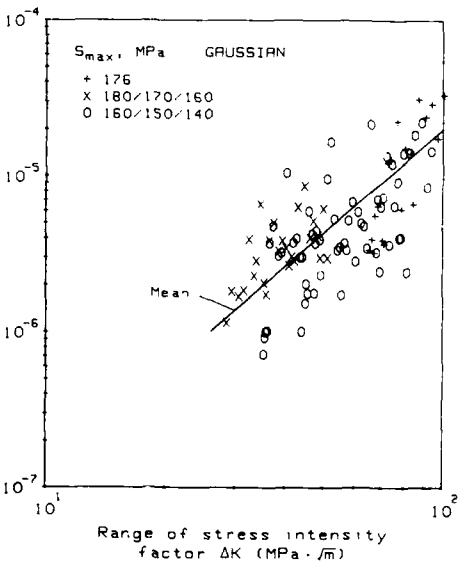

Figure H4.- Summary of long-crack growth rate data from all GAUSSIAN load tests.

ANNEX I

DATABASE PROGRAM FOR CRACK PROPAGATION DATA ACQUIRED IN THE AGARD SHORT CRACKS COLLABORATIVE EFFORT

P. R. Edwards
P. P. Data Ltd
Fleet, Hampshire
United Kingdom

INTRODUCTION

This annex describes the operation of a database program developed for use in the AGARD short cracks collaborative effort. Data are stored as files of crack length against number of cycles. If desired, sets of polynomial coefficients describing curves fitted to the data in each file are available. Any of the sets of data can be plotted, either a plot of crack length against number of cycles or a log-log plot of ΔK (alternating stress intensity factor) against da/dN (crack growth rate), with adjustable scales in both cases. The object of the program is to enable easy cross-plotting of different sets of data on the same graph. The plots can be output to an external plotter if required, either for incorporation into technical reports or to produce viewgraphs. These features have been extensively used in this report. Least squares fit straight lines on log-log plots can be calculated and plotted for any set or sets of data.

Provision exists for the fitting of polynomials to each set of data. This can be carried out interactively, because polynomials are plotted quickly on the graphics screen, and different orders of polynomial curve fit compared. If a suitable digitising tablet is available then additional points can be added to the length against cycles curve, so as to "force" the polynomial to follow a desired curve, in particular, to follow the correct slope at the beginning and end of defined crack propagation curves.

The program will run on Hewlett-Packard 9836/9816 or 9817/217/310/320 computers with virtually any kind of disc storage (although the medium for distribution of the program and database is single sided 3.5 inch floppy disk). At the present stage of development of the program, the series 300 computers must be used with a display compatibility interface, type 98546A, to give full compatibility with the earlier 9836/9816 machines. Additionally, a graphics printer of the HP 2225A ink-jet type, HP 2671G or similar is required with optionally a plotter using the HPGL language (HP 7470A, HP 9872 or similar). A digitising tablet (HP 7114A or similar) is highly desirable.

SOFTWARE REQUIREMENTS

The program was written using BASIC 3.0 with graphics extensions, and has been run exclusively with that system and BASIC 4.0. However, it should be noted that later computer models in the Hewlett-Packard series 200-300 range tend not to operate with earlier BASIC systems. The program should run on later versions of BASIC with, perhaps, minor modifications. The program uses some matrix operations. Note that if it is found that some lines of the program are single asterisks (*) then one or more BASIC system binary programs are missing.

GETTING STARTED

Definitions and General Operation of the Program

A "Database" consists of two binary disc files. The first file contains 110 sets of data, which are referred to in this note as "Files". Each File may contain up to 50 values of crack length and up to 50 corresponding values of number of cycles applied in the laboratory programmes of crack measurement. In addition, each File may contain up to 10 coefficients for polynomial "best fit" curves to the data. The second file consists of up to 110 "information strings" of up to 80 characters each. Each string is associated with a particular File and contains information relating to the source of the test data (participant), the loading action, the stress level and the crack type. In all file operations the two binary disc files are handled by the database program as one.

On any disc containing the two binary files defining a particular Database, the File containing the numeric data has a particular name, for example, UKC_DB, the complete database for the UK contribution to the AGARD programme. The second File, containing information strings, has the same name as the other, but with an additional character "1" at the end of the name, so the corresponding information string file name for UKC_DB is UKC_DB1. In addition, databases have been subjected to the "non-interaction" criterion as described in Section 4.2. These "filtered" data are contained in databases with names including an "X". For instance, UKXC_DB and UKXC_DB1 constitute the UK data subjected to the "non-interaction" criterion. More details of the Files constituting the complete AGARD Core Program Database are given in Tables I1 (raw data) and I2 (data filtered by the non-interaction criterion).

In order to plot any of the data Files, to add more information to the Database, or to edit any existing Files, the appropriate Database File must first be read into the computer. As previously stated, where Database File operations require the specification of the File name, then only the name of the main file (the one with the name not ending in "1") needs to be specified. The accompanying file is dealt with automatically by the software. If the Database File is edited in any way, then it must be re-stored onto the disc at the end of the current operation, or else the modification will be lost when the computer is switched off.

Loading and Running the Program

The program is supplied as a Standard BASIC program file and is loaded in the normal way once all of the appropriate system files have also been loaded. For series 300 or 9817/217 computers, before the program is executed, the following command should be typed:

CONTROL KBD;15,1

This command configures the soft keys on these computers to be the same as on the 9836/9816 machines. The program name is NEW_DPLOT although subsequent versions are called NEW_PLOT1, NEW_PLOT2 and etc. The current version at the time of writing this report is NEW_PLOT1. On pressing the "Run" key, after a short pause, a set of soft key labels is displayed, as shown below (referred to here as Group 1a):

Group 1a

INPUT DBASE	**INPUT FILE**	**EXT PLOTTER**	**ERASE FILE**	**NEXT DADN**
SAVE DBASE	**SAVE FILE**	**PLOTTER VEL**	**PEN NUMBER**	**LEN VS CYCLES**

Note that the layout for the soft keys on the Series 300 or 9817/217 computers is slightly different to that shown above. The layout for Group 1a soft keys on these computers is in one line rather than two. As an example, the equivalent layout for the Group 1a soft keys is as follows:

INPUT DBASE	**INPUT FILE**	**EXT PLOTTER**	**ERASE FILE**	**NEXT DADN**	**SAVE DBASE**	**SAVE FILE**	**PLOTTER VEL**	**PEN NUMBER**	**LEN VS CYCLES**

At this point there exists in the memory of the computer an empty Database File. If the intention is to create a new Database File then the operator needs to go to the "Edit" routine, which will enable input of data, both by the keyboard and from the digitising tablet. This is accomplished by pressing the bottom right soft key labelled "LEN VS CYCLES" twice (after the first press, the soft key label changes to "EDIT DATA"). Data may then be input as described below. Alternatively, an existing Database can be loaded by pressing the top left soft key labelled "INPUT DBASE" and then on the request of the computer, type the appropriate Database name. More details are given below.

Soft Key Description

The soft keys are in two basic groups: (a) those dealing with plotting crack growth rate (da/dN) against ΔK, handling of individual data Files (without actually changing their content) and setting plotting parameters; and (b) those dealing with plotting crack length against cycles and editing the data.

(a) There are four sets of soft keys in the 'Group a' category and the selection of the particular group in this category is accomplished by pressing the top right soft key labelled "NEXT DADN". Pressing this key causes the computer to cycle through the various groups of soft keys. Group 1a has already been discussed. The other three groups or soft keys in this class are as follows (referred to here as Groups 2a, 3a and 4a):

Group 2a

AXES DADN	**GRID DADN**	**DUMP GRAPH**	**SCALE DADN**	**NEXT DADN**
TITLE DADN	**POLY DADN**	**CLEAR GRAPH**	**POINTS DADN**	**LEN VS CYCLES**

Group 3a

INSERT FILE	**SELECT PARAM**	**SEARCH START**	**NEXT FILE ^**	**NEXT DADN**
COPY FILE	**ENTER PARAM**	**SEARCH CONT**	**FILE BEFOREv**	**LEN VS CYCLES**

Group 4a

PLOT LC	**CLEAR STAT**	**PLOT STAT**		**NEXT DADN**
PRINT STAT	**SEARCH PLOT**			**LEN VS CYCLES**

(b) There are two groups of soft keys for creating the crack length against cycles plots and for editing the data. The first deals with plotting the length against cycles graph and fitting polynomials to the data. This is obtained by pressing the bottom right soft key labelled "LEN VS CYCLES" in any of the groups of soft keys (1a, 2a, 3a or 4a). This group of soft keys is as follows (referred to here as Group 1b):

Group 1b

AXES LvC	**POINTS LvC**	**DUMP GRAPH**		**DADN PLOT**
TITLE LvC	**POLY LvC**	**CLEAR GRAPH**	**FIT POL LvC**	**EDIT DATA**

Return to groups 1a, 2a, 3a and 4a is effected by means of the "DADN PLOT" soft key.

The final set of soft keys, those for the Editor, is obtained by pressing the bottom right soft key labelled "EDIT DATA" in Group 1b. Where there is no data in the File currently accessed, the following display will be shown (together with the group of soft keys referred to here as Group 2b):

Manual data input

Crack origin (mm from notch centre)

```
X        Y

 0,   0

Cycles    Crack length (mm)

At end
```

Group 2b

```
  ^       | DATA START ^ | INSERT BEFORE| TABLET INIT | GRAPH
  v       | TO END     v |    DELETE    | SET LENGTH  | END EDIT
```

If there are data in the data File then the first pair of values in the list will be displayed as the coordinates of the crack origin (in mm from the centre of the grid on the AGARD Data Charts). Subsequent values in the File are displayed as a list of cycles against crack length which can be modified by overtyping, deleted in turn or have additional values inserted as described in the next section.

EDITING AND ENTERING DATA FROM THE KEYBOARD AND DIGITISER

Additional data can be entered at the end of the File displayed in the editor by typing it as sets of cycles and crack length data separated by a comma. This should be typed over the text "At end" or over any other value in the File, using soft keys to set the editing position as described below. Hitting any key except one of the soft keys is regarded as a signal that the operator desires to input values of cycles and crack length. If this is done the soft key labels disappear, a prompt describing the format of the data is displayed and the input must be completed. If at any time the values "0,0" are input (except for the position of the crack origin), then this defines the end of File and all following values are erased.

Editing functions are assisted by the Group 2b soft keys. The position at which data is input to the File is controlled by the soft keys "^" and "v" (pressing 'ENTER' is exactly equivalent to pressing the "v" soft key). In order to move the editing position to the start of the File, press the "DATA START ^" soft key, and to move the editing position to the end of the File press the "TO END v" soft key. When pressing the "DELETE" soft key, the data for the current point being edited will be deleted, and pressing the "INSERT BEFORE" soft key enables a point to be inserted before the current position. Pressing the "GRAPH" soft key will enable a continuous graphical display of the data in terms of a crack length against cycles plot while the data is being input. It should be borne in mind, however, that there is automatic scaling on the cycles axis and the complete graph is redrawn every time that the editing operation is carried out. This may make the editing process rather slow and so it is recommended that graphics should be switched on only occasionally. To disable the 'graphics' function, press the "GRAPH" soft key again, which will have been relabelled *"ALPHA"*. *The current data* point being edited always appears on the graphical display as a "@" symbol. The "SET LENGTH" soft key is used to change the scaling of the crack length axis. The "TABLET INIT" soft key is used to initiate input from the digitising tablet, which should be set with the address 6 and is referred to in the program as "706". The data being digitised is assumed to be in the form of a crack length against cycles plot. Following the activation of this soft key the operator is asked to digitise the origin and maximum points on the cycles and crack length axes, respectively. Any further presses of the digitising stylus onto the graph on the digitising tablet will transmit the coordinates of that point to the data File. Normally this facility is used to input additional data points into a File in order to force a polynomial curve to follow a desired behaviour. Therefore, the graph which is digitised on the digitising tablet is normally one from the current File being edited, and which has been output in crack length against cycles format, using the Group 1b soft key "DUMP GRAPH".

An example of the use of the digitiser to improve the quality of a 'best fit' curve is shown in Figures I1 and I2. Figure I1 shows such a curve fitted to six points and is clearly unacceptable because of the cyclic swings, even though it does go through all the points. Figure I2 shows a much improved fitted curve which was induced by the addition, using the digitiser, of a single point, shown ringed in the Figure. Once an acceptable curve has been produced, the added points can be deleted. The polynomial coefficients are stored in the data File and the fitted curve is unchanged by the deletion. It must be remembered, however that the data File must be saved to disc before the program is halted.

To leave the editor and return to the Group 2a soft keys, relating to the length against cycles plot, press the "END EDIT" soft key, whereupon the computer displays any information string code relating to this particular data File, the format of which is described later in this Annex. If "ENTER" is pressed at this point then any existing code describing the test data is left unchanged. Alternatively, the user may edit the displayed information string, and exit via the "ENTER" key.

LOADING AND STORING DATABASE FILES AND INDIVIDUAL DATA FILES

Input and output of DATABASE FILES is controlled by the Group 1a soft keys "INPUT DBASE" and "SAVE DBASE".

To load an entire Database File into memory, press the "INPUT DBASE" soft key. Following a request from the computer for the name of the database, the name of the main data File should be typed, (eg. "UKC_DB"). Alternatively, pressing the 'ENTER' key will cancel the operation. Various error messages will appear if, for instance, the disc is not in the disc drive or the File name is wrong. In all cases the operator is able to repeat the operation once the error condition has been rectified without losing the program or data.

Following editing, the entire Database is stored again on the disc using the "SAVE DBASE" soft key. The typing procedure is similar to that for input of a Database File.

The "INPUT FILE" and "SAVE FILE" soft keys work in almost exactly the same way as the "INPUT DBASE" and "SAVE DBASE" soft keys, except that the data loaded or stored is one of the possible 110 component Files in a Database File, i.e. one set of length against cycles data. The data transfer will be between a disc File and the particular component File which is being accessed by the computer in a Database File in the computer's memory.

MOVING BETWEEN COMPONENT FILES IN THE DATABASE STORED IN THE COMPUTER'S MEMORY

This is carried out by the Group 3a soft keys "NEXT FILE ^" and "FILE BEFORE v", respectively. When Group 3a soft keys are selected any graphics are temporarily removed from the screen and the information relating to the current component File accessed in the Database File in the computer's memory are displayed on the screen. When the Database File is read into the computer memory, the computer is left accessing component File 1 in that Database File. Pressing the "NEXT FILE ^" soft key will enable the computer to access the next component File in the Database File, and pressing the "FILE BEFORE v" soft key enables the computer to access the component File before. Every time a new component File is accessed the information relating to that File, which is an interpretation of the data contained in the relevant information string, is displayed on the screen. An example of such a display is given below:

RAE Farnborough UK
Gaussian - irreg 0.99
Peak stress 125
Crack number 1
---Single crack (Spec A_66_20)
File number 2

P1L6S125R1T1:---Single crack (Spec A_66_20)

At the top of the screen is displayed the interpretation of the information string. The actual information string (in the example above starting with P1...) is printed at the bottom of the screen. (Remember that on leaving Group 2b soft keys the operator has a chance to enter a new information string or modify the existing one. Further details concerning the information string are given later in this Annex).

MOVING AND COPYING OF COMPONENT FILES

When the program is first run, as described above, an empty Database File exists in the memory of the computer. In this case every information string contains the words 'NO DATA'. If it is desired to erase a particular File in a Database and set the information string to 'NO DATA', the Group 1a soft key labelled "ERASE FILE" should be used. On pressing this key the interpretation of the information string of the current component File is printed on the screen and the computer asks for confirmation that this File should be erased. Typing 'Y' followed by 'ENTER' erases the File, and typing 'N' followed by 'ENTER' leaves it unchanged.

The process of saving a component File separately on to a disc, so that perhaps it can be stored on a different Database File later, and loading such a File back was described earlier in this Annex. Two soft keys in Group 3a enable the insertion of component Files into the Database in the computer memory and the copying of Files to other positions in the Database File. Soft key "INSERT FILE" moves up all the Files above the current File position by one and copies the current File into the newly created space. Soft key "COPY FILE" will copy the current File into the first File in the Database that is empty, i.e. having the information string equal to "NO DATA". An advantage of the copying procedure relates to the fact that in the AGARD programme multiple cracks are recorded on replicas and so the numbers of cycles in each component File for each crack on one specimen will in fact be largely the same (e.g. one replica taken at, say, 250,000 cycles may have four cracks on it and so the value 250,000 will be a value in each of the four Files referring to each of the four cracks). Consequently the first File, which would normally show a major crack on the specimen, will have a complete list of all the numbers of cycles in the subsequent four Files, and if this File is copied four times the facilities of the edit group of soft keys (Group 1b) can be used to modify the data for the major crack to that of the subsequent cracks, by changing the crack length values and perhaps deleting some data points. This is normally less trouble than typing all the data from the start. Similarly, the information string will normally need only minor modification to convert it from one set of data to that for the next component File.

SEARCHING THROUGH COMPONENT FILES IN THE DATABASE FILE IN THE COMPUTER MEMORY

It is sometimes useful to carry out searches on the basis of information in the information string. For instance, if all the data under FALSTAFF starts at File No. 83, then the computer can search for the first and subsequent Files that refer to FALSTAFF loading and the operator will not need to press the "NEXT FILE" soft key 83 times. Searches can be carried out starting at the current component File or from the first component File in the Database File. The soft keys relating to this search system are in Group 3a.

The "SELECT PARAM" soft key is used to select the parameter or parameters that will be searched for. Each press of the "SELECT PARAM" key will give a display at the bottom of the screen of the following in turn:

Participant
Peak Stress

Crack No
Crack Type
Loading
Participant
Peak Stress

and etc.

As an example, if it is required to search for the first component File containing information under FALSTAFF, then press the "SELECT PARAM" soft key until the word "Loading" appears at the bottom of the screen. Then press the "ENTER PARAM" soft key and on each press the name of a different loading action will appear at the top of the screen, e.g. FALSTAFF, Gaussian - irreg 0.99 or "NOT ALLOCATED". Whatever appears at the top of the screen is the parameter that will be searched for. If it is wished in any subsequent search not to search for that parameter, then first use the "SELECT PARAM" to find the relevant one, and then keep pressing the "ENTER PARAM" soft key until the corresponding display at the top of the screen disappears. Other parameters such as participant and crack type are selected in the same way. For peak stress values, pressing the "ENTER PARAM" soft key requests operator input of the value. Following this procedure a list of parameters searched for will be displayed at the top of the screen and the search will look for a combination of all of these parameters (AND function rather than OR).

The Group 3a soft keys "SEARCH START" and "SEARCH CONT" respectively start the search from the beginning of the Database File or from the component File currently being accessed.

USING THE EXTERNAL PLOTTER

The external plotter should be set to Device Code 5 and is referred to in the program as 705. The plotter is activated by pressing the Group 1a soft key "EXT PLOTTER" and deactivated by pressing the same soft key, which if the external plotter is activated should read "INT PLOTTER". With the external plotter function enabled all graphics output will be directed to the plotter in virtually the same form as it normally appears on the internal graphics screen.

The plotting speed for the external plotter may be input following the pressing of the Group 1a soft key "PLOTTER VEL". The operator then inputs a number between 1 and 36 so as to obtain either a relatively fast plot (eg. 36) or a slower one with greater definition (eg. 5).

The pen on the plotter is selected by using the "PEN NUMBER" soft key in Group 1a. It should be noted that if pen number -1 is selected, when the internal graphics operation is used (i.e. plotting on the graphics screen) then the plot will erase rather than draw.

PLOTTING CRACK RATE AGAINST STRESS INTENSITY FACTOR

At the beginning of the program standard values of axis scales are set. These can be changed by the Group 2a soft key "SCALE DADN". The operator inputs in turn values for the power of 10 relating to the maximum and minimum scale values of stress intensity factor and crack rate. These numbers do not need to be integers. Typing 'ENTER' with no other input in response to the request for a particular value will leave the value as it was before.

The three Group 2a soft keys "AXES DADN", "GRID DADN" and "POINTS DADN" draw on the selected plotter the axes, a logarithmic grid and the points from the File currently selected, respectively. However, a detail of the "POINTS DADN" soft key operation needs to be understood. When the program is first run the standard plotting symbol is an asterisk (*). When the "POINTS DADN" soft key is activated the computer requests a new plotting symbol. Typing 'ENTER' with no other input leaves the symbol unchanged. If a single plotting symbol is requested (i.e. single asterisk as set by the program on the initial running), then plotting will be of the symbols with lines drawn between them. The rates are calculated as described in Section 3.5.2. If two symbols are input in response to the request for a plotting symbol, then one symbol is plotted but lines are not drawn between consecutive symbols.

The "TITLE DADN" soft key in Group 2a enables the input of a title at the bottom of the plot (actually vertically upwards because the plot is sideways). Two lines of title are permitted and the maximum length of the title which avoids going over the edges of the plot is indicated by the computer prompt. The title is self-centering.

The "POLY DADN" soft key plots any polynomial which has previously been fitted using the "FIT POL LVC" soft key in Group 1b. The coefficients for the polynomial are stored permanently in the appropriate component File in the Database File once fitting has occurred.

AUTOMATIC PLOTTING OF MORE THAN ONE SET OF DATA ON ONE GRAPH

The search facility described earlier has been extended to enable automatic plotting of more than one File on the same set of Crack rate against ΔK axes. As described in the earlier part of this Annex, using the Group 3a soft keys, enter the parameters which are required in the search. An example of the parameters set could be "FALSTAFF" and "275", meaning all FALSTAFF results at a maximum stress of 275 MPa. Next select the appropriate plotter using the appropriate group 1a soft key and draw the axis and grid if desired using the "AXES DADN" and "GRID DADN" soft keys of Group 2a. Pressing the "SEARCH PLOT" soft key in Group 4a will then initiate a search through the data base in which any component Files complying with the search specification will be plotted.

HARD COPY OUTPUT TO PRINTER AND CLEARING GRAPHICS

Output of whatever has been drawn on the graphics screen is accomplished by the "DUMP GRAPH" soft keys in Groups 2a and 1b. A dot by dot image of the screen is sent to the graphics printer. The screen is cleared by the "CLEAR GRAPH" soft keys in the same Groups 2a and 1b. It should be noted that the "CLEAR GRAPH" soft key will not function if plotting is currently directed to the external plotter.

INFORMATION STRING

On leaving the Group 2b soft keys, by pressing the "END EDIT" soft key, the interpretation of the information string is printed on the screen and the information string itself is displayed at the bottom of the screen. An example of this display was given earlier in this Annex. The operator can then move the cursor and edit this display if desired.

Each information string relates to a particular component File in a Database File. It consists of the following elements:

(a) The letter 'P' followed by a number from 1 to 20. This refers to the participant in the AGARD Short Crack Programme according to the following table:

P1 = RAE Farnborough UK
P2 = NASA/LANGLEY Hampton Va USA
P3 = CEAT Toulouse France
P4 = DFVLR Koeln W.Germany
P5 = IABG Ottobrunn W.Germany
P6 = NLR Emmeloord Netherlands
P7 = University of Pisa Italy
P8 = METU Ankara Turkey
P9 = FFA Stockholm Sweden
P10 = Johns Hopkins University Baltimore Md USA
P12 = WPAFB Dayton Oh USA
P14 = LNETI/CEMUL Lisbon Portugal

P11, P13 and P15 to P20 are not allocated and can be added by modifying the program as described later.

(b) The letter 'L' followed by a number between 1 and 20 inclusive refers to the following loading actions:

L1 = Constant amplitude R = -2
L2 = Constant amplitude R = -1
L3 = Constant amplitude R = 0
L4 = Constant amplitude R = 0.5
L5 = FALSTAFF
L6 = Gaussian - irreg 0.99
L7 = Felix

L8 to L20 are not allocated and can be added by modifying the program as described later.

(c) The letter "S" followed by a number which denotes the peak stress value in MPa.

(d) The letter "N" followed by an integer number represents the "crack number" (i.e. where there are four cracks on one specimen the cracks would be numbered 1 to 4).

(e) The letter 'T' followed by an integer number from 1 to 4, represents the type of crack:

T1 = Centre crack
T2 = Corner crack

T3 to T4 are not allocated and can be added by modifying the program as described later.
A "Centre crack" is a surface crack located along the notch root and a "Corner crack" is located at the edge of the notch and sheet surface.

(f) The preceding text is terminated by a colon (:) and after this may be typed further description to identify the test, for instance a specimen number.

PLOTTING CRACK LENGTH AGAINST NUMBER OF CYCLES

The plotting of the crack length against cycles graph is carried out using Group 1b soft keys. The following soft keys are used in virtually the same manner as for the crack rate plot described earlier in this Annex.

"AXES LvC"
"TITLE LvC"
"POLY LvC", and
"POINTS LvC"

The only difference is that whether or not two plotting symbols are defined, lines are never drawn between the test points, whereas for the crack rate plot described earlier, if a double symbol is defined then lines are not drawn.

FITTING POLYNOMIALS TO CRACK LENGTH AGAINST CYCLES DATA

This is accomplished using the "FIT POL LvC" soft key in Group 1b. On pressing the soft key the polynomial is fitted to the data of the File currently being accessed, following a request from the computer for the degree of polynomial and operator input of an integer from 1 to 8. If only 'ENTER' is typed in response to this question then the curve is not fitted and any previously fitted coefficients are retained. If a degree of polynomial is requested which is too large for the number of points existing in the File then an error message will be output but the data will not be lost. The fitted polynomial is drawn on the screen after fitting has been completed.

If the fitted polynomial is not satisfactory, and in particular it is possible that the fitted curve may deviate suddenly from the desired line towards the ends of the data, then additional data points can be added using the digitiser, as described earlier in this Annex.

FITTING A LEAST SQUARES STRAIGHT LINE TO CRACK GROWTH RATE DATA

When plotting a File of crack rate data, the following quantities are accumulated for each point plotted:

N = number of points plotted
ΣX = sum of log of crack growth rate
ΣY = sum of log of stress intensity factor
ΣXX = sum of log of crack growth rate times log of crack growth rate
ΣXY = sum of log of crack growth rate times log of stress intensity factor

These values may be used to plot a least squares fit straight line through the data. The line passes through the point

$$\Sigma X/N \ , \ \Sigma Y/N$$

with a slope of

$$\frac{N\ \Sigma XY - \Sigma X\ \Sigma Y}{N\ \Sigma XX - \Sigma X\ \Sigma X}$$

The line defined from the above values can be plotted at any time by using the "PLOT STAT" soft key of Group 4a (provided the graph axes have already been plotted). Because the values are accumulated as each File is plotted, they must be cleared before plotting any group of Files for which a least squares fit is desired. This is accomplished using the "CLEAR STAT" soft key of Group 4a. If it is desired to inspect the accumulated values, then press the "PRINT STAT" soft key of Group 4a and they will be displayed on the screen.

It will be appreciated that a least squares fit straight line can be drawn for a complete set of data plotted in a "SEARCH PLOT" operation, as described earlier.

PLOTTING LONG CRACK DATA

Long crack data, acquired in the AGARD short crack programme and described in Annex G and H, is stored in the database program in piecewise linear form as presented in Table G1. In order to plot any of the long crack results, press soft key "PLOT LC" in Group 4a. In response to a question asking for the "selection code", type one of the following to plot the appropriate data:

Selection code	Data plotted
-2	Constant amplitude loading R = -2
-1	Constant amplitude loading R = -1
0	Constant amplitude loading R = 0
0.5	Constant amplitude loading R = 0.5
FA	FALSTAFF
GA	Gaussian (irreg - 0.99)

POSSIBLE MODIFICATIONS TO THE DATA BASE PROGRAM

The data base program may freely be passed on to third parties and/or modified. It is not intended to give a comprehensive description of possible modifications here, but the following may be useful to the user.

Adding to the list of participants

As previously described, there are spaces for a total of 20 participants. In the first few lines of the program the participants in the AGARD crack programme are defined in statements such as

```
Participant$(3)="CEAT Toulouse France"
```

The user may introduce another participant by adding a line of similar form and using one of the free participant strings as, for example,

```
Participant$(15)="University of Anywhere Anytown Anyland"
```

New loading action

It is important to understand that two variables must be set in order to introduce a new loading action to the program. In a manner similar to that described for the participants, the value of

Loading$(n)

should be set to the name of the loading, where 'n' is a free value of the loading string array (currently from 8 to 20 inclusive). However, the corresponding value of the variable

P_r_fac(n)

must also be set. The reason for introducing the value 'P_r_fac' is that in the AGARD programme all loading actions were defined as the maximum peak stress in the sequence, and it is that peak stress which is entered into the information string of this program in order to define the overall stress value of the loading. However, it was agreed for the short crack programme that stress intensity factors would be plotted as the maximum elastic calculated range. 'P_r_fac' is the value by which the peak stress of the loading must be multiplied in order to obtain the full elastic range of stress. An examination of the program will show that for constant amplitude loading at R = -1 the corresponding 'P_r_fac' value is '2' because the range of the loading is twice the peak value. Examining other values in the program listing should provide further clarification if required.

Changing crack type

As can be seen from the early part of the listing of the program, two types of crack are defined -- centre crack and corner crack. If it is desired to classify cracks in any other manner, then the variable

Crk_type$(n)

should be set, where 'n' is an integer from 3 to 4 inclusive.

Changing default scales

The default scales of the crack rate plot are set early in the program after the label 'Set_default'. The values that are set are logs to the base 10, as follows:

Mik = -.5 (Minimum alternating stress intensity factor)
Mak = 1.7 (Maximum alternating stress intensity factor)
Mir = -8 (Minimum crack rate)
Mar = -3 (Maximum crack rate)

The default values can be set easily in the program if desired, to save the user the necessity of changing them every time the program is executed.

Stress intensity factor calculation

This is carried out by the Subroutine 'Stress_int'. It is carefully commented and is consistent with the definition of stress intensity factor in Section 3.5.1 except that the angle ϕ is assumed to be equal to $\pi/2$ radians. It is a relatively simple matter to change this formula if desired.

Introducing new sets of long crack data to be plotted

Plotting of the long crack data starts at label 'Plotr' shortly after the beginning of the program. It is a simple matter to introduce a new set of values to be plotted. Further details are given in program comments.

FUTURE MODIFICATION

The full set of data charts or crack maps (eg. Fig. 14) are available from the RAE or NASA as described below. However, the next version of the Database program will incorporate a system of drawing the short crack data charts automatically.

OBTAINING COPIES OF THE DATABASE AND PROGRAM

Copies of the Database and Program should be obtainable through the Executive of the Structures and Materials Panel at the following address:

From Europe:

SMP Executive
AGARD
7, rue Ancelle
92200 Neuilly-sur-Seine
France

Telephone: 33 (1) 4738-5790
Telex : 610176F

From USA & CANADA

AGARD/NATO
APO New York 09777
Attn: SMP Executive

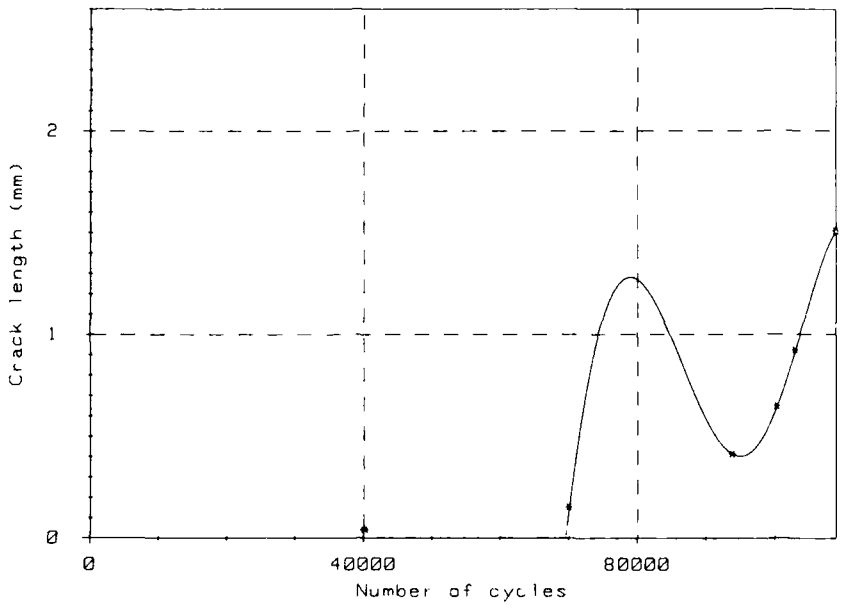

Figure 11.- Initial best-fit polynomial.

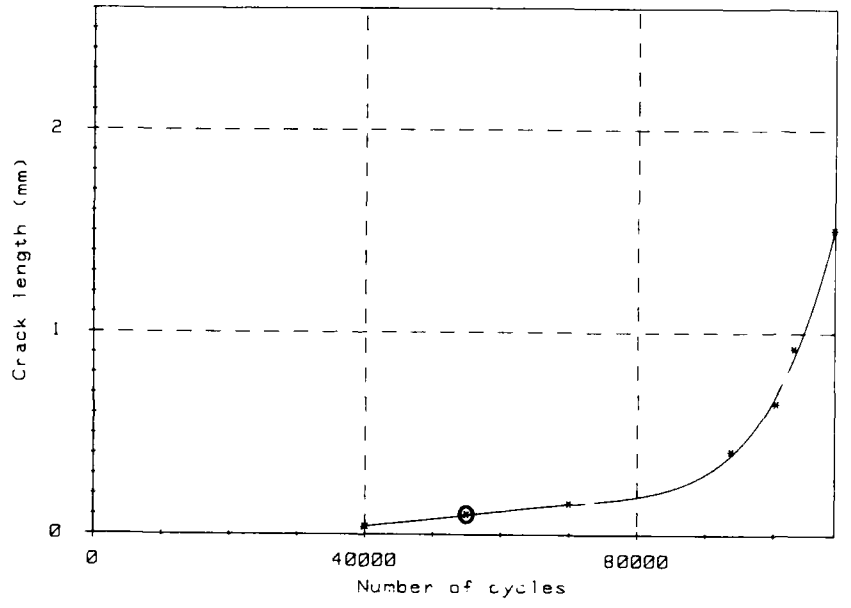

Figure 12.- Best-fit polynomial following the addition of one extra point (circled).

Table II.- Summary of Databases - Raw Data

NAME OF DATABASE		PORTC	TURKC	CEATC	1ABUC1 •1ABUC2	DFVC	SWEC	NLRC	ITAC •ITAC1	UKC	NAS3C •NAS2C	JHUBC	WPAC •WPAC1
PARTICIPANT		PORTUGAL LNETI	TURKEY METU	FRANCE CEAT	GERMANY IABG	GERMANY DFVLR	SWEDEN FFA	NETHERLANDS NLR	ITALY UNIVERSITY OF PISA	UK RAE	USA NASA	USA J HOPKINS UNIVERSITY	USA AFWAL/FIBEC
	STRESS LEVEL MPa	SPEC 1 | 2 | 3 CRACKS	SPEC 1 | 2 | 3 CRACKS	SPEC 1 | 2 | 3 CRACKS	SPEC 1 | 2 | 3 CRACKS	SPEC 1 | 2 | 3 CRACKS	SPEC 1 | 2 | 3 CRACKS	SPEC 1 | 2 | 3 CRACKS	SPEC 1 | 2 | 3 CRACKS	SPEC 1 | 2 | 3 CRACKS	SPEC 1 | 2 | 3 CRACKS	SPEC 1 | 2 | 3 CRACKS	SPEC 1 | 2 | 3 CRACKS
FALSTAFF	275			5/5	5/5 5/5	5/5	6/6		5/5 5/5 •5/5	6/6	5/6 5/5		•5/5 •5/5
	205			5/5	5/5 5/5	5/5	7/7 7/7		5/5 5/5 5/5	5/5	•5/11 3/4		•5/5 •5/5
	170				5/5 5/5	5/5				5/5	4/7 5/6		5/5 2/4
GAUSSIAN	170				•5/5 •5/5	5/5		5/5 5/5		5/5			
	145				•5/5 •5/5	5/5		6/6 5/5		5/5			
	125				•5/5 •5/5	5/5		2/2 3/3		2/2			
CONSTANT AMPLITUDE	R = -2												
	75	5/5	5/5	5/5			8/8 4/4			5/5	2/3 5/5	5/5	6/6 6/6 5/5
	60	5/5	5/5	5/5			7/7 4/4			5/5	5/7 5/6	5/5 5/5	5/5 5/5
	50	4/4	5/5	2/2			3/3 2/2			5/5	3/3 5/5	1/1 4/4	2/2 3/3
	R = -1												
	105	6/6	5/5	5/5	5/5 5/5	5/5	10/12	8/8 7/7	5/5 5/5 5/5	5/5	5/5 •4/6	5/5 5/5	5/5 5/5 5/5
	80	5/5	5/5	5/5	5/5 5/5		8/8 6/6	1/1 5/5 5/5	5/5 5/5 5/5	5/5	4/4 6/6	5/5 1/1	5/5 5/5
	70	2/2	3/5	2/2	2/2 1/1			1/1 1/1	1/1 2/2	2/2	2/2 1/1 1/2	4/4 5/5	5/5 5/5
	R = 0												
	145	5/5	5/5	5/5 5/5 5/5	5/5 5/5 5/5		5/5 2/2		5/5 5/5 4/4	5/5	2/3 1/1	5/5 4/4	5/5 5/5 5/5 5/5
	120	5/5	3/3	4/4	1/1 5/5 3/3		4/4 1/1		3/3 1/1 5/5	5/5	1/2 3/5	1/1	3/3 1/1 2/2 3/3 1/1
	110	2/2	1/1	3/3	5/6 1/1 4/4				1/1	2/2	4/5	3/3 1/1	1/1 1/1 1/1 1/1
	R = 0.5												
	225	1/1	5/5						5/7 5/5 2/2	5/5	1/1 5/6	1/1 5/5	
	205	1/1	4/4						2/2 2/2 5/5	1/1	2/2 1/1	5/5 2/2	
	195	1/1	2/2						2/2 5/5 1/1	1/1	2/2 4/5	1/1 4/4	

KEY: A/B

A = Number of cracks
B = Number of files

Table 12.- Summary of Databases - Data Subjected to Non-Interaction Criterion.

NAME OF DATABASE		PORTXC	TURXC	CEATXC	IAU1XC •IAU2XC	DFVXC	SWEXC	NLRXC	ITAXC	UKXC	NAS3XC •NAS2XC	JHUXC	•PAXC
PARTICIPANT		PORTUGAL LNETI	TURKEY METU	FRANCE CEAT	GERMANY IABG	GERMANY DFVLR	SWEDEN FFA	NETHERLANDS NLR	ITALY UNIVERSITY OF PISA	UK RAE	USA NASA	USA J HOPKINS UNIVERSITY	USA AFWAL/FIBEC
	STRESS LEVEL MPa	SPEC 1 2 3 CRACKS	SPEC 1 2 3 CRACKS	SPEC 1 2 3 CRACKS	SPEC 1 2 3 CRACKS	SPEC 1 2 3 CRACKS	SPEC 1 2 3 CRACKS	SPEC 1 2 3 CRACKS	SPEC 1 2 3 CRACKS	SPEC 1 2 3 CRACKS	SPEC 1 2 3 CRACKS	SPEC 1 2 3 CRACKS	SPEC 1 2 3 4 5 6 CRACKS
FALSTAFF	275			4/4	5/5 5/5		4/4		5/5 5/5 3/3		5/6 5/5		5/5
	205				5/5 5/5	2/2	4/4 4/4		5/5 1/1	4/4	•5/8 3/4		5/5 4/4
	170				5/5 4/4	5/5				3/3	4/7 5/5		2/5
GAUSSIAN	170				•5/5 •5/5	5/5		4/4 5/5		4/4			
	145				•5/5 •5/5	3/3		6/7		5/5			
	125				•5/5 •5/5	2/2		2/2 1/1		1/1			
CONSTANT AMPLITUDE	R = -2												
	75	5/5	5/5	5/5			4/4				2/3 5/5	4/4	2/2 4/4
	60	3/3	5/5	5/5			7/7			3/3	5/5 4/5	4/4 5/5	2/2
	50	1/2	5/5	1/2			2/2			4/5 4/5	3/3 5/5	1/1 3/3	1/2 2 2
	R = -1												
	100	6/7	5/5	4/4	5/5 5/5	1/1	1/1		3/3	5/6	•4/4 5/5	5/5 3/3	5/5 5/5 5/5
	90	5/5	5/5	3/3	5/5 4/4		3/3 3/3	1/1 2/2	5/5 5/5 4/4	4/5	3/3 5/5	4/4 1/1	4/4 3/3
	75	1/3	3/3	1/1	2/2 1/1			1/1 1/1	1/1 1/2	2/2	1/1 1/1 1/2	3/3 5/5	4/6 3/4
	R = 0												
	145	5/6	5/5	4/4 5/5 5/5	5/5 5/5 5/5		2/2 2/2		5/5 5/5 3/3	4/4	1/1 2/1	4/4 3/3	3/3 1/1 2/2 5/5
	130	4/5	3/3	3/3	1/1 4/4 2/2		4/4 1/1		1/1 1/1 5/5	3/3	1/2 3/5	1/1	3/3 1/1 1/1 1/1
	110	2/3	1/1	3/5	5/5 1/1 2/2				1/1	2/2	4/5	3/3 1/1	1/1 1/1 1/1
	R = 0.5												
	235	1/1	5/5						4/4 5/5 1/1	4/5	1/1 5/6	1/1 4/4	
	205	1/2	2/2						1/1 2/3 4/4	1/1	2/2 1/1	2/2 2/2	
	190	1/2	2/2						2/2 1/1	1/1	2/2 4/5	1/1	

KEY A/B A Number of cracks
B Number of files

REPORT DOCUMENTATION PAGE

1. Recipient's Reference	2. Originator's Reference	3. Further Reference	4. Security Classification of Document
	AGARD-R-732	ISBN 92-835-0493-3	UNCLASSIFIED

5. Originator Advisory Group for Aerospace Research and Development
North Atlantic Treaty Organization
7 rue Ancelle, 92200 Neuilly sur Seine, France

6. Title SHORT-CRACK GROWTH BEHAVIOUR IN AN ALUMINUM ALLOY — AN AGARD COOPERATIVE TEST PROGRAMME

7. Presented at

8. Author(s)/Editor(s) J.C.Newman, Jr and P.R.Edwards

9. Date December 1988

10. Author's/Editor's Address See flyleaf.

11. Pages 104

12. Distribution Statement This document is distributed in accordance with AGARD policies and regulations, which are outlined on the Outside Back Covers of all AGARD publications.

13. Keywords/Descriptors

Aluminum alloys
Crack propagation
Mathematical models
Experimental data
Fatigue life
Comparison

14. Abstract

An AGARD test programme on the growth of "short" fatigue cracks was conducted to define the significance of the short-crack effect, to compare test results from various laboratories and to evaluate an existing analytical model to predict the growth of such cracks. The first phase of this programmme, the Core Programme, was aimed at test procedure and specimen standardisation and calibration of the various laboratories. A detailed working document has been prepared and is included in this report. It describes the testing fundamentals and procedures and includes the analysis procedures used for handling the test data.

The results from the test programme showed good agreement among the participants on short-crack growth rates, on fatigue life to various crack sizes and breakthrough (surface- or corner-crack became a through crack), and on crack shapes. A crack-growth model, incorporating crack-closure effects was used to analyse the growth of short cracks from small (inclusion) defects in the material along the notch surface. The closure model indicated that the "short-crack" effect was greatest in those tests involving significant compressive loads, such as constant-amplitude loading at stress ratios of -1 and -2, and the Gaussian spectrum loading.

This publication was sponsored by the Structures and Materials Panel of AGARD.

AGARD
NATO OTAN
7 rue Ancelle · 92200 NEUILLY-SUR-SEINE
FRANCE
Telephone (1)47.38.57.00 · Telex 610 176

DISTRIBUTION OF UNCLASSIFIED AGARD PUBLICATIONS

AGARD does NOT hold stocks of AGARD publications at the above address for general distribution. Initial distribution of AGARD publications is made to AGARD Member Nations through the following National Distribution Centres. Further copies are sometimes available from these Centres, but if not may be purchased in Microfiche or Photocopy form from the Purchase Agencies listed below.

NATIONAL DISTRIBUTION CENTRES

BELGIUM
Coordonnateur AGARD — VSL
Etat-Major de la Force Aérienne
Quartier Reine Elisabeth
Rue d'Evere, 1140 Bruxelles

CANADA
Director Scientific Information Services
Dept of National Defence
Ottawa, Ontario K1A 0K2

DENMARK
Danish Defenc
Ved Idraetspa
2100 Copenha

FRANCE
O.N.E.R.A. (D
29 Avenue de
92320 Châtillo

GERMANY
Fachinformatio
Physik, Mathen
Karlsruhe
D-7514 Eggen

GREECE
Hellenic Air Fo
Aircraft Suppo
Department of
Holargos, Athe

ICELAND
Director of Aviation
c/o Flugrad
Reykjavik

ITALY
Aeronautica Militare
Ufficio del Delegato Nazionale all'AGARD
3 Piazzale Adenauer
00144 Roma/EUR

LUXEMBOURG
See Belgium

NETHERLANDS
Netherlands Delegation to AGARD
National Aerospace Laboratory, NLR
P.O. Box 126
2600 AC Delft

NORWAY

Kentigern House
65 Brown Street
Glasgow G2 8EX

UNITED STATES
National Aeronautics and Space Administration (NASA)
Langley Research Center
M/S 180
Hampton, Virginia 23665

THE UNITED STATES NATIONAL DISTRIBUTION CENTRE (NASA) DOES NOT HOLD STOCKS OF AGARD PUBLICATIONS, AND APPLICATIONS FOR COPIES SHOULD BE MADE DIRECT TO THE NATIONAL TECHNICAL INFORMATION SERVICE (NTIS) AT THE ADDRESS BELOW.

PURCHASE AGENCIES

National Technical Information Service (NTIS)
5285 Port Royal Road
Springfield
Virginia 22161, USA

ESA/Information Retrieval Service
European Space Agency
10, rue Mario Nikis
75015 Paris, France

The British Library
Document Supply Division
Boston Spa, Wetherby
West Yorkshire LS23 7BQ
England

Requests for microfiche or photocopies of AGARD documents should include the AGARD serial number, title, author or editor, and publication date. Requests to NTIS should include the NASA accession report number. Full bibliographical references and abstracts of AGARD publications are given in the following journals:

Scientific and Technical Aerospace Reports (STAR)
published by NASA Scientific and Technical Information Branch
NASA Headquarters (NIT-40)
Washington D.C. 20546, USA

Government Reports Announcements (GRA)
published by the National Technical Information Services, Springfield
Virginia 22161, USA

Printed by Specialised Printing Services Limited
40 Chigwell Lane, Loughton, Essex IG10 3TZ

ISBN 92-835-0493-3